POLITECNICO DI TORINO
Repository ISTITUZIONALE

3D capability of refined GDQ models for the bending analysis of composite and sandwich plates, spherical and doubly-curved shells

(Article begins on next page)

26 April 2024

3D CAPABILITY OF REFINED GDQ MODELS FOR THE BENDING ANALYSIS OF COMPOSITE AND SANDWICH PLATES, SPHERICAL AND DOUBLY-CURVED SHELLS

Francesco Tornabene[1], Salvatore Brischetto[2]

ABSTRACT. The paper proposes a comparative study between different analytical and numerical three-dimensional (3D) and two-dimensional (2D) shell models for the bending analysis of composite and sandwich plates, spherical and doubly-curved shells subjected to a transverse normal load applied at the top surface. 3D shell models, based on the equilibrium equations written in mixed orthogonal curvilinear coordinates, are proposed in closed form considering harmonic forms for displacements, stresses and loads and simply supported boundary conditions. The partial differential equations in the normal direction are solved in analytical form using the Exponential Matrix (EM) method and in numerical form by means of the Generalized Differential Quadrature (GDQ) method. The first 3D model is here defined as 3D EM model and the second one is here defined as 3D GDQ model. Two-dimensional shell solutions are based on the unified formulation which allows to obtain several refined and classical 2D shell theories in both Equivalent Single Layer (ESL) and Layer Wise (LW) form. Classical theories such as the First order Shear Deformation Theory (FSDT), the Third order Shear Deformation Theory (TSDT) and the Kirchhoff-Love (KL) theory are obtained as particular cases of refined 2D ESL models. 2D shell solutions are proposed by means of a complete generic numerical method such as the GDQ method which allows the investigation of complicated geometries, lamination schemes, materials, loading conditions and boundary conditions. The analyses and comparisons are proposed in terms of displacements, stresses and strains. In 2D GDQ models the transverse shear and transverse normal stresses are recovered from the 3D equilibrium equations allowing results in accordance with the 3D shell solutions. After these validations, the refined 2D GDQ shell models are used for the investigations of new cases which cannot be analyzed by means of closed form solutions. In the present work, the static analysis of an elliptic pseudo-sphere is proposed. Considerations about the typical zigzag form of displacements for multilayered structures are given. The interlaminar continuity in terms of compatibility and equilibrium conditions are also discussed for all the proposed assessments and benchmarks.

[1]*DICAM Department - School of Engineering and Architecture, University of Bologna, Italy.* *francesco.tornabene@unibo.it.*
[2]*DIMEAS – Department of Mechanical and Aerospace Engineering, Politecnico di Torino, Italy.* *salvatore.brischetto@polito.it.*

KEYWORDS: 3D shell models; refined 2D shell models; closed form solutions; generalized differential quadrature method; exponential matrix method; sandwich and laminated structures; stress recovery; zigzag effect; interlaminar continuity.

1. INTRODUCTION

Multilayered composite and sandwich structures give high level performances, increasing the safety requirements and improving the dynamic behavior, and they can be employed to design stiffer structures with limited weight. These structures have a great diffusion in aerospace, marine, building and automotive engineering fields where they are analyzed as shell and plate elements [1-3]. Shell and plate structures can be investigated using analytical and numerical three-dimensional (3D) or two-dimensional (2D) shell models. 3D shell models give more accurate results but they are heavy from the computational and mathematical point of view. For these reasons, 2D shell models have a great diffusion in practical engineering applications. They propose an approximation though the thickness of the structure but they allow a drastic reduction of the computational time and the complexity of the formulation.

3D plate and shell formulations proposed in the literature show a restricted range of applications when they are developed in analytical form. These limitations could be overcome when they are implemented in numerical form. Pagano [4-6] proposed the bending investigation of multilayered composite and sandwich plates showing several benchmarks frequently used in the literature to perform model comparisons. The 3D numerical plate model by Xu and Zhou [7] allowed the bending analysis of plates with variable thickness. The elasticity beam/plate solution by Meyer-Piening [8] is of particular interest for the bending analysis of sandwich structures with soft core. Demasi [9] proposed a 3D analytical elasticity solution for plates using the mixed form of constitutive equations. Ren [10] proposed the exact 3D bending analysis of composite cylindrical panels subjected to transverse normal loads. Varadan and Bhaskar [11] developed an exact 3D model for composite cylinders subjected to transverse normal loads. Composite spherical panels were analyzed by Fan and Zhang [12-13] using 3D static shell solutions. Soldatos and Ye [14] proposed a similar formulation in the case of composite cylinders subjected to harmonic loads. The three-dimensional elasticity solution by Fan and Ye [15] was devoted to composite plates with classical load applications. A typical 3D exact plate solution extended to the static analysis of single-layered Functionally Graded Material (FGM) structures was that by Kashtalyan [16]. This method was extended to sandwich plates embedding FGM cores by Kashtalyan and Menshykova [17]. 3D

2

free vibration and dynamic models for plates can be found in [18-21]. Three-dimensional elasticity solutions for free vibration and dynamic analysis of shells are typical of works [22-24]. Further interesting 3D solutions in numerical form can be found in [25-30] for free frequency, dynamic and bending analysis of plate and shell structures. All the discussed 3D models in [4]-[30] are very accurate but they were developed only for particular geometries. Recently, this limit has been overcome by Brischetto which developed a general analytical 3D exact shell model for the investigation of plates, cylinders and spherical/cylindrical shell panels embedding isotropic, composite and functionally graded layers. Free vibration problems were proposed in [31-34] in the case of one-layered, laminated composite, sandwich and functionally graded structures and for single-walled carbon nanotubes. Static analyses with the applications of transverse shear and transverse normal loads at the external surfaces were proposed in [35-38] for multilayered composite, sandwich and functionally graded plates and shells. The 3D exact model by Brischetto [31-38] uses the exponenetial matrix method, the layer-wise approach, the interlaminar continuity conditions in terms of displacements and transverse stresses and the 3D equilibrium equations in mixed orthogonal curvilinear coordinates. It is a generalization of the plate and shell models already presented in [13-14] and [20].

2D plate and shell models are developed in order to reduce the degrees of freedom of the system and to have a simpler formulation. In this way, the computational cost of the models is reduced. Moreover, numerical models allow the solution of more complicated problems in terms of loads, boundary conditions and lamination schemes. The most popular numerical methods available in the literature are based on the weak formulation of the governing equations, a typical example is the Finite Element Method (FEM). Recently, alternative methods have been proposed in terms of strong form of the governing equations. A typical example of these methods is the Generalized Differential Quadrature (GDQ) method proposed by Shu [39-40]. This approach and further methods related with this procedure allow the accurate and complete analysis of composite and sandwich structures. Several examples about GDQ methods used for the analysis of composite and sandwich structures can be found in [41-50]. The present new 2D GDQ shell models include more refined 2D kinematic models (in both equivalent single layer (ESL) and layer wise (LW) form) and a more general geometrical approach. Tornabene developed classical and refined 2D GDQ models for the analysis of plates and doubly-curved shells using the differential geometry of curves and surfaces. The free vibration analysis of doubly-curved laminated shells and plates was performed in [51] using general higher-order shear deformation theories developed in the framework of the GDQ method. The same models was extended to the static analysis of doubly-curved laminated shells and

panels in [52]. The extension to higher order equivalent single layer theories was made in [53] extending the Carrera Unified Formulation (CUF) [54-55] to GDQ solutions for the free vibration analysis. The same formulation [54-55] was used in [56] to analyze the static behaviour of doubly-curved anisotropic shells and panels. The use of a posteriori shear and normal stress recovery in the GDQ static analysis of composite plates and shells was introduced by Tornabene and his collaborators in [57-60]. In particular, the a posteriori recovery procedure was applied previously to the First-order Shear Deformation Theory [57-58], and secondly to various Higher-order Shear Deformation Theories [59-60]. Furthermore, in the present new paper, the recovery procedure is not compared with 3D FEM solutions, but with different analytical and numerical three-dimensional (3D) shell models, which are more accurate with respect the previous adopted FEM solutions.

In the area of plate- and shell-type structures, many contributions were published in the past. In particular, different approches were considered such as Discrete Sigular Convolution Methodology [61-63], Meshless Local Petrov-Galerkin Method [64], Semi-Analytical Procedures [65-66], Finite Element Method [67-68] and Isogeometric Analysis [69-71]. Finally, a new methodology, called Variational Differential Quadrature (VDQ) Technique [72], was recently proposed. In particular, the VDQ method was based on the variational formulation of the considered problem and it presented very accurate and converging properties as shown in the paper by Shojaei and Ansari [72]. The 2D GDQ models here proposed are more general from the geometrical and kinematic point of view because they include higher order ESL and LW models able to investigate plates and complicated double-curved structures.

The present paper proposes the static analysis of laminated composite/sandwich plates and spherical or double-curved shells subjected to transverse normal loads applied at the top surface in harmonic form. The choice of these geometries, lamination schemes, materials and loads allows to clearly evaluate the zigzag form of displacements and the problems connected with the interlaminar conditions in terms of displacement and transverse stress continuity. Classical and refined GDQ shell models by Tornabene [40-45], [51-53], [56-57], [73-74] have been compared with two different closed-form three-dimensional shell theories. The first form uses mixed orthogonal curvilinear coordinates, layer-wise approach, interlaminar continuity for transverse stresses and displacements and exponential matrix methodology for the analytical resolution of differential equations in the normal direction. This form was developed by Brischetto in [31-38]. The second form, here presented for the first time, uses mixed orthogonal curvilinear coordinates, layer-wise approach, interlaminar continuity for transverse stresses and displacements and the GDQ method by Tornabene [40-45], [51-53], [56-57], [73-74] to

numerically solve the differential equations in the normal direction. The proposed refined and classical 2D GDQ theories use a posteriori shear and normal stress recovery in order to improve the evaluation of these quantities through the thickness direction. The proposed 3D and 2D shell models are accurate enough in terms of displacements, stresses and strains. This feature easily allows their extention to non-linear problems for large elastic deformations.

The main novelties and new contributions of the present work are summarized as follows. First of all, the proposed closed-form 3D shell model, which includes the solution of differential equations in normal direction by means of the GDQ method (here called as 3D GDQ shell model), is for the first time proposed in the present paper in the framework of a general formulation for the geometry able to investigate plates, cylinders, cylindrical shells and spherical shells. To the best of authors' knowledges, in the literature this idea has never been proposed. The other 3D shell model in closed form, which uses the Exponential Matrix method for the solution of differential equations in normal direction (here called as 3D EM shell model), was already proposed by one of the two authors in [31-38]. 3D EM model has been included in the present paper for comparison purposes in order to validate the new 3D GDQ model. Secondly, GDQ combined with CUF was already proposed by one of the two authors in [56-60], but it is now developed in a more general way which allows a complete static analysis for several geometries (also including one of the novelty of the present paper which is the elliptic pseudosphere). The proposed 2D GDQ models based on CUF are very general because they analyze true double-curved shells and not only plates, cylindrical and spherical shells. Moreover, they also consider complicated boundary conditions and they use the "a posteriori stress" recovery. Finally, to the best of authors' knowledge, there are no papers in the literature which propose a complete static investigation as the present one. In fact, stress, displacement and strain results are proposed for plates, spherical shells and true double curved shells by comparing different classical and refined 2D theories, a 3D closed-form shell model based on the exponential matrix method, and a 3D closed-form shell model based on the generalized differential quadrature method. The comparisons of these three methodologies, which are very different between them, always guarantee correct results and the possibility to give fundamental considerations about the modelling of plates and shells. In fact, zigzag form of displacements and stresses, and interlaminar continuity in terms of displacements (compatibility conditions) and transverse stresses (equilibrium conditions) are clearly shown in the proposed graphical results.

2. 3D SHELL THEORY AND NAVIER EXACT SOLUTION

The 3D shell theory is based on the 3D equilibrium equations written in principal curvilinear coordinates (s_1, s_2, ζ) [73]. Figure 1 shows the curvilinear coordinates, the geometrical features, the several possibilities for thickness coordinates and the meaning of the mean radii of curvature $R_1(s_1, s_2)$ and $R_2(s_1, s_2)$ along the two directions s_1 and s_2. For a generic isotropic or cross-ply k-th lamina we can write the kinematic, costitutive and equilibrium equations [73] as follows:

$$
\begin{bmatrix} \varepsilon_1^{(k)} \\ \varepsilon_2^{(k)} \\ \gamma_{12}^{(k)} \\ \gamma_{13}^{(k)} \\ \gamma_{23}^{(k)} \\ \varepsilon_3^{(k)} \end{bmatrix} =
\begin{bmatrix}
\dfrac{1}{H_1^{(k)}}\dfrac{\partial}{\partial s_1} & 0 & \dfrac{1}{H_1^{(k)}R_1} \\[2mm]
0 & \dfrac{1}{H_2^{(k)}}\dfrac{\partial}{\partial s_2} & \dfrac{1}{H_2^{(k)}R_2} \\[2mm]
\dfrac{1}{H_2^{(k)}}\dfrac{\partial}{\partial s_2} & \dfrac{1}{H_1^{(k)}}\dfrac{\partial}{\partial s_1} & 0 \\[2mm]
\dfrac{\partial}{\partial \zeta^{(k)}} - \dfrac{1}{H_1^{(k)}R_1} & 0 & \dfrac{1}{H_1^{(k)}}\dfrac{\partial}{\partial s_1} \\[2mm]
0 & \dfrac{\partial}{\partial \zeta^{(k)}} - \dfrac{1}{H_2^{(k)}R_2} & \dfrac{1}{H_2^{(k)}}\dfrac{\partial}{\partial s_2} \\[2mm]
0 & 0 & \dfrac{\partial}{\partial \zeta^{(k)}}
\end{bmatrix}
\begin{bmatrix} U_1^{(k)} \\ U_2^{(k)} \\ U_3^{(k)} \end{bmatrix}
\tag{1}
$$

$$
\begin{bmatrix} \sigma_1^{(k)} \\ \sigma_2^{(k)} \\ \tau_{12}^{(k)} \\ \tau_{13}^{(k)} \\ \tau_{23}^{(k)} \\ \sigma_3^{(k)} \end{bmatrix} =
\begin{bmatrix}
\bar{C}_{11}^{(k)} & \bar{C}_{12}^{(k)} & \bar{C}_{16}^{(k)} & 0 & 0 & \bar{C}_{13}^{(k)} \\
\bar{C}_{12}^{(k)} & \bar{C}_{22}^{(k)} & \bar{C}_{26}^{(k)} & 0 & 0 & \bar{C}_{23}^{(k)} \\
\bar{C}_{16}^{(k)} & \bar{C}_{26}^{(k)} & \bar{C}_{66}^{(k)} & 0 & 0 & \bar{C}_{36}^{(k)} \\
0 & 0 & 0 & \bar{C}_{44}^{(k)} & \bar{C}_{45}^{(k)} & 0 \\
0 & 0 & 0 & \bar{C}_{45}^{(k)} & \bar{C}_{55}^{(k)} & 0 \\
\bar{C}_{13}^{(k)} & \bar{C}_{23}^{(k)} & \bar{C}_{36}^{(k)} & 0 & 0 & \bar{C}_{33}^{(k)}
\end{bmatrix}
\begin{bmatrix} \varepsilon_1^{(k)} \\ \varepsilon_2^{(k)} \\ \gamma_{12}^{(k)} \\ \gamma_{13}^{(k)} \\ \gamma_{23}^{(k)} \\ \varepsilon_3^{(k)} \end{bmatrix}
\tag{2}
$$

$$
\frac{1}{H_1^{(k)}}\frac{\partial \sigma_1^{(k)}}{\partial s_1} + \frac{1}{H_2^{(k)}}\frac{\partial \tau_{12}^{(k)}}{\partial s_2} + \frac{\partial \tau_{13}^{(k)}}{\partial \zeta^{(k)}} + \tau_{13}^{(k)}\left(\frac{2}{H_1^{(k)}R_1} + \frac{1}{H_2^{(k)}R_2} \right) + f_1^{(k)} = 0
$$

$$
\frac{1}{H_2^{(k)}}\frac{\partial \sigma_2^{(k)}}{\partial s_2} + \frac{1}{H_1^{(k)}}\frac{\partial \tau_{12}^{(k)}}{\partial s_1} + \frac{\partial \tau_{23}^{(k)}}{\partial \zeta^{(k)}} + \tau_{23}^{(k)}\left(\frac{1}{H_1^{(k)}R_1} + \frac{2}{H_2^{(k)}R_2} \right) + f_2^{(k)} = 0
\tag{3}
$$

$$
\frac{1}{H_1^{(k)}}\frac{\partial \tau_{13}^{(k)}}{\partial s_1} + \frac{1}{H_2^{(k)}}\frac{\partial \tau_{23}^{(k)}}{\partial s_2} + \frac{\partial \sigma_3^{(k)}}{\partial \zeta^{(k)}} + \sigma_3^{(k)}\left(\frac{1}{H_1^{(k)}R_1} + \frac{1}{H_2^{(k)}R_2} \right) - \frac{\sigma_1^{(k)}}{H_1^{(k)}R_1} - \frac{\sigma_2^{(k)}}{H_2^{(k)}R_2} + f_3^{(k)} = 0
$$

where the parametric coefficients $H_1^{(k)}$ and $H_2^{(k)}$ have the following form:

$$H_1^{(k)} = 1 + \frac{\zeta}{R_1}$$

$$H_2^{(k)} = 1 + \frac{\zeta}{R_2} \tag{4}$$

In the equations (1)-(3), $U_1(s_1, s_2, \zeta)$, $U_2(s_1, s_2, \zeta)$ and $U_3(s_1, s_2, \zeta)$ are the 3D displacements components, $f_i^{(k)}$ are the body forces, $\varepsilon_1^{(k)}, \varepsilon_2^{(k)}, \gamma_{12}^{(k)}, \gamma_{13}^{(k)}, \gamma_{23}^{(k)}, \varepsilon_3^{(k)}$ and $\sigma_1^{(k)}, \sigma_2^{(k)}, \tau_{12}^{(k)}, \tau_{13}^{(k)}, \tau_{23}^{(k)}, \sigma_3^{(k)}$ are the strain and stress components for the k-th ply. Symbol ∂ indicates partial derivatives and $\bar{C}_{ij}^{(k)}$ are the elastic coefficients. Structures are considered simply supported and with harmonic forms for displacements, stresses, loads and body forces:

$$\left\{ U_1^{(k)}, f_1^{(k)}, \tau_{13}^{(k)} \right\}(s_1, s_2, \zeta) = \left\{ U_1^{(k)}, f_1^{(k)}, T_{13}^{(k)} \right\}(\zeta) \cos\left(\frac{n\pi}{L_1} s_1 \right) \sin\left(\frac{m\pi}{L_2} s_2 \right) \tag{5}$$

$$\left\{ U_2^{(k)}, f_2^{(k)}, \tau_{23}^{(k)} \right\}(s_1, s_2, \zeta) = \left\{ U_2^{(k)}, f_2^{(k)}, T_{23}^{(k)} \right\}(\zeta) \sin\left(\frac{n\pi}{L_1} s_1 \right) \cos\left(\frac{m\pi}{L_2} s_2 \right) \tag{6}$$

$$\left\{ U_3^{(k)}, f_3^{(k)}, \sigma_1^{(k)}, \sigma_2^{(k)}, \sigma_3^{(k)} \right\}(s_1, s_2, \zeta) = \left\{ U_3^{(k)}, f_3^{(k)}, \Sigma_1^{(k)}, \Sigma_2^{(k)}, \Sigma_3^{(k)} \right\}(\zeta) \sin\left(\frac{n\pi}{L_1} s_1 \right) \sin\left(\frac{m\pi}{L_2} s_2 \right) \tag{7}$$

$$\tau_{12}^{(k)}(s_1, s_2, \zeta) = T_{12}^{(k)}(\zeta) \cos\left(\frac{n\pi}{L_1} s_1 \right) \cos\left(\frac{m\pi}{L_2} s_2 \right) \tag{8}$$

where m and n are the half-wave numbers, and L_1 and L_2 are the dimensions of the structures. $U_i^{(k)}$ are the amplitudes of displacements $U_i^{(k)}$. $f_i^{(k)}$ are the amplitudes of body forces $f_i^{(k)}$. $T_{ij}^{(k)}$ are the amplitudes of shear stresses $\tau_{ij}^{(k)}$ and $\Sigma_{ij}^{(k)}$ are the amplitudes of normal stresses $\sigma_i^{(k)}$.

The considered Navier's solution (5)-(8) (see Reddy [1]) may exist only when the laminate staking sequences regard to isotropic or cross-ply laminates for which we have the following zero elastic coefficients:

$$\bar{C}_{16}^{(k)} = \bar{C}_{26}^{(k)} = \bar{C}_{36}^{(k)} = \bar{C}_{45}^{(k)} = 0 \tag{9}$$

The substitution of Eqs. (5)-(8) in the 3D governing equations (1)-(3) allows a closed-form solution of the system:

$$\left(\bar{C}_{44}^{(k)} \frac{\partial^2}{\partial \zeta^2} + \left(\frac{\bar{C}_{44}^{(k)}}{H_1^{(k)} R_1} + \frac{\bar{C}_{44}^{(k)}}{H_2^{(k)} R_2} \right) \frac{\partial}{\partial \zeta} - \frac{n^2 \pi^2}{L_1^2} \frac{\bar{C}_{11}^{(k)}}{H_1^{(k)2}} - \frac{m^2 \pi^2}{L_2^2} \frac{\bar{C}_{66}^{(k)}}{H_2^{(k)2}} - \frac{\bar{C}_{44}^{(k)}}{H_1^{(k)} H_2^{(k)} R_1 R_2} - \frac{\bar{C}_{44}^{(k)}}{H_1^{(k)2} R_1^2} \right) U_1^{(k)} +$$

$$+ \left(-\frac{n\pi}{L_1} \frac{m\pi}{L_2} \frac{\bar{C}_{12}^{(k)} + \bar{C}_{66}^{(k)}}{H_1^{(k)} H_2^{(k)}} \right) U_2^{(k)} + \left(\frac{n\pi}{L_1} \frac{\bar{C}_{13}^{(k)} + \bar{C}_{44}^{(k)}}{H_1^{(k)}} \frac{\partial}{\partial \zeta} + \frac{n\pi}{L_1} \left(\frac{\bar{C}_{12}^{(k)} + \bar{C}_{44}^{(k)}}{H_1^{(k)} H_2^{(k)} R_2} + \frac{\bar{C}_{11}^{(k)} + \bar{C}_{44}^{(k)}}{H_1^{(k)2} R_1} \right) \right) U_3^{(k)} + f_1^{(k)} = 0 \tag{10}$$

7

$$\left(-\frac{n\pi}{L_1}\frac{m\pi}{L_2}\frac{\bar{C}_{12}^{(k)}+\bar{C}_{66}^{(k)}}{H_1^{(k)}H_2^{(k)}}\right)U_1^{(k)}+\left(\bar{C}_{55}^{(k)}\frac{\partial^2}{\partial\zeta^2}+\left(\frac{\bar{C}_{55}^{(k)}}{H_1^{(k)}R_1}+\frac{\bar{C}_{55}^{(k)}}{H_2^{(k)}R_2}\right)\frac{\partial}{\partial\zeta}-\frac{n^2\pi^2}{L_1^2}\frac{\bar{C}_{66}^{(k)}}{H_1^{(k)2}}-\frac{m^2\pi^2}{L_2^2}\frac{\bar{C}_{22}^{(k)}}{H_2^{(k)2}}-\frac{\bar{C}_{55}^{(k)}}{H_1^{(k)}H_2^{(k)}R_1R_2}-\frac{\bar{C}_{55}^{(k)}}{H_2^{(k)2}R_2^2}\right)U_2^{(k)}+$$

$$+\left(\frac{m\pi}{L_2}\frac{\bar{C}_{23}^{(k)}+\bar{C}_{55}^{(k)}}{H_2^{(k)}}\frac{\partial}{\partial\zeta}+\frac{m\pi}{L_2}\left(\frac{\bar{C}_{12}^{(k)}+\bar{C}_{55}^{(k)}}{H_1^{(k)}H_2^{(k)}R_1}+\frac{\bar{C}_{22}^{(k)}+\bar{C}_{55}^{(k)}}{H_2^{(k)2}R_2}\right)\right)U_3^{(k)}+f_2^{(k)}=0 \tag{11}$$

$$\left(-\frac{n\pi}{L_1}\frac{\bar{C}_{13}^{(k)}+\bar{C}_{44}^{(k)}}{H_1^{(k)}}\frac{\partial}{\partial\zeta}-\frac{n\pi}{L_1}\left(\frac{\bar{C}_{13}^{(k)}-\bar{C}_{12}^{(k)}}{H_1^{(k)}H_2^{(k)}R_2}-\frac{\bar{C}_{11}^{(k)}+\bar{C}_{44}^{(k)}}{H_1^{(k)2}R_1}\right)\right)U_1^{(k)}+\left(-\frac{m\pi}{L_2}\frac{\bar{C}_{23}^{(k)}+\bar{C}_{55}^{(k)}}{H_2^{(k)}}\frac{\partial}{\partial\zeta}-\frac{m\pi}{L_2}\left(\frac{\bar{C}_{23}^{(k)}-\bar{C}_{12}^{(k)}}{H_1^{(k)}H_2^{(k)}R_1}-\frac{\bar{C}_{22}^{(k)}+\bar{C}_{55}^{(k)}}{H_2^{(k)2}R_2}\right)\right)U_2^{(k)}+$$

$$+\left(\bar{C}_{33}^{(k)}\frac{\partial^2}{\partial\zeta^2}+\left(\frac{\bar{C}_{33}^{(k)}}{H_1^{(k)}R_1}+\frac{\bar{C}_{33}^{(k)}}{H_2^{(k)}R_2}\right)\frac{\partial}{\partial\zeta}-\frac{n^2\pi^2}{L_1^2}\frac{\bar{C}_{44}^{(k)}}{H_1^{(k)2}}-\frac{m^2\pi^2}{L_2^2}\frac{\bar{C}_{55}^{(k)}}{H_2^{(k)2}}+\frac{\bar{C}_{13}^{(k)}+\bar{C}_{23}^{(k)}-2\bar{C}_{12}^{(k)}}{H_1^{(k)}H_2^{(k)}R_1R_2}-\frac{\bar{C}_{11}^{(k)}}{H_1^{(k)2}R_1^2}-\frac{\bar{C}_{22}^{(k)}}{H_2^{(k)2}R_2^2}\right)U_3^{(k)}+f_3^{(k)}=0 \tag{12}$$

The proposed 3D theory is given in layer-wise form and for this reason the compatibility conditions for displacements and equilibrium conditions for transverse stresses are imposed at each interface:

$$U_1^{(k)}\left(s_1,s_2,\zeta_{k+1}\right)=U_1^{(k+1)}\left(s_1,s_2,\zeta_{k+1}\right)$$
$$U_2^{(k)}\left(s_1,s_2,\zeta_{k+1}\right)=U_2^{(k+1)}\left(s_1,s_2,\zeta_{k+1}\right) \tag{13}$$
$$U_3^{(k)}\left(s_1,s_2,\zeta_{k+1}\right)=U_3^{(k+1)}\left(s_1,s_2,\zeta_{k+1}\right)$$

$$\tau_{13}^{(k)}\left(s_1,s_2,\zeta_{k+1}\right)=\tau_{13}^{(k+1)}\left(s_1,s_2,\zeta_{k+1}\right)$$
$$\tau_{23}^{(k)}\left(s_1,s_2,\zeta_{k+1}\right)=\tau_{23}^{(k+1)}\left(s_1,s_2,\zeta_{k+1}\right) \tag{14}$$
$$\sigma_{33}^{(k)}\left(s_1,s_2,\zeta_{k+1}\right)=\sigma_{33}^{(k+1)}\left(s_1,s_2,\zeta_{k+1}\right)$$

The load conditions at the external surfaces in the three directions s_1,s_2,ζ are imposed as:

$$\tau_{13}^{(1,l)}\left(s_1,s_2,\pm\frac{h}{2}\right)=q_1^{(1,l)}\left(s_1,s_2\right)=q_1^{(\pm)}\cos\left(\frac{n\pi}{L_1}s_1\right)\sin\left(\frac{m\pi}{L_2}s_2\right)$$

$$\tau_{23}^{(1,l)}\left(s_1,s_2,\pm\frac{h}{2}\right)=q_2^{(1,l)}\left(s_1,s_2\right)=q_2^{(\pm)}\sin\left(\frac{n\pi}{L_1}s_1\right)\cos\left(\frac{m\pi}{L_2}s_2\right) \tag{15}$$

$$\sigma_3^{(1,l)}\left(s_1,s_2,\pm\frac{h}{2}\right)=q_3^{(1,l)}\left(s_1,s_2\right)=q_3^{(\pm)}\sin\left(\frac{n\pi}{L_1}s_1\right)\sin\left(\frac{m\pi}{L_2}s_2\right)$$

1 means the first layer and l is the last layer. h is the global thickness of the structure. $+$ means the top of the structure and $-$ means the bottom of the structure. The sistem of differential equations in the thickness direction is given in closed form as shown in Eqs. (10)-(12). This system can be solved in analytical form by means of the exponential matrix method:

$$\mathbf{U}^{(j)}\left(\tilde{z}^j\right)=\exp\left(\mathbf{A}^{j*}\tilde{z}^j\right)\mathbf{U}^{(j)}(0)\quad\text{with}\quad\tilde{z}^j\in\left[0,h^j\right] \tag{16}$$

j is the general mathematical layer and $\tilde{z}^j$ is defined in each j layer. $\mathbf{A}^{j*}$ is the exponential matrix and it is defined by means of the material and geometrical information of each j layer as clearly explained in past works

[31-38] where all the details were given. The vector $\mathbf{U}^{(j)}$ contains the three displacement components and their derivatives made with respect to the thickness coordinate. This vector can be evaluated at each thickness coordinate $\tilde{z}^j$ of the j layer starting from its value at the bottom of the considered j layer ($\mathbf{U}^{(j)}(0)$). The exponential term $\exp\left(\mathbf{A}^{j*}\tilde{z}^j\right)$ can be rewritten by means of a Taylor expansion in order to pass from a system of differential equations in z to an algebraic system (see works [31-38] for further details). In the section about results this solution is called as "3D EM" because the Exponential Matrix method is employed for an analytical solution of partial differential equations in ζ. More details about its development can be found in [31-38]. In these works the "3D EM" solution has been validated by means of several comparisons with other 3D solutions presented in the literature. In particular, comparisons have been performed with the well- known 3D solution by Pagano [4-6] for sandwich and laminated plates, with the 3D solution by Ren [10] for the bending of laminated cylindrical panels, with the elasticity solution by Varadan and Bhaskar [11] for the static analysis of composite cylinders, with the exact solutions of Fan and Zhang [12] for thick laminated spherical shells, with the 3D model by Soldatos and Ye [14] for hollow cylinders, with the 3D exact solutions by Kashtalyan [16] and Kashtalyan and Menshykova [17] for bending analysis of one-layered and multilayered functionally graded plates, with the elasticity model by Vel and Batra [18] for the vibration of functionally graded plates and with the 3D exact solution by Messina [20] for the free vibration analysis of laminated composite plates.

The other closed form 3D shell solution proposed in the results is called as "3D GDQ". The model uses the same procedure already described in Eqs. (1)-(15). In this second case, the closed form of partial differential equations in ζ has been solved in numerical way by the first author using the generalized differential quadrature model (GDQ) described in the past works [40-45], [51-53] and [56-57], [73-74] for the two-dimensional analysis of plates and shells. For a one-dimensional domain defined in the interval $[x_1, x_T]$, the GDQ method permits to approximate the n-th derivative in a generic point x_i of a sufficiently smooth function $f(x)$ by means of a weighted linear sum of the function values at some defined points

$$\left.\frac{d^n f(x)}{dx^n}\right|_{x=x_i} \cong \sum_{j=1}^{T} \varsigma_{ij}^{(n)} f(x_j) \tag{17}$$

for $i = 1, 2, ..., T$, where T indicates the total number of grid points. $\varsigma_{ij}^{(n)}$ are the weighting coefficients calculated using the recursive expressions presented by Shu (see [40], [74]). This method allows the evaluation

of the derivative of a function for each point of the domain. The nodes must be positioned within the domain according to a specific grid distribution. In the proposed work, the Chebyshev-Gauss-Lobatto grid distribution is used because of its stability and accuracy (see [40], [74]). In this case, the discrete points are defined as

$$x_i = \left(1 - \cos\left(\frac{i-1}{T-1}\pi\right)\right)\frac{\left(x_T - x_1\right)}{2} + x_1 \tag{18}$$

for $i = 1, 2, ..., T$ and $x \in \left[x_1, x_T\right]$. The numerical solution of partial differential equations (10)-(12) in ζ by means of the GDQ method allows a reduction of the computational cost without significantly modifying the precision of the results as can be seen in the section 4 where "3D EM" and "3D GDQ" theories are compared for several benchmarks. By means of these comparisons, 3D GDQ model can be considered validated for the static analysis of composite and sandwich plates and spherical shells.

3.   REFINED 2D GDQ MODELS

The equations of the present formulation describe the doubly-curved surfaces by means of the differential geometry. These surfaces constitute the reference surface as defined in the book [73]. The two-dimensional structural analysis of a general doubly-curved shell is strictly connected with the mechanical behavior of its reference surface. The reference surface coincides with the middle surface of the shell in the case of multilayered configuration as shown in Figure 1. A shell is a three-dimensional body in the space defined by the global reference system $Ox_1 x_2 x_3$. The thickness of the shell is defined as the distance between the two external curved surfaces. In the case of multilayered shells, the global thickness is defined as:

$$h = \sum_{k=1}^{l} h_k \tag{19}$$

h_k is the thickness of the generic layer k which goes from the first layer 1 to the last layer l. A local reference system $O'\alpha_1\alpha_2\zeta$ can be employed as shown in Figure 1. In this case, a shell is bounded by the following limits

$$\begin{aligned}
\alpha_1 &\in \left[\alpha_1^0, \alpha_1^1\right] \\
\alpha_2 &\in \left[\alpha_2^0, \alpha_2^1\right] \\
\zeta &\in \left[-h/2, h/2\right]
\end{aligned} \tag{20}$$

The curvilinear orthogonal coordinates α_1, α_2 coincide with the lines of principal curvature of the reference surface of the shell. This basic hypothesis has been discussed in the book [73]. h is the global thickness. α_1, α_2

10

are a generic couple of principal coordinates and this feature allows different meanings. For example, $\alpha_1 = \varphi, \alpha_2 = \vartheta$ in the case of shells of revolution, $\alpha_1 = \varphi, \alpha_2 = y$ in the case of singly-curved panels of translation, $\alpha_1 = s_1 = x, \alpha_2 = s_2 = y$ for a rectangular plate. The following vector identifies each point P of the three-dimensional body

$$\mathbf{R}(\alpha_1, \alpha_2, \zeta) = \mathbf{r}(\alpha_1, \alpha_2) + \frac{h}{2} z \mathbf{n}(\alpha_1, \alpha_2) \tag{21}$$

$z = 2\zeta/h(\alpha_1, \alpha_2) \in [-1,1]$ is a no-dimensional coordinate. It indicates the distance of the point P from its projection P' on the reference surface of the shell. $\mathbf{r}(\alpha_1, \alpha_2)$ is the position vector and it indicates each point of the reference surface. This vector changes its expression according to the investigated structural element. $\mathbf{n}(\alpha_1, \alpha_2)$ is the outward unit normal

$$\mathbf{n} = \frac{\mathbf{r}_{,1} \wedge \mathbf{r}_{,2}}{|\mathbf{r}_{,1} \wedge \mathbf{r}_{,2}|} \tag{22}$$

$\mathbf{r}_{,i} = \partial \mathbf{r}/\partial \alpha_i$, for $i = 1, 2$. The symbol " $\wedge$ " indicates the vector product. The position vector $\mathbf{r}(\alpha_1, \alpha_2)$ permits the calculation of the first fundamental forms of the reference surface [73]. The Lamè parameters $A_1(\alpha_1, \alpha_2)$ and $A_2(\alpha_1, \alpha_2)$ are calculated as

$$A_1 = \sqrt{\mathbf{r}_{,1} \cdot \mathbf{r}_{,1}} \\ A_2 = \sqrt{\mathbf{r}_{,2} \cdot \mathbf{r}_{,2}} \tag{23}$$

the symbol " $\cdot$ " is used for the scalar product. When the curvilinear orthogonal coordinates match the lines of principal curvature of the reference surface of the shell, the principal radii of curvature of the surface $R_1(\alpha_1, \alpha_2)$ and $R_2(\alpha_1, \alpha_2)$ are defined as

$$R_1 = -\frac{\mathbf{r}_{,1} \cdot \mathbf{r}_{,1}}{\mathbf{r}_{,11} \cdot \mathbf{n}} \\ R_2 = -\frac{\mathbf{r}_{,2} \cdot \mathbf{r}_{,2}}{\mathbf{r}_{,22} \cdot \mathbf{n}} \tag{24}$$

In the case of a generic doubly-curved shell, the principal radii of curvature vary in each point of the domain. The described approach is valid for both static and dynamic analyses of thick and moderately thick shells that mean

$$0.01 \leq \max\left(\frac{h}{R_{\min}}, \frac{h}{L_{\min}}\right) \leq 0.2 \qquad (25)$$

$R_{\min}$ and $L_{\min}$ are the minimum radius of curvature and the lowest size of the structure. The three displacement components of a generic shell are developed by means of the Carrera Unified Formulation (CUF) [73]. The displacement field is developed as

$$\begin{aligned}
U_1 &= F_0\, u_1^{(0)} + F_1\, u_1^{(1)} + F_2\, u_1^{(2)} + F_3\, u_1^{(3)} + \ldots + F_N u_1^{(N)} + F_{N+1} u_1^{(N+1)} \\
U_2 &= F_0\, u_2^{(0)} + F_1\, u_2^{(1)} + F_2\, u_2^{(2)} + F_3\, u_2^{(3)} + \ldots + F_N u_2^{(N)} + F_{N+1} u_2^{(N+1)} \\
U_3 &= F_0\, u_3^{(0)} + F_1\, u_3^{(1)} + F_2\, u_3^{(2)} + F_3\, u_3^{(3)} + \ldots + F_N u_3^{(N)} + F_{N+1} u_3^{(N+1)}
\end{aligned} \qquad (26)$$

$U_1(\alpha_1, \alpha_2, \zeta)$, $U_2(\alpha_1, \alpha_2, \zeta)$, $U_3(\alpha_1, \alpha_2, \zeta)$ are the 3D displacements components. $u_1^{(\tau)}(\alpha_1, \alpha_2)$, $u_2^{(\tau)}(\alpha_1, \alpha_2)$, $u_3^{(\tau)}(\alpha_1, \alpha_2)$ are the generalized displacement components τ which represent the degrees of freedom and the unknown variables of the problem written inside the algebraic vector $\mathbf{u}^{(\tau)} = \mathbf{u}^{(\tau)}(\alpha_1, \alpha_2)$. $F_\tau = F_\tau(\zeta)$ are the thickness functions used for the τ-th order of the kinematic expansion [73]. Several kinematic models can be developed according to the order of expansion τ and the type of thickness function $F_\tau(\zeta)$. Several Higher-order Shear Deformation Theories (HSDTs) are developed in a unified manner to analyze the mechanical behavior of shell structures. The Reissner-Mindlin theory or the First-order Shear Deformation Theory (FSDT) can also be obtained as particular cases. The zigzag Murakami's function $Z = Z(\zeta)$ can be added as the $(N+1)$-th degree of freedom in order to capture the zig-zag effect along the shell thickness in the case of transverse anisotropy. The Murakami's function is defined as

$$Z = (-1)^k \left(\frac{2}{\zeta_{k+1} - \zeta_k} \zeta - \frac{\zeta_{k+1} + \zeta_k}{\zeta_{k+1} - \zeta_k} \right) \qquad (27)$$

where ζ_k is the coordinate of the k-th layer through the thickness direction. Further details about the zigzag Murakami's function can be found in [73]. The Equivalent Single Layer (ESL) theories of the present paper are developed using power functions ζ^τ, with $\tau = 0, 1, 2, \ldots, N$, as thickness functions $F_\tau(\zeta)$ [73]. Using the maximum order of kinematic expansion $\tau = N$, the following theories are obtained for $N \leq 4$

$$\begin{array}{cc}
\overbrace{\text{ED1} \quad \text{EDZ1}}^{N=1} & \overbrace{\text{ED2} \quad \text{EDZ2}}^{N=2} \\[6pt]
\overbrace{\text{ED3} \quad \text{EDZ3}}^{N=3} & \overbrace{\text{ED4} \quad \text{EDZ4}}^{N=4}
\end{array} \qquad (28)$$

"E" indicates ESL, "D" indicates that the generalized displacements are the main variables of the problem, "Z" indicates the Murakami's function. The τ-th order generalized strain components evaluated on the reference surface can be included in the vector $\boldsymbol{\varepsilon}^{(\tau)} = \boldsymbol{\varepsilon}^{(\tau)}(\alpha_1, \alpha_2)$

$$\boldsymbol{\varepsilon}^{(\tau)} = \begin{bmatrix} \varepsilon_1^{(\tau)} & \varepsilon_2^{(\tau)} & \gamma_1^{(\tau)} & \gamma_2^{(\tau)} & \gamma_{13}^{(\tau)} & \gamma_{23}^{(\tau)} & \omega_{13}^{(\tau)} & \omega_{23}^{(\tau)} & \varepsilon_3^{(\tau)} \end{bmatrix}^T \tag{29}$$

The τ-th order generalized strain component vector is linked to the τ-th order generalized displacement component vector $\mathbf{u}^{(\tau)}$ by means of the following compact form

$$\boldsymbol{\varepsilon}^{(\tau)} = \mathbf{D}_\Omega \mathbf{u}^{(\tau)} \tag{30}$$

the operator matrix $\mathbf{D}_\Omega$ has both differential and geometrical contributions

$$\mathbf{D}_\Omega = \begin{bmatrix} \dfrac{1}{A_1}\dfrac{\partial}{\partial\alpha_1} & \dfrac{1}{A_1 A_2}\dfrac{\partial A_2}{\partial\alpha_1} & -\dfrac{1}{A_1 A_2}\dfrac{\partial A_1}{\partial\alpha_2} & \dfrac{1}{A_2}\dfrac{\partial}{\partial\alpha_2} & -\dfrac{1}{R_1} & 0 & 1 & 0 & 0 \\ \dfrac{1}{A_1 A_2}\dfrac{\partial A_1}{\partial\alpha_2} & \dfrac{1}{A_2}\dfrac{\partial}{\partial\alpha_2} & \dfrac{1}{A_1}\dfrac{\partial}{\partial\alpha_1} & -\dfrac{1}{A_1 A_2}\dfrac{\partial A_2}{\partial\alpha_1} & 0 & -\dfrac{1}{R_2} & 0 & 1 & 0 \\ \dfrac{1}{R_1} & \dfrac{1}{R_2} & 0 & 0 & \dfrac{1}{A_1}\dfrac{\partial}{\partial\alpha_1} & \dfrac{1}{A_2}\dfrac{\partial}{\partial\alpha_2} & 0 & 0 & 1 \end{bmatrix}^T \tag{31}$$

The stress resultant vector $\mathbf{S}^{(\tau)} = \mathbf{S}^{(\tau)}(\alpha_1, \alpha_2)$ for the τ-th order of kinematic expansion is

$$\mathbf{S}^{(\tau)} = \begin{bmatrix} N_1^{(\tau)} & N_2^{(\tau)} & N_{12}^{(\tau)} & N_{21}^{(\tau)} & T_1^{(\tau)} & T_2^{(\tau)} & P_1^{(\tau)} & P_2^{(\tau)} & S_3^{(\tau)} \end{bmatrix}^T \tag{32}$$

and it is related to τ-th order generalized displacements according to the following compact equation

$$\mathbf{S}^{(\tau)} = \sum_{\eta=0}^{N+1} \mathbf{A}^{(\tau\eta)} \mathbf{D}_\Omega \mathbf{u}^{(\eta)} \tag{33}$$

where $\tau = 0, 1, 2, ..., N, N+1$. The term $\mathbf{A}^{(\tau\eta)}$, for $\tau, \eta = 0, 1, 2, ..., N, N+1$, is the stiffness matrix. For a generic laminated composite shell including l orthotropic elastic layers we can write

$$
\mathbf{A}^{(\tau\eta)} = \begin{bmatrix}
A_{11(20)}^{(\tau\eta)} & A_{12(11)}^{(\tau\eta)} & A_{16(20)}^{(\tau\eta)} & A_{16(11)}^{(\tau\eta)} & 0 & 0 & 0 & 0 & A_{13(10)}^{(\tau\tilde{\eta})} \\
A_{12(11)}^{(\tau\eta)} & A_{22(02)}^{(\tau\eta)} & A_{26(11)}^{(\tau\eta)} & A_{26(02)}^{(\tau\eta)} & 0 & 0 & 0 & 0 & A_{23(01)}^{(\tau\tilde{\eta})} \\
A_{16(20)}^{(\tau\eta)} & A_{26(11)}^{(\tau\eta)} & A_{66(20)}^{(\tau\eta)} & A_{66(11)}^{(\tau\eta)} & 0 & 0 & 0 & 0 & A_{36(10)}^{(\tau\tilde{\eta})} \\
A_{16(11)}^{(\tau\eta)} & A_{26(02)}^{(\tau\eta)} & A_{66(11)}^{(\tau\eta)} & A_{66(02)}^{(\tau\eta)} & 0 & 0 & 0 & 0 & A_{36(01)}^{(\tau\tilde{\eta})} \\
0 & 0 & 0 & 0 & A_{44(20)}^{(\tau\eta)} & A_{45(11)}^{(\tau\eta)} & A_{44(10)}^{(\tau\tilde{\eta})} & A_{45(10)}^{(\tau\tilde{\eta})} & 0 \\
0 & 0 & 0 & 0 & A_{45(11)}^{(\tau\eta)} & A_{55(02)}^{(\tau\eta)} & A_{45(01)}^{(\tau\tilde{\eta})} & A_{55(01)}^{(\tau\tilde{\eta})} & 0 \\
0 & 0 & 0 & 0 & A_{44(10)}^{(\tilde{\tau}\eta)} & A_{45(01)}^{(\tilde{\tau}\eta)} & A_{44(00)}^{(\tilde{\tau}\tilde{\eta})} & A_{45(00)}^{(\tilde{\tau}\tilde{\eta})} & 0 \\
0 & 0 & 0 & 0 & A_{45(10)}^{(\tilde{\tau}\eta)} & A_{55(01)}^{(\tilde{\tau}\eta)} & A_{45(00)}^{(\tilde{\tau}\tilde{\eta})} & A_{55(00)}^{(\tilde{\tau}\tilde{\eta})} & 0 \\
A_{13(10)}^{(\tilde{\tau}\eta)} & A_{23(01)}^{(\tilde{\tau}\eta)} & A_{36(10)}^{(\tilde{\tau}\eta)} & A_{36(01)}^{(\tilde{\tau}\eta)} & 0 & 0 & 0 & 0 & A_{33(00)}^{(\tilde{\tau}\tilde{\eta})}
\end{bmatrix}
\tag{34}
$$

where the elastic coefficients are calculated as

$$
A_{nm(pq)}^{(\tau\eta)} = \sum_{k=1}^{l} \int_{\zeta_k}^{\zeta_{k+1}} \overline{B}_{nm}^{(k)} F_\eta\, F_\tau\, \frac{H_1 H_2}{H_1^p H_2^q}\, d\zeta
$$

$$
A_{nm(pq)}^{(\tilde{\tau}\eta)} = \sum_{k=1}^{l} \int_{\zeta_k}^{\zeta_{k+1}} \overline{B}_{nm}^{(k)} F_\eta\, \frac{\partial F_\tau}{\partial \zeta}\, \frac{H_1 H_2}{H_1^p H_2^q}\, d\zeta
$$

$$
A_{nm(pq)}^{(\tau\tilde{\eta})} = \sum_{k=1}^{l} \int_{\zeta_k}^{\zeta_{k+1}} \overline{B}_{nm}^{(k)} \frac{\partial F_\eta}{\partial \zeta}\, F_\tau\, \frac{H_1 H_2}{H_1^p H_2^q}\, d\zeta
$$

$$
A_{nm(pq)}^{(\tilde{\tau}\tilde{\eta})} = \sum_{k=1}^{l} \int_{\zeta_k}^{\zeta_{k+1}} \overline{B}_{nm}^{(k)} \frac{\partial F_\eta}{\partial \zeta}\, \frac{\partial F_\tau}{\partial \zeta}\, \frac{H_1 H_2}{H_1^p H_2^q}\, d\zeta
$$

(35)

for $\tau, \eta = 0, 1, 2, ..., N, N+1$, $n, m = 1, 2, 3, 4, 5, 6$ and $p, q = 0, 1, 2$. The terms τ, η specify the thickness functions

F_τ, F_η and $\tilde{\tau}, \tilde{\eta}$ their derivatives with respect to the ζ. The parameters $H_1 = 1 + \zeta/R_1$ and $H_2 = 1 + \zeta/R_2$ are

representative of the shell curvature. The stiffness terms $\overline{B}_{nm}^{(k)}$ are

$$
\begin{aligned}
\overline{B}_{nm}^{(k)} &= \overline{E}_{nm}^{(k)} && \text{for} \quad n, m = 1, 2, 3, 6 \\
\overline{B}_{nm}^{(k)} &= \kappa \overline{E}_{nm}^{(k)} && \text{for} \quad n, m = 4, 5
\end{aligned}
\tag{36}
$$

Terms $\overline{E}_{nm}^{(k)}$ are used to specify the elastic constants and they depend on the mechanical properties of the body.

This general notation allows the use of the reduced elastic coefficients ($\overline{E}_{nm}^{(k)} = \overline{Q}_{nm}^{(k)}$) or the classical ones (

$\overline{E}_{nm}^{(k)} = \overline{C}_{nm}^{(k)}$), as explained in [73]. The reduced stiffness values must be used when the stretching effect is

discarded or considered as constant through the thickness. The subscript RS is used for structural theories,

which do not consider this effect (e.g., the Reissner-Mindlin theory). If a HSDT includes a linear stretching

effect, the non-reduced elastic coefficients are employed. These elastic constants are defined in geometric

reference system $O'\alpha_1\alpha_2\zeta$. Similar considerations can be made for the shear correction factor κ. It is equal to

14

the constant value of $5/6$ in the case of a structural theory which considers a non-parabolic shear stress through the thickness. In the other cases, it is neglected. Its value will be specified in the notation of the employed structural model via an opportune superscript [73]. The HSDTs here proposed do not require the shear correction factor. The integrals in (35) must be numerically computed. Different numerical approaches can be used for this calculation. A possibility is the Generalized Integral Quadrature (GIQ) technique as proposed in [74].

The equilibrium equations are obtained via the Hamilton's principles and can be written as

$$\mathbf{D}_\Omega^* \mathbf{S}^{(\tau)} + \mathbf{q}^{(\tau)} = \mathbf{0} \tag{37}$$

where $\mathbf{q}^{(\tau)}$ indicates the load vector including the forces applied at the external surfaces of the shell. This expression is valid for each order $\tau = 0,1,2,...,N,N+1$ of the kinematic expansion. The equilibrium differential operator $\mathbf{D}_\Omega^*$ has the following form

$$\mathbf{D}_\Omega^* = \begin{bmatrix} \dfrac{1}{A_1}\dfrac{\partial}{\partial\alpha_1} + \dfrac{1}{A_1 A_2}\dfrac{\partial A_2}{\partial\alpha_1} & -\dfrac{1}{A_1 A_2}\dfrac{\partial A_1}{\partial\alpha_2} & -\dfrac{1}{R_1} \\[2ex] -\dfrac{1}{A_1 A_2}\dfrac{\partial A_2}{\partial\alpha_1} & \dfrac{1}{A_2}\dfrac{\partial}{\partial\alpha_2} + \dfrac{1}{A_1 A_2}\dfrac{\partial A_1}{\partial\alpha_2} & -\dfrac{1}{R_2} \\[2ex] \dfrac{1}{A_1 A_2}\dfrac{\partial A_1}{\partial\alpha_2} & \dfrac{1}{A_1}\dfrac{\partial}{\partial\alpha_1} + \dfrac{1}{A_1 A_2}\dfrac{\partial A_2}{\partial\alpha_1} & 0 \\[2ex] \dfrac{1}{A_2}\dfrac{\partial}{\partial\alpha_2} + \dfrac{1}{A_1 A_2}\dfrac{\partial A_1}{\partial\alpha_2} & \dfrac{1}{A_1 A_2}\dfrac{\partial A_2}{\partial\alpha_1} & 0 \\[2ex] \dfrac{1}{R_1} & 0 & \dfrac{1}{A_1}\dfrac{\partial}{\partial\alpha_1} + \dfrac{1}{A_1 A_2}\dfrac{\partial A_2}{\partial\alpha_1} \\[2ex] 0 & \dfrac{1}{R_2} & \dfrac{1}{A_2}\dfrac{\partial}{\partial\alpha_2} + \dfrac{1}{A_1 A_2}\dfrac{\partial A_1}{\partial\alpha_2} \\[2ex] -1 & 0 & 0 \\[1ex] 0 & -1 & 0 \\[1ex] 0 & 0 & -1 \end{bmatrix}^T \tag{38}$$

Three load components for each order $\tau = 0,1,2,...,N,N+1$ of the kinematic expansion are considered

$$\mathbf{q}^{(\tau)} = \begin{bmatrix} q_1^{(\tau)} & q_2^{(\tau)} & q_n^{(\tau)} \end{bmatrix}^T \tag{39}$$

The principle of static equivalence is employed to transform these external loads in statically equivalent forces applied on the shell reference surface. The structure is loaded only by external pressures applied along the principal curvilinear coordinate directions, on the top surface $q_1^{(+)}, q_2^{(+)}, q_n^{(+)}$ and on the bottom one $q_1^{(-)}, q_2^{(-)}, q_n^{(-)}$. The generalized external forces are given as

$$q_1^{(\tau)} = q_1^{(-)} F_\tau^{(-)} H_1^{(-)} H_2^{(-)} + q_1^{(+)} F_\tau^{(+)} H_1^{(+)} H_2^{(+)}$$

$$q_2^{(\tau)} = q_{2a}^{(-)} F_\tau^{(-)} H_1^{(-)} H_2^{(-)} + q_{2a}^{(+)} F_\tau^{(+)} H_1^{(+)} H_2^{(+)} \tag{40}$$

$$q_n^{(\tau)} = q_n^{(-)} F_\tau^{(-)} H_1^{(-)} H_2^{(-)} + q_n^{(+)} F_\tau^{(+)} H_1^{(+)} H_2^{(+)}$$

The external loads are applied on the outer surfaces, and both the thickness function $F_\tau^{(\pm)}$ and the geometric

parameters $H_1^{(\pm)}, H_2^{(\pm)}$ must be evaluated on the external surfaces of the shell. These surfaces are identified by

$\zeta = \pm h/2$. All these features can be shown as one differential system, which has the following form

$$\sum_{\eta=0}^{N+1} \mathbf{L}^{(\tau\eta)} \mathbf{u}^{(\eta)} + \mathbf{q}^{(\tau)} = \mathbf{0} \tag{41}$$

The system is valid for each order $\tau = 0,1,2,...,N,N+1$ of the kinematic expansion and it is the fundamental

nucleus of the present unified formulation. The fundamental operator $\mathbf{L}^{(\tau\eta)} = \mathbf{D}_\Omega^* \mathbf{A}^{(\tau\eta)} \mathbf{D}_\Omega$, for

$\tau, \eta = 0,1,2,...,N,N+1$, is

$$\mathbf{L}^{(\tau\eta)} = \begin{bmatrix} L_{11}^{(\tau\eta)} & L_{12}^{(\tau\eta)} & L_{13}^{(\tau\eta)} \\ L_{21}^{(\tau\eta)} & L_{22}^{(\tau\eta)} & L_{23}^{(\tau\eta)} \\ L_{31}^{(\tau\eta)} & L_{32}^{(\tau\eta)} & L_{33}^{(\tau\eta)} \end{bmatrix} \tag{42}$$

Each term $L_{fg}^{(\tau\eta)}$ is defined in [73], for $f, g = 1, 2, 3$ and $\tau, \eta = 0,1,2,...,N,N+1$ of the fundamental operator. The

fundamental system has $3 \times (N+2)$ equilibrium equations for a generic N order of kinematic expansion. The

opportune boundary conditions must be enforced to solve the static problem. In the numerical applications,

completely clamped (C), simply-supported (S) and free (F) edges are investigated. Therefore, for $\alpha_1 = \alpha_1^0$ or

$\alpha_1 = \alpha_1^1$ and $\alpha_2 \in \left[\alpha_2^0, \alpha_2^1 \right]$ we have

$$\begin{aligned} \text{C} \quad &\rightarrow \quad u_1^{(\tau)} = u_2^{(\tau)} = u_3^{(\tau)} = 0 \\ \text{S} \quad &\rightarrow \quad N_1^{(\tau)} = 0, \quad u_2^{(\tau)} = u_3^{(\tau)} = 0 \\ \text{F} \quad &\rightarrow \quad N_1^{(\tau)} = N_{12}^{(\tau)} = T_1^{(\tau)} = 0 \end{aligned} \tag{43}$$

For $\alpha_2 = \alpha_2^0$ or $\alpha_2 = \alpha_2^1$ and $\alpha_1 \in \left[\alpha_1^0, \alpha_1^1 \right]$, these conditions are

$$\begin{aligned} \text{C} \quad &\rightarrow \quad u_1^{(\tau)} = u_2^{(\tau)} = u_3^{(\tau)} = 0 \\ \text{S} \quad &\rightarrow \quad N_2^{(\tau)} = 0, \quad u_1^{(\tau)} = u_3^{(\tau)} = 0 \\ \text{F} \quad &\rightarrow \quad N_{21}^{(\tau)} = N_2^{(\tau)} = T_2^{(\tau)} = 0 \end{aligned} \tag{44}$$

Equations (43) and (44) must be enforced for each order τ of the kinematic expansion. A clamped (C) or free

edge (F) condition must be specified on each edge of a generic doubly-curved panel. Each side is identified by means of an appropriate value of the curvilinear coordinates. The West edge (W) is defined by $\alpha_2 = \alpha_2^0$ and $\alpha_1^0 \leq \alpha_1 \leq \alpha_1^1$; the South edge (S) is defined by $\alpha_1 = \alpha_1^1$ and $\alpha_2^0 \leq \alpha_2 \leq \alpha_2^1$; the coordinates $\alpha_2 = \alpha_2^1$ and $\alpha_1^0 \leq \alpha_1 \leq \alpha_1^1$ define the East edge (E); $\alpha_1 = \alpha_1^0$ and $\alpha_2^0 \leq \alpha_2 \leq \alpha_2^1$ define the North edge (N). After the definitions of the four edges, the boundary conditions are indicated by means of the sequence WSEN. For example, the notation CFCF means that the West and the East edges are clamped (C) and the other sides are free (F). Furthermore, the higher-order layer-wise theory adopted in the present work is based on the following displacement field:

$$\mathbf{U}^{(k)} = \sum_{\tau=0}^{N+1} \mathbf{F}_\tau^{(k)} \mathbf{u}^{(k\tau)} = \mathbf{F}_\tau^{(k)} \mathbf{u}^{(k\tau)} \quad \text{for} \quad k = 1, 2, ..., l \tag{45}$$

similar to what has already done in the previous work [73-75]. The only difference from the ESL theory presented above is that all the quantities are referred to each k-th layer. In order to simplify the notation, it is possible to use the following representation:

$$\text{LD -}
\begin{matrix}
(\alpha_1) & [F_0][F_1][F_2][F_3]\cdots[F_N][F_{N+1}] \\
(\alpha_2) & [F_0][F_1][F_2][F_3]\cdots[F_N][F_{N+1}] \\
(\zeta) & [F_0][F_1][F_2][F_3]\cdots[F_N][F_{N+1}]
\end{matrix} \tag{46}$$

where L indicates that a layer-wise theory is considered; D specifies that the governing equations are only expressed in terms of generalized displacements; $\alpha_1, \alpha_2, \zeta$ denote the principal directions of the variable expansion in the kinematical model, respectively; $[F_\tau]$ stands for the type of thickness function $F_\tau(\zeta)$ chosen for the τ-th order of expansion in each principal direction and in each layer. The symbology (46) can be simplified when the same thickness functions $F_\tau^{(k)}\left(\zeta^{(k)}\right) = F_\tau\left(\zeta^{(k)}\right)$ are chosen in each layer and for each displacement of the kinematical model assumed (45):

$$
\begin{aligned}
&\text{LD -}
\begin{matrix}
(\alpha_1) & [F_0][F_1][F_2][F_3][F_4] \\
(\alpha_2) & [F_0][F_1][F_2][F_3][F_4] \\
(\zeta) & [F_0][F_1][F_2][F_3][F_4]
\end{matrix} = \text{LD -}[F_0][F_1][F_2][F_3][F_4] = \text{LD4} \\
&\text{LD -}
\begin{matrix}
(\alpha_1) & [F_0][F_1][F_2][F_3] \\
(\alpha_2) & [F_0][F_1][F_2][F_3] \\
(\zeta) & [F_0][F_1][F_2][F_3]
\end{matrix} = \text{LD -}[F_0][F_1][F_2][F_3] = \text{LD3} \\
&\text{LD -}
\begin{matrix}
(\alpha_1) & [F_0][F_1][F_2] \\
(\alpha_2) & [F_0][F_1][F_2] \\
(\zeta) & [F_0][F_1][F_2]
\end{matrix} = \text{LD -}[F_0][F_1][F_2] = \text{LD2} \\
&\text{LD -}
\begin{matrix}
(\alpha_1) & [F_0][F_1] \\
(\alpha_2) & [F_0][F_1] \\
(\zeta) & [F_0][F_1]
\end{matrix} = \text{LD -}[F_0][F_1] = \text{LD1}
\end{aligned} \tag{47}
$$

3.1 Numerical Procedure

The system of governing equations is numerically solved using the Generalized Differential Quadrature (GDQ) method (17) as described in the review paper [40] and in the book [74]. This method allows the evaluation of the derivative of a function for each point of the domain (17). In the proposed work, the Chebyshev-Gauss-Lobatto grid distribution (18) is used as reported above. Now, the structural problems at issue are two-dimensional, and the grid distribution (18) must be used along the two principal curvilinear coordinates α_1, α_2. Therefore, the total number of grid points must be separately given for each principal direction. In details, $T = I_N$ indicates the number of points along α_1, whereas $T = I_M$ is for the other coordinate α_2. The equation (17) can be extended to the two-dimensional case in accordance with [40]. The Generalized Integral Quadrature (GIQ) method uses the same ideas of the GDQ technique, as demonstrated in [40, 74]. The static problem is numerically solved. The fundamental equilibrium equations and the related boundary conditions are given in discrete form using the GDQ method. Therefore, the fundamental system (41) can be written as

$$\mathbf{K}\boldsymbol{\delta} = \mathbf{f} \tag{48}$$

where $\mathbf{K}$ is the stiffness matrix, $\boldsymbol{\delta}$ is the displacement vector, and $\mathbf{f}$ is the external load vector. Equation (48) is an algebraic linear problem. The static condensation permits to reduce the problem size by separating the degrees of freedom of the inner points of the domain (d) from the points linked to the boundaries (b). Therefore, the new system is

$$\begin{aligned}
\mathbf{K}_{bb}\boldsymbol{\delta}_b + \mathbf{K}_{bd}\boldsymbol{\delta}_d &= \mathbf{f}_b \\
\mathbf{K}_{db}\boldsymbol{\delta}_b + \mathbf{K}_{dd}\boldsymbol{\delta}_d &= \mathbf{f}_d
\end{aligned} \tag{49}$$

where the vector of the degrees of freedom related to the boundary $\boldsymbol{\delta}_b$ is

$$\boldsymbol{\delta}_b = \mathbf{K}_{bb}^{-1}\left(\mathbf{f}_b - \mathbf{K}_{bd}\boldsymbol{\delta}_d\right) \tag{50}$$

The substitution of equation (50) in equation (49) gives the final algebraic system containing the unknown variable vector $\boldsymbol{\delta}_d$

$$\left(\mathbf{K}_{dd} - \mathbf{K}_{db}\mathbf{K}_{bb}^{-1}\mathbf{K}_{bd}\right)\boldsymbol{\delta}_d = \mathbf{f}_d - \mathbf{K}_{db}\mathbf{K}_{bb}^{-1}\mathbf{f}_b \tag{51}$$

In this way, the generalized displacements for each order of kinematic expansion are obtained.

3.2 Strain and Stress Recovery Procedure

The proposed shell problem is a two-dimensional model. Therefore, a posteriori recovery procedure based on the

three-dimensional elasticity [73] permits the evaluation of the effective shear and normal stresses through the thickness of the shell. The 3D equilibrium equations in principal curvilinear coordinates for a shell are

$$
\begin{aligned}
\frac{\partial \tau_{13}}{\partial \zeta} + \tau_{13}\left(\frac{2}{R_1+\zeta} + \frac{1}{R_2+\zeta}\right) = \\
= -\frac{1}{A_1\left(1+\zeta/R_1\right)}\frac{\partial \sigma_1}{\partial \alpha_1} + \frac{\sigma_2-\sigma_1}{A_1 A_2\left(1+\zeta/R_2\right)}\frac{\partial A_2}{\partial \alpha_1} + \\
-\frac{1}{A_2\left(1+\zeta/R_2\right)}\frac{\partial \tau_{12}}{\partial \alpha_2} - \frac{2\tau_{12}}{A_1 A_2\left(1+\zeta/R_1\right)}\frac{\partial A_1}{\partial \alpha_2}
\end{aligned}
\tag{52}
$$

$$
\begin{aligned}
\frac{\partial \tau_{23}}{\partial \zeta} + \tau_{23}\left(\frac{1}{R_1+\zeta} + \frac{2}{R_2+\zeta}\right) = \\
= -\frac{1}{A_2\left(1+\zeta/R_2\right)}\frac{\partial \sigma_2}{\partial \alpha_2} + \frac{\sigma_1-\sigma_2}{A_1 A_2\left(1+\zeta/R_1\right)}\frac{\partial A_1}{\partial \alpha_2} + \\
-\frac{1}{A_1\left(1+\zeta/R_1\right)}\frac{\partial \tau_{12}}{\partial \alpha_1} - \frac{2\tau_{12}}{A_1 A_2\left(1+\zeta/R_2\right)}\frac{\partial A_2}{\partial \alpha_1}
\end{aligned}
\tag{53}
$$

$$
\begin{aligned}
\frac{\partial \sigma_3}{\partial \zeta} + \sigma_3\left(\frac{1}{R_1+\zeta} + \frac{1}{R_2+\zeta}\right) = \\
= -\frac{1}{A_1\left(1+\zeta/R_1\right)}\frac{\partial \tau_{13}}{\partial \alpha_1} - \frac{\tau_{13}}{A_1 A_2\left(1+\zeta/R_2\right)}\frac{\partial A_2}{\partial \alpha_1} + \\
-\frac{1}{A_2\left(1+\zeta/R_2\right)}\frac{\partial \tau_{23}}{\partial \alpha_2} - \frac{\tau_{23}}{A_1 A_2\left(1+\zeta/R_1\right)}\frac{\partial A_1}{\partial \alpha_2} + \frac{\sigma_1}{R_1+\zeta} + \frac{\sigma_2}{R_2+\zeta}
\end{aligned}
\tag{54}
$$

The meaning of the symbols employed in Eqs. (52)-(54) is the same already seen in Section 2. These equations must also be developed in discrete form in order to be evaluated in each point of the three-dimensional shell domain [74]. The GDQ method (17) is used for this purpose and the discrete system in each point $\left(\alpha_{1i},\alpha_{2j}\right)$ of the reference surface of the shell is

$$
\begin{aligned}
\sum_{k=1}^{I_T}\varsigma_{mk}^{\zeta(1)}\tau_{13(ijk)} + \tau_{13(ijm)}\left(\frac{2}{R_{1(ij)}+\zeta_m} + \frac{1}{R_{2(ij)}+\zeta_m}\right) = \\
= -\frac{1}{A_{1(ij)}\left(1+\zeta_m/R_{1(ij)}\right)}\left.\frac{\partial \sigma_1}{\partial \alpha_1}\right|_{(ijm)} + \frac{\sigma_{2(ijm)}-\sigma_{1(ijm)}}{A_{1(ij)}A_{2(ij)}\left(1+\zeta_m/R_{2(ij)}\right)}\left.\frac{\partial A_2}{\partial \alpha_1}\right|_{(ij)} + \\
-\frac{1}{A_{2(ij)}\left(1+\zeta_m/R_{2(ij)}\right)}\left.\frac{\partial \tau_{12}}{\partial \alpha_2}\right|_{(ijm)} - \frac{2\tau_{12(ijm)}}{A_{1(ij)}A_{2(ij)}\left(1+\zeta_m/R_{1(ij)}\right)}\left.\frac{\partial A_1}{\partial \alpha_2}\right|_{(ij)}
\end{aligned}
\tag{55}
$$

19

$$\sum_{k=1}^{I_T} \varsigma_{mk}^{\zeta(1)} \tau_{23(ijk)} + \tau_{23(ijm)} \left(\frac{1}{R_{1(ij)} + \zeta_m} + \frac{2}{R_{2(ij)} + \zeta_m} \right) =$$

$$= -\frac{1}{A_{2(ij)} \left(1 + \zeta_m / R_{2(ij)}\right)} \frac{\partial \sigma_2}{\partial \alpha_2}\bigg|_{(ijm)} + \frac{\sigma_{1(ijm)} - \sigma_{2(ijm)}}{A_{1(ij)} A_{2(ij)} \left(1 + \zeta_m / R_{1(ij)}\right)} \frac{\partial A_1}{\partial \alpha_2}\bigg|_{(ij)} + \tag{56}$$

$$- \frac{1}{A_{1(ij)} \left(1 + \zeta_m / R_{1(ij)}\right)} \frac{\partial \tau_{12}}{\partial \alpha_1}\bigg|_{(ijm)} - \frac{2\tau_{12(ijm)}}{A_{1(ij)} A_{2(ij)} \left(1 + \zeta_m / R_{2(ij)}\right)} \frac{\partial A_2}{\partial \alpha_1}\bigg|_{(ij)}$$

$$\sum_{k=1}^{I_T} \varsigma_{mk}^{\zeta(1)} \sigma_{3(ijk)} + \sigma_{3(ijm)} \left(\frac{1}{R_{1(ij)} + \zeta_m} + \frac{1}{R_{2(ij)} + \zeta_m} \right) =$$

$$= \frac{\sigma_{1(ijm)}}{R_{1(ij)} + \zeta_m} + \frac{\sigma_{2(ijm)}}{R_{2(ij)} + \zeta_m} - \frac{1}{A_{1(ij)} \left(1 + \zeta_m / R_{1(ij)}\right)} \frac{\partial \tau_{13}}{\partial \alpha_1}\bigg|_{(ijm)} - \frac{\tau_{13(ijm)}}{A_{1(ij)} A_{2(ij)} \left(1 + \zeta_m / R_{2(ij)}\right)} \frac{\partial A_2}{\partial \alpha_1}\bigg|_{(ij)} + \tag{57}$$

$$- \frac{1}{A_{2(ij)} \left(1 + \zeta_m / R_{2(ij)}\right)} \frac{\partial \tau_{23}}{\partial \alpha_2}\bigg|_{(ijm)} - \frac{\tau_{23(ijm)}}{A_{1(ij)} A_{2(ij)} \left(1 + \zeta_m / R_{1(ij)}\right)} \frac{\partial A_1}{\partial \alpha_2}\bigg|_{(ij)}$$

for $m = 1, 2, ..., I_T$. The Chebyshev-Gauss-Lobatto grid distribution (18) containing I_T points is used to discretize the system along the normal direction ζ. In the proposed results, the value $I_T = 31$ is used for each numerical investigation. The equilibrium relations (55)-(56) are expressed as a function of the shear stresses τ_{13} and τ_{23} which are the unknown variables. These stresses are obtained using the opportune boundary conditions at the bottom

$$\overline{\tau}_{13(ij1)} = q_{1(ij)}^{(-)}$$
$$\overline{\tau}_{23(ij1)} = q_{2(ij)}^{(-)} \tag{58}$$

and at the top

$$\overline{\tau}_{13(ijI_T)} = q_{1(ij)}^{(+)}$$
$$\overline{\tau}_{23(ijI_T)} = q_{2(ij)}^{(+)} \tag{59}$$

The through-the-thickness profile of the shear stresses is given by

$$\tau_{13(ijm)} = \tilde{\tau}_{13(ijm)} + \frac{q_{1(ij)}^{(+)} - \tilde{\tau}_{13(ijI_T)}}{h} \left(\zeta_m + \frac{h}{2} \right) \tag{60}$$

$$\tau_{23(ijm)} = \tilde{\tau}_{23(ijm)} + \frac{q_{2(ij)}^{(+)} - \tilde{\tau}_{23(ijI_T)}}{h} \left(\zeta_m + \frac{h}{2} \right) \tag{61}$$

for $m = 2, 3, ..., I_T$, where $\tilde{\tau}_{13}$ and $\tilde{\tau}_{23}$ are the shear stresses connected with the boundary conditions on the top surface. The third equilibrium equation (57) permits the evaluation of the normal stress σ_3, imposing the

appropriate boundary conditions on the shell external surfaces

$$\bar{\sigma}_{3(ij1)} = q^{(-)}_{3(ij)}$$
$$\bar{\sigma}_{3(ijI_T)} = q^{(+)}_{3(ij)}$$

(62)

The effective through-the-thickness profile of the normal stress is

$$\sigma_{3(ijm)} = \tilde{\sigma}_{3(ijm)} + \frac{q^{(+)}_{3(ij)} - \tilde{\sigma}_{3(ijI_T)}}{h}\left(\zeta_m + \frac{h}{2}\right)$$

(63)

for $m = 2, 3, ..., I_T$, where $\tilde{\sigma}_3$ is the normal stress connected with the boundary conditions on the top surface. It needs the correct imposition of boundary conditions at the top. Remembering the constitutive relations for an orthotropic body (2), the shear strains γ_{13}, γ_{23} and the normal strain ε_3 can be calculated using the computed shear stresses τ_{13}, τ_{23} and normal stress σ_3. Thus, the through-the-thickness profiles of the strains are

$$\gamma_{13(ijm)} = \frac{\overline{C}^{(m)}_{55}\tau_{13(ijm)} - \overline{C}^{(m)}_{45}\tau_{23(ijm)}}{\overline{C}^{(m)}_{55}\overline{C}^{(m)}_{44} - \left(\overline{C}^{(m)}_{45}\right)^2}$$

(64)

$$\gamma_{23(ijm)} = \frac{\overline{C}^{(m)}_{44}\tau_{23(ijm)} - \overline{C}^{(m)}_{45}\tau_{13(ijm)}}{\overline{C}^{(m)}_{55}\overline{C}^{(m)}_{44} - \left(\overline{C}^{(m)}_{45}\right)^2}$$

(65)

$$\varepsilon_{3(ijm)} = \frac{\sigma_{3(ijm)} - \overline{C}^{(m)}_{13}\varepsilon_{1(ijm)} - \overline{C}^{(m)}_{23}\varepsilon_{2(ijm)} - \overline{C}^{(m)}_{36}\gamma_{12(ijm)}}{\overline{C}^{(m)}_{33}}$$

(66)

A trivial error could occur in the strain profiles because equations (64)-(66) do not guarantee the strain compatibility between the different layers. A more accurate through-the-thickness profile can be calculated for the membrane stresses employing the effective value of the computed normal strain component ε_3 using the constitutive law (2).

4. RESULTS

The proposed benchmarks consider simply supported square plates, spherical shell panels and elliptic pseudospheres. In the first two proposed geometries, the transverse normal load is applied at the top surface in harmonic form with amplitude $q^{(+)}_3 = 10000\,\mathrm{Pa}$, half-wave numbers $n = m = 1$ and simply supported sides. The third geometry has a uniform transverse normal load applied at the top as $q^{(+)}_3 = -10000\,\mathrm{Pa}$, and the sequence clamped-free-clamped-free (CFCF) for the boundary conditions. The three geometries are proposed in images

21

(a), (b) and (c) of Figure 2. The square plate has dimensions $a = b = 1\text{m}$ and the investigated thickness ratios are $a/h = 10$ (moderately thick plate) and $a/h = 100$ (moderately thin plate). The spherical shell panel has radii of curvature $R_1 = R_2 = 10\text{m}$ and dimensions $a = b = R_1 \pi/4 = R_2 \pi/4$. The investigated thickness ratios are $R_1/h = 20$ (moderately thick shell) and $R_1/h = 100$ (moderately thin shell). The elliptic pseudosphere has a total thickness $h = 0.2m$ and dimension $a = 2m$. In each proposed geometry, h indicates the global thickness of the structure. The first benchmark proposes a square multi-layered composite $(0/90/0/90)$ plate where the thickness of each layer is $h_1 = h_2 = h_3 = h_4 = h/4$. The second benchmark considers a sandwich square plate with external skins made of Titanium Alloy and an internal Foam core. The two skins have thickness $h_1 = h_3 = 0.15h$ and the core has thickness value $h_2 = 0.7h$. The third benchmark proposes a spherical shell panel with the same lamination scheme already discussed for the benchmark one about the multi-layered composite plate. The fourth benchmark considers a spherical shell panel with the same lamination scheme already employed for the sandwich plate of the benchmark two. The fifth benchmark is a composite laminated $(20/35/45/70)$ elliptic pseudosphere where the thickness for each layer is $h_1 = h_4 = 0.03\text{m}$ and $h_2 = h_3 = 0.07\text{m}$. Material for the layers 1 and 3 of the fifth benchmark is the Graphite-Epoxy (Young modulus $E_1 = 137.9\,\text{GPa}$ and $E_2 = E_3 = 8.96\,\text{GPa}$, shear modulus $G_{12} = G_{13} = 7.1\,\text{GPa}$ and $G_{23} = 6.21\,\text{GPa}$, Poisson ratio $\nu_{12} = \nu_{13} = 0.3$ and $\nu_{23} = 0.49$). Material for the layers 2 and 4 of the fifth benchmark is the Boron-Epoxy (Young modulus $E_1 = 206.9\,\text{GPa}$ and $E_2 = E_3 = 20.69\,\text{GPa}$, shear modulus $G_{12} = G_{13} = 6.9\,\text{GPa}$ and $G_{23} = 4.14\,\text{GPa}$, Poisson ratio $\nu_{23} = \nu_{13} = 0.25$ and $\nu_{12} = 0.3$). For the first four benchmarks, the employed composite material is a carbon fibre reinforced material with Young modulus $E_1 = 172\,\text{GPa}$ and $E_2 = E_3 = 6.9\,\text{GPa}$, shear modulus $G_{12} = G_{13} = 3.4\,\text{GPa}$ and $G_{23} = 1.4\,\text{GPa}$ and Poisson ratio $\nu_{12} = \nu_{13} = \nu_{23} = 0.25$. The Foam used as core in the sandwich configurations is an isotropic material with Young modulus $E = 232\,\text{GPa}$ and Poisson ratio $\nu = 0.2$. The Titanium Alloy used for the skins in the sandwich configurations is isotropic and has Young modulus $E = 114\,\text{GPa}$ and Poisson ratio $\nu = 0.3$. Furthermore, we indicate $\tau_{13} = \tau_{1n}$, $\tau_{23} = \tau_{2n}$ and $\sigma_3 = \sigma_n$ in order to simplify the figure reading. These particular geometries, lamination schemes, materials and load conditions have been chosen for the five proposed benchmarks in order to clearly show the zigzag form of displacements and the correct imposition of congruence conditions for displacements and equilibrium conditions for transverse stresses in the proposed refined 2D models and 3D shell theories.

Moreover, these benchmarks allow to see the differences between the classical 2D models and the refined 2D or 3D models, and the importance of the "a posteriori" stress recovery. Shell geometries give a full coupling between all the displacement components, and the sandwich and composite configurations show important in-plane and transverse anisotropy. All these features generate complicated through-the-thickness displacement and stress forms which can be evaluated only by means of refined 2D models or 3D shell theories.

Figures 3, 4 and 5 show the six strain components, the six stress components and the three displacement components evaluated through the thickness direction for a position in the plane (0.25, 0.25) of the square composite $(0/90/0/90)$ plate in the case of thickness ratio $a/h = 10$. The comparison has been proposed for the 3D EM shell model, the 3D GDQ shell model and several classical and refined 2D GDQ shell models. The employed 2D GDQ shell models are the Kirchhoff-Love theory (KL), the First order Shear Deformation Theory (FSDT), the Third order Shear Deformation Theory (TSDT), the Equivalent single layer model in displacement formulation with a fourth order of expansion through the thickness for each displacement component (ED4), the ED4 model where the typical Zigzag effect for displacements has been obtained by means of the addition of the Murakami zigzag function (EDZ4) and the Layer wise model with fourth order of expansion for the three displacement components at each layer k (LD4). In Figures 3-5, the two 3D shell models (EM and GDQ form) are always coincident for all the strains, stresses and displacements. In the strain plots of Figure 3, it is clear the typical zigzag effect of multi-layered structures and the discontinuity of transverse shear and transverse normal strains at each interface. The stresses of Figure 4 have the typical form of multi-layered composite structures. In-plane stresses can be discontinuous because no interlaminar continuity has been imposed for these quantities. Transverse shear and transverse normal stresses are continuous at each layer interface because equilibrium conditions have been correctly imposed at each interface for both 3D shell models. Moreover, transverse shear and transverse normal stresses exactly fulfil the boundary loading conditions which are τ_{1n} and τ_{2n} equal zero at the external surfaces because no external transverse shear loads have been applied, and transverse normal stress σ_n equals the applied external transverse normal load at the top ($5000\,\text{Pa}$ in the position (0.25, 0.25)). The displacements in Figure 5 are continuous at each interface because the 3D layer-wise shell models have correctly imposed the compatibility conditions. Displacements are not constant through the thickness direction because the plate is thick and multi-layered composite. In Figures 3-5, it is clear how the best possible 2D theory is always the LD4 for all the displacement, strain and stress components. However, the stress recovery by means of equilibrium equations gives satisfactory analyses for all the stress components also using refined equivalent

single layer models (ED4 and EDZ4) and classical theories such as KL, FSDT and TSDT. This feature is possible because the multi-layered cross-ply composite plate does not have a great value for the transverse anisotropy. Figures 6-8 show the same quantities and analyses already seen for the thick plate in the case of multi-layered composite $(0/90/0/90)$ plate with thickness ratio $a/h = 100$. The small values for the transverse anisotropy and the thickness of the structure allow obtaining results where all the 3D and 2D shell theories are always very close.

Figures 9, 10 and 11 propose strains, stresses and displacements for the same plate geometry seen in the first case but considering a sandwich configuration. The considered plate is thick ($a/h = 10$) and the transverse anisotropy is high because of the great difference between the Young modulus of the external skins made of Titanium alloy and the Young modulus of the internal soft Foam core. Figure 9 shows the typical zigzag form of strain components in the case of sandwich structures. The discontinuity of transverse shear and transverse normal strains at each interface is clearly shown. The two proposed 3D shell theories are always coincident. Satisfactory results are also given by the LD4 and EDZ4 models. ED4 model shows some difficulties to recover the typical zigzag form of sandwich plates. This problem is more evident for classical equivalent single layer models such as KL, TSDT and FSDT. In Figure 10 is clear how the stress recovery works very well for the LD4 and EDZ4 models but it shows several difficulties for equivalent single layer models (both classical and refined theories). Figure 11 about displacement components confirms the great capability of LD4 and EDZ4 models to obtain the typical zigzag effect of displacements for sandwich structures and the evident difficulties of classical and refined equivalent single layer models (KL, FSDT, TSDT and ED4). The thin sandwich plate ($a/h = 100$) is investigated in Figures 12-14. The reduced value of the thickness allows satisfactory analyses also for equivalent single layer classical and refined theories.

Figures 15, 16 and 17 propose the strain, stress and displacement evaluations for a multi-layered spherical panel (thickness ratio $R_1/h = 20$) with the same lamination scheme already proposed for the composite plate investigated in Figures 3-8. The presence of the two radii of curvature $R_1 = R_2$ generates a full coupling between the three displacement components which gives a complicated evaluation of strains, stresses and displacements through the thickness. For this reason, even if the transverse anisotropy is not elevated, the difference between the layer wise approaches (3D EM, 3D GDQ and LD4 GDQ theories) and the equivalent single layer approaches (ED4, TSDT, FSDT and KL) is important for each proposed quantity. The presence of the Murakami zigzag

function in EDZ4 gives an improvement with respect to the other classical and refined equivalent single layer models. The presence of the curvature in the spherical shell gives also problems in classical 2D GDQ models even if a thin structure ($R_1/h = 100$) is investigated. This last feature is clearly remarked in results proposed in Figures 18-20.

The sandwich spherical shell is investigated in Figures 21-23 for thickness ratio $R_1/h = 20$ and in Figures 24-26 for thickness ratio $R_1/h = 100$. In these cases, the transverse anisotropy is more evident with respect to the multi-layered composite shell because of the soft Foam core. This high transverse anisotropy combined with the presence of the two radii of curvature (full coupling between the three displacement components) give complicated behaviours of strains, stresses and displacements through the thickness direction. For both thick and thin shells, the 3D EM and the 3D GDQ shell models are always coincident because of their layer wise approach and closed form solution based on the harmonic forms for displacements. The most accurate 2D GDQ shell models are the LD4 theory based on the layer wise approach and the EDZ4 theory (which introduces the Murakami zigzag function in the equivalent single layer kinematic approach). Classical and refined equivalent single layer theory always gives important errors because they are not capable of considering the typical zigzag effect of sandwich structures.

In the four proposed benchmarks the best 2D GDQ solutions are LD4 and EDZ4 theories because they are capable of obtaining the zigzag effect for displacements and stresses. LD4 shows some small differences in the spherical shell cases because of some small problems in the connection between the layer-wise assembling procedure and the differential geometry. These small problems are missing in the equivalent single layer approach and for this reason the best results appear those where the Murakami zigzag function has been added.

Figures 27-29 show the displacements, strains and stresses for the composite laminated elliptic pseudosphere. Only 2D GDQ results are proposed because the structure is not simply supported. Moreover, uniform loads different from the harmonic ones and lamination sequences different from 0° and 90° are employed. For these conditions the 3D closed-form solutions are not possible. Results clearly show the importance of layer-wise approach and the Murakami zigzag function. 2D GDQ classical theories are inadequate. This new benchmark is fundamental for those scientists interested in the validation of their new 2D numerical shell models.

5. CONCLUSIONS

The paper proposed the static analysis of multilayered composite and sandwich square plates, spherical and

double-curved shells. Plate and spherical shell structures are considered as simply supported with a transverse normal load applied at the top in harmonic form. Double-curved shell structure has different boundary and load conditions. The proposed results show a comparison, in terms of strain, stress and displacement components through the thickness, between several 3D and 2D shell theories. 3D shell models are based on the differential equilibrium relations given in closed form where the differential equations in the normal direction can be solved by means of the Exponential Matrix method (3D EM) or the Generalized Differential Quadrature method (3D GDQ). 2D results are in numerical form by means of the GDQ solution. Classical and refined equivalent single layer (also including the Murakami zigzag function) and advanced layer wise theories are proposed. In the stress evaluation by means of 2D GDQ models, the transverse stress components are a posteriori recovered by using the differential equilibrium equations. This last method gives an important improvement in the results with respect to theories where the transverse stresses are obtained from the constitutive law. This improvement is evident for each investigated geometry, lamination, material and thickness ratio. 3D EM and 3D GDQ results are always coincident demonstrating how the closed-form does not introduce any numerical approximation. However, closed-from solutions are not general and they are valid only for simple cases where the sides are simply supported and the loads are in harmonic form. For this reason, the developing of opportune 2D numerical theories such as the proposed 2D GDQ shell models is mandatory. Advanced layer wise (LD4) and zigzag refined equivalent single theories (EDZ4) theories appear as the most promising because they are very close to the 3D shell solutions for all the proposed benchmarks. Moreover, LD4 and EDZ4 theories give a satisfactory description of the main features of multilayered sandwich and composite structures (zigzag effects of displacements and interlaminar continuity in terms of compatibility conditions for displacements and equilibrium conditions for transverse stresses).

REFERENCES

[1]   J.N. Reddy, Mechanics of Laminated Composite Plates and Shells. Theory and Analysis. Second Edition, CRC Press, New York, 2004.
[2]   S.W. Tsai, Composites Design, Think Composites, Dayton OH, 1987.
[3]   J.R. Vinson, The Behavior of Sandwich Structures of Isotropic and Composite Materials, Technomic Publishing Company, Inc., Lancaster, Pennsylvania USA, 1999.
[4]   N.J. Pagano, Exact solutions for composite laminates in cylindrical bending, Journal of Composite Materials, 3, 398-411, 1969.
[5]   N.J. Pagano, Exact solutions for rectangular bidirectional composites and sandwich plates, Journal of Composite Materials, 4, 20-34, 1970.
[6]   N.J. Pagano and A.S.D. Wang, Further study of composite laminates under cylindrical bending, Journal of Composite Materials, 5, 521-528, 1971.
[7]   Y. Xu and D. Zhou, Three-dimensional elasticity solution of functionally graded rectangular plates with

variable thickness, Composite Structures, 91, 56-65, 2009.

[8] H.-R. Meyer-Piening, Application of the elasticity solution to linear sandwich beam, plate and shell analyses, Journal of Sandwich Structures and Materials, 6, 295-312, 2004.

[9] L. Demasi, Three-dimensional closed form solutions and exact thin plate theories for isotropic plates, Composite Structures, 80, 183-195, 2007.

[10] J.G. Ren, Exact solutions for laminated cylindrical shells in cylindrical bending, Composite Science and Technology, 29, 169-187, 1987.

[11] T.K. Varadan and K. Bhaskar, Bending of laminated orthotropic cylindrical shells - an elasticity approach, Composite Structures, 17, 141-156, 1991.

[12] J.-R. Fan and J.-Y. Zhang, Exact solutions for thick laminated shells, Science in China, 35, 1343-1355, 1992.

[13] J.-R. Fan and J.-Y. Zhang, Analytical solutions for thick, doubly curved, laminated shells, Journal of Engineering Mechanics, 118, 1338-1356, 1992.

[14] K.P. Soldatos and J. Ye, Axisymmetric static and dynamic analysis of laminated hollow cylinders composed of monoclinic elastic layers, Journal of Sound and Vibration, 184, 245-259, 1995.

[15] J.-R. Fan and J. Ye, An exact solution for the statics and dynamics of laminated thick plates with orthotropic layers, International Journal of Solids and Structures, 26, 655-662, 1990.

[16] M. Kashtalyan, Three-dimensional elasticity solution for bending of functionally graded rectangular plates, European Journal of Mechanics - A/Solids, 23, 853-864, 2004.

[17] M. Kashtalyan and M. Menshykova, Three-dimensional elasticity solution for sandwich panels with a functionally graded core, Composite Structures, 87, 36-43, 2009.

[18] S.S. Vel and R.C. Batra, Three-dimensional exact solution for the vibration of functionally graded rectangular plates, Journal of Sound and Vibration, 172, 703-730, 2004.

[19] S. Srinivas, A.K. Rao and C.V.J. Rao, Flexure of simply supported thick homogeneous and laminated rectangular plates, Zeitschrift fur Angewandte Mathematik und Mechanik, 49, 449-458, 1969.

[20] A. Messina, Three dimensional free vibration analysis of cross-ply laminated plates through 2D and exact models, 3rd International Conference on Integrity, Reliability and Failure, Porto (Portugal), 20-24 July 2009.

[21] Q. Li, V.P. Iu and K.P. Kou, Three-dimensional vibration analysis of functionally graded material sandwich plates, Journal of Sound and Vibration, 311, 498-515, 2008.

[22] A.E. Armenakas, D.C. Gazis and G. Herrmann, Free Vibrations of Circular Cylindrical Shells, Pergamon Press, Oxford, 1969.

[23] N.N. Huang, Exact analysis for three-dimensional free vibrations of cross-ply cylindrical and doubly-curved laminates, Acta Mechanica, 108, 23-34, 1995.

[24] P. Zahedinejad, P. Malekzadeh, M. Farid and G. Karami, A semi-analytical three-dimensional free vibration analysis of functionally graded curved panels, International Journal of Pressure Vessels and Piping, 87, 470-480, 2010.

[25] P. Malekzadeh, A.R. Fiouz and H. Razi, Three-dimensional dynamic analysis of laminated composite plates subjected to moving load, Composite Structures, 90, 105-114, 2009.

[26] P. Malekzadeh, A. Afsari, P. Zahedinejad and R. Bahadori, Three-dimensional layerwise-finite element free vibration analysis of thick laminated annular plates on elastic foundation, Applied Mathematical Modelling, 34, 776-790, 2010.

[27] P. Malekzadeh, H. Monfared Maharloei and A.R. Vosoughi, A three-dimensional layerwise differential quadrature free vibration of thick skew laminated composite plates, Mechanics of Advanced Materials and Structures, 21, 792-801, 2014.

[28] P. Malekzadeh and M. Ghaedsharaf, Three-dimensional free vibration of laminated cylindrical panels with functionally graded layers, Composite Structures, 108, 894-904, 2014.

[29] P. Malekzadeh and M. Ghaedsharaf, Three-dimensional thermoelastic analysis of finite length laminated cylindrical panels with functionally graded layers, Meccanica, 49, 887-906, 2014.

[30] P. Malekzadeh and Y. Heydarpour, Mixed Navier-layerwise differential quadrature three-dimensional static and free vibration analysis of functionally graded carbon nanotube reinforced composite laminated plates, Meccanica, 50, 143-167, 2015.

[31] S. Brischetto, Three-dimensional exact free vibration analysis of spherical, cylindrical, and flat one-layered panels, Shock and Vibration, vol.2014, 1-29, 2014.

[32] S. Brischetto, An exact 3D solution for free vibrations of multilayered cross-ply composite and sandwich plates and shells, International Journal of Applied Mechanics, 6, 1-42, 2014.

[33] S. Brischetto, Exact elasticity solution for natural frequencies of functionally graded simply-supported structures, Computer Modeling in Engineering & Sciences, 95, 391-430, 2013.

[34] S. Brischetto, A continuum elastic three-dimensional model for natural frequencies of single-walled carbon nanotubes, Composites. Part B, Engineering, 61, 222-228, 2014.

[35] S. Brischetto, A general exact elastic shell solution for bending analysis of functionally graded structures, Composite Structures, 175, 70-85, 2017.

[36] S. Brischetto, Exact three-dimensional static analysis of single- and multi-layered plates and shells, Composites. Part B, Engineering, 119, 230-252, 2017.

[37] S. Brischetto, A closed-form 3D shell solution for multilayered structures subjected to different load combinations, Aerospace Science and Technology, 70, 29-46, 2017.

[38] S. Brischetto, A 3D layer-wise model for the correct imposition of transverse shear/normal load conditions in FGM shells, International Journal of Mechanical Sciences, 136, 50-66, 2018.

[39] C. Shu, Differential quadrature and its application in engineering, Springer, London, 2000.

[40] F. Tornabene, F. Fantuzzi, F. Ubertini and E. Viola, Strong formulation finite element method based on differential quadrature: a survey. Applied Mechanics Review, 67, 020801 (55 pages), 2015.

[41] F. Tornabene and F. Fantuzzi, Strong formulation isogeometric analysis (SFIGA) for laminated composite arbitrarily shaped plates, Composites. Part B, Engineering, 96, 173-203, 2016.

[42] F. Tornabene, F. Fantuzzi, M. Bacciocchi, A.M.A. Neves and A.J.M. Ferreira, MLSDQ based on RBFs for the free vibrations of laminated composite doubly-curved shells, Composites. Part B, Engineering, 99, 30-47, 2016.

[43] N. Fantuzzi, R. Dimitri and F. Tornabene, A SFEM-based evaluation of Mode-I stress intensity factor in composite structures, Composite Structures, 145, 162-185, 2016.

[44] F. Tornabene, R. Dimitri and E. Viola, Transient dynamic response of generally shaped arches based on a GDQ-Time-stepping method, International Journal of Mechanical Sciences, 114, 277-314, 2016.

[45] R. Dimitri, N. Fantuzzi, F. Tornabene and G. Zavarise, Innovative numerical methods based on SFEM and IGA for computing stress concentrations in isotropic plates with discontinuities, International Journal of Mechanical Sciences, 118, 166-187, 2016.

[46] H. Kurtaran, Geometrically nonlinear transient analysis of moderately thick laminated composite shallow shells with generalized differential quadrature method, Composite Structures, 125, 605-614, 2015.

[47] M.A. De Rosa and M. Lippiello, Nonlocal frequency analysis of embedded single-walled carbon nanotube using the Differential Quadrature Method, Composites. Part B, Engineering, 84, 41-51, 2016.

[48] F. Mehralian and Y.T. Beni, Size-dependent torsional buckling analysis of functionally graded cylindrical shell, Composites. Part B, Engineering, 94, 11-25, 2016.

[49] R. Ansari, J. Torabi and M.F. Shojaei, Buckling and vibration analysis of embedded functionally graded carbon nanotube-reinforced composite annular sector plates under thermal loading, Composites. Part B, Engineering, 109, 197-213, 2017.

[50] M. Mohammadimeh and S. Shahedi, High-order buckling and free vibration analysis of two types sandwich beam including AL or PVC-foam flexible core and CNTs reinforced nanocomposite face sheets using GDQM, Composites. Part B, Engineering, 108, 91-107, 2017.

[51] E. Viola, F. Tornabene and N. Fantuzzi, General higher-order shear deformation theories for the free vibration analysis of completely doubly-curved laminated shells and panels, Composite Structures, 95, 639-666, 2013.

[52] E. Viola, F. Tornabene and N. Fantuzzi, Static analysis of completely doubly-curved laminated shells and panels using general higher-order shear deformation theories, Composite Structures, 101, 59-93, 2013.

[53] F. Tornabene, E. Viola, N. Fantuzzi, General higher-order equivalent single layer theory for free vibrations of doubly-curved laminated composite shells and panels, Composite Structures, 104, 94-117, 2013.

[54] E. Carrera, Theories and finite elements for multilayered, anisotropic, composite plates and shells, Archives of Computational Methods in Engineering, 9, 87-140, 2002.

[55] E. Carrera, On the use of the Murakami's zig-zag function in the modeling of layered plates and shells, Computers and Structures, 82, 541-554, 2002.

[56] F. Tornabene, N. Fantuzzi, E. Viola, E. Carrera, Static analysis of doubly-curved anisotropic shells and panels using CUF approach, Differential Geometry and Differential Quadrature Method, Composite Structures, 107, 675-697, 2014.

[57] F. Tornabene, A. Liverani, G. Caligiana, Laminated composite rectangular and annular plates: A GDQ solution for static analysis with a posteriori shear and normal stress recovery, Composites. Part B, engineering, 43, 1847-1872, 2012.

[58] F. Tornabene, E. Viola, Static analysis of functionally graded doubly-curved shells and panels of revolution, Meccanica 48, 901-930, 2013.

[59] E. Viola, F. Tornabene, N. Fantuzzi, Static analysis of completely doubly-curved laminated shells and

panels using general higher-order shear deformation theories, Composite Structures 101, 59-93, 2013.

[60] F. Tornabene, N. Fantuzzi, E. Viola, E. Carrera, Static analysis of doubly-curved anisotropic shells and panels using CUF approach, differential geometry and differential quadrature method, Composite Structures 107, 675-697, 2014.

[61] M. Gurses, O. Civalek, A.K. Korkmaz, H. Ersoy, Free vibration analysis of symmetric laminated skew plates by discrete singular convolution technique based on first-order shear deformation theory, International Journal for Numerical Methods in Engineering, 79, 290-313, 2009.

[62] O. Civalek, Analysis of thick rectangular plates with symmetric cross-ply laminates based on First-order Shear Deformation Theory, Journal of Composite Materials, 42, 2853-2867, 2008.

[63] O. Civalek, A. Korkmaz, C. Demir, Discrete singular convolution approach for buckling analysis of rectangular Kirchhoff plates subjected to compressive loads on two-opposite edges, Advances in Engineering Software, 41, 557-560, 2010.

[64] S.N. Atluri, T.Zhu, A new Meshless Local Petrov-Galerkin (MLPG) approach in computational mechanics, Computational Mechanics, 22, 117-127, 1998.

[65] R. Ansari, R. Gholami, A. Norouzzadeh, Size-dependent thermo-mechanical vibration and instability of conveying fluid functionally graded nanoshells based on Mindlin's strain gradient theory, Thin-Walled Structures, 105, 172-184, 2016.

[66] R. Ansari, R. Gholami, A. Norouzzadeh, S. Sahmani, Size-dependent vibration and instability of fluid-conveying functionally graded microshells based on the modified couple stress theory, Microfluid Nanofluid, 19, 509-522, 2015.

[67] M. Bischoff, E. Ramm, On the physical significance of higher order kinematic and static variables in a three-dimensional shell formulation, International Journal of Solids and Structures, 37, 6933-6960, 2000.

[68] R.A. Arciniega, J.N. Reddy, Tensor-based finite element formulation for geometrically nonlinear analysis of shell structures, Computer Methods in Applied Mechanics and Engineering, 196, 1048-1073, 2007.

[69] R. Echter, B. Oesterle, M. Bischoff, A hierarchic family of isogeometric shell finite elements, Computer Methods in Applied Mechanics and Engineering, 254, 170-180, 2013.

[70] R. Ansari, A. Norouzzadeh, Non local and surface effects on the buckling behaviour of functionally graded nanoplates: An isogeometric analysis, Physica E, 84, 84-97, 2016.

[71] F. Tornabene, N. Fantuzzi, M. Bacciocchi, A new doubly-curved shell element for the free vibrations of arbitrarily shaped laminated structures based on weak formulation isogeometric analysis, Composite Structures 171, 429-461, 2017.

[72] M. F. Shojaei, R. Ansari, Variational differential quadrature: A technique to simplify numerical analysis of structures, Applied Mathematical Modelling, 49, 705-738, 2017.

[73] F. Tornabene, N. Fantuzzi, M. Bacciocchi, E. Viola, Laminated Composite Doubly-Curved Shell Structures. Differential Geometry. Higher-order Structural Theories, Esculapio, Bologna, Italy, 2016.

[74] F. Tornabene, N. Fantuzzi, M. Bacciocchi, E. Viola, Laminated Composite Doubly-Curved Shell Structures. Differential and Integral Quadrature. Strong Formulation Finite Element Method, Esculapio, Bologna, Italy, 2016.

[75] F. Tornabene, General higher-order layer-wise theory for free vibrations of doubly-curved laminated composite shells and panels, Mechanics of Advanced Materials and Structures, 23, 1046-1067, 2016.

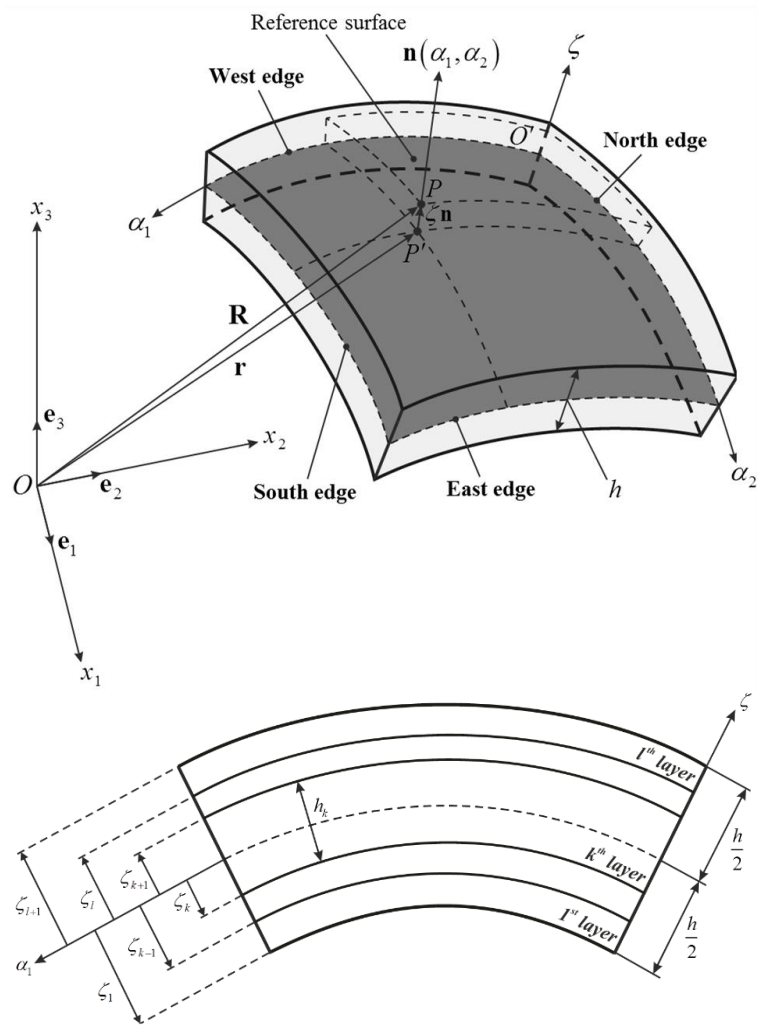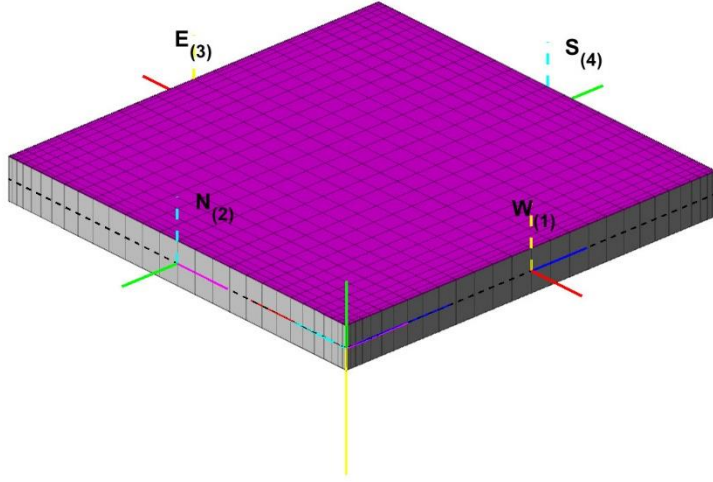29

Figure 1. Local reference system and lamination scheme of a general doubly-curved shell element.

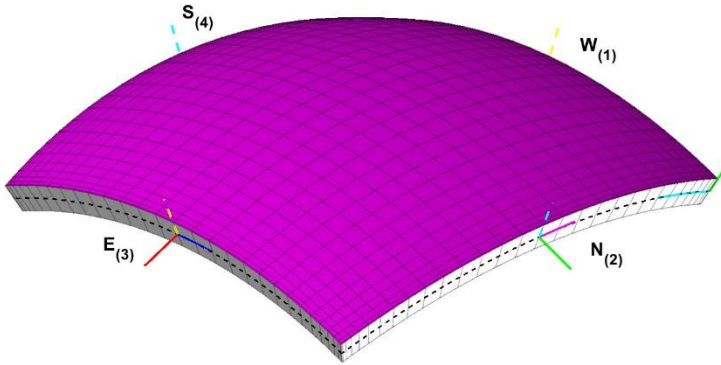$$\mathbf{r}(s_1, s_2) = s_1\mathbf{e}_1 + s_2\mathbf{e}_2$$
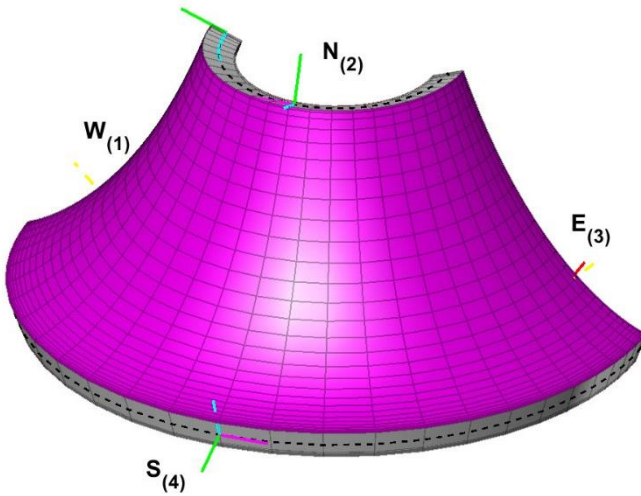$$s_1 \in [0, a]$$
$$s_2 \in [0, b]$$

$$\mathbf{r}(\alpha_1, \alpha_2) = R\sin\alpha_1\cos\alpha_2\,\mathbf{e}_1 - R\sin\alpha_1\sin\alpha_2\,\mathbf{e}_2 +$$
$$+ R(1-\cos\alpha_1)\mathbf{e}_3$$
$$\alpha_1 \in \left[\alpha_1^0, \alpha_1^1\right], \quad \alpha_2 \in \left[\alpha_2^0, \alpha_2^1\right]$$
$$R = R_1 = R_2$$

$$\mathbf{r}(\alpha_1, \alpha_2) = a\sin\alpha_1\cos\alpha_2\,\mathbf{e}_1 - a\sin\alpha_1\sin\alpha_2\,\mathbf{e}_2 +$$
$$+ a\left(\cos\alpha_1 + \log\left(\tan\left(\frac{\alpha_1}{2}\right)\right)\right)\mathbf{e}_3$$
$$\alpha_1 \in \left[\alpha_1^0, \alpha_1^1\right], \quad \alpha_2 \in \left[\alpha_2^0, \alpha_2^1\right]$$
$$\alpha_1^0 = \pi/9 \quad \alpha_1^1 = \pi/3 \quad \alpha_2^0 = 0 \quad \alpha_2^1 = 5\pi/6$$
$$a = 2\text{m}$$

Figure 2. Geometry representation, GDQ discrete point distribution and local coordinate reference system for proposed benchmarks.
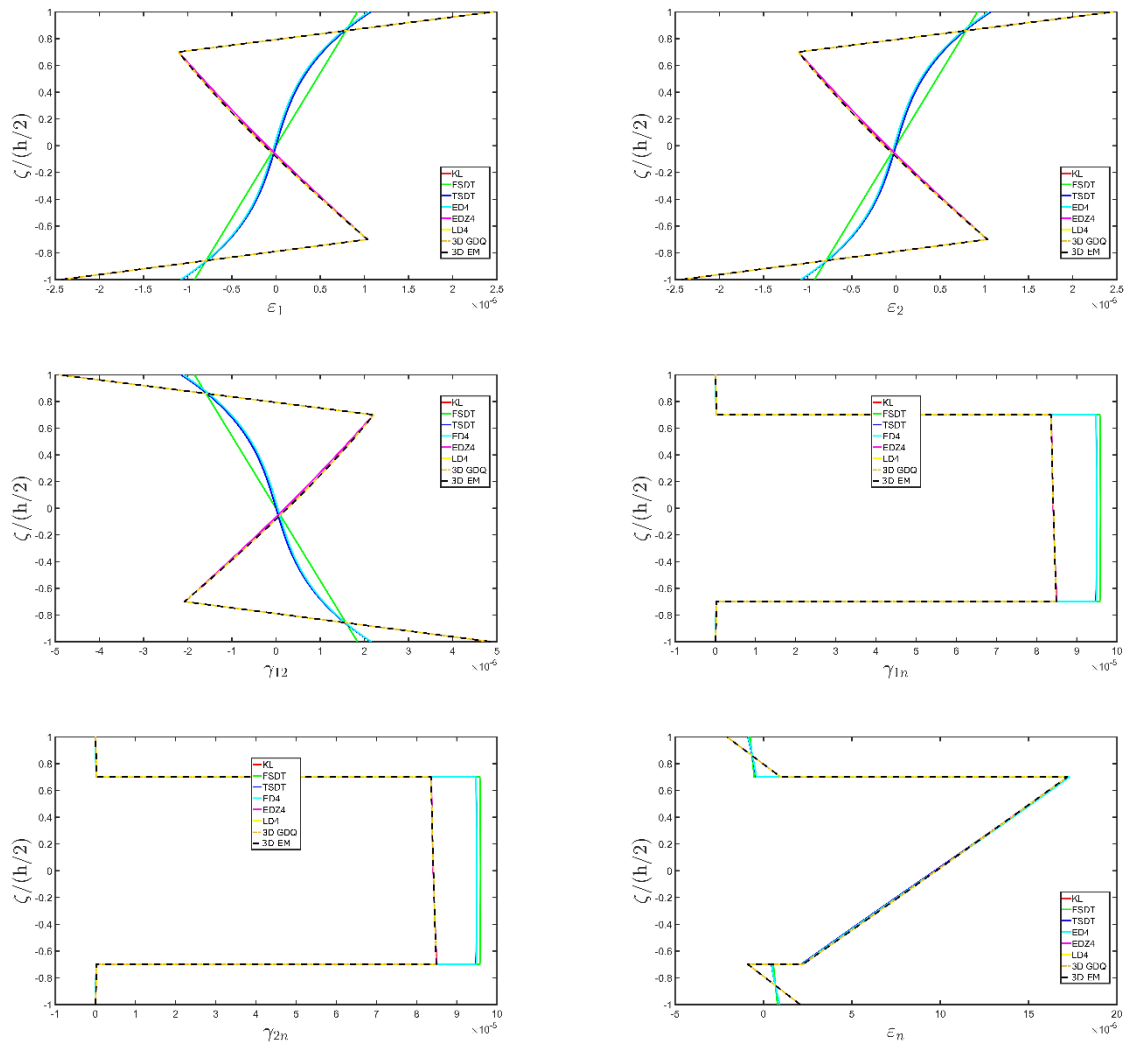
31
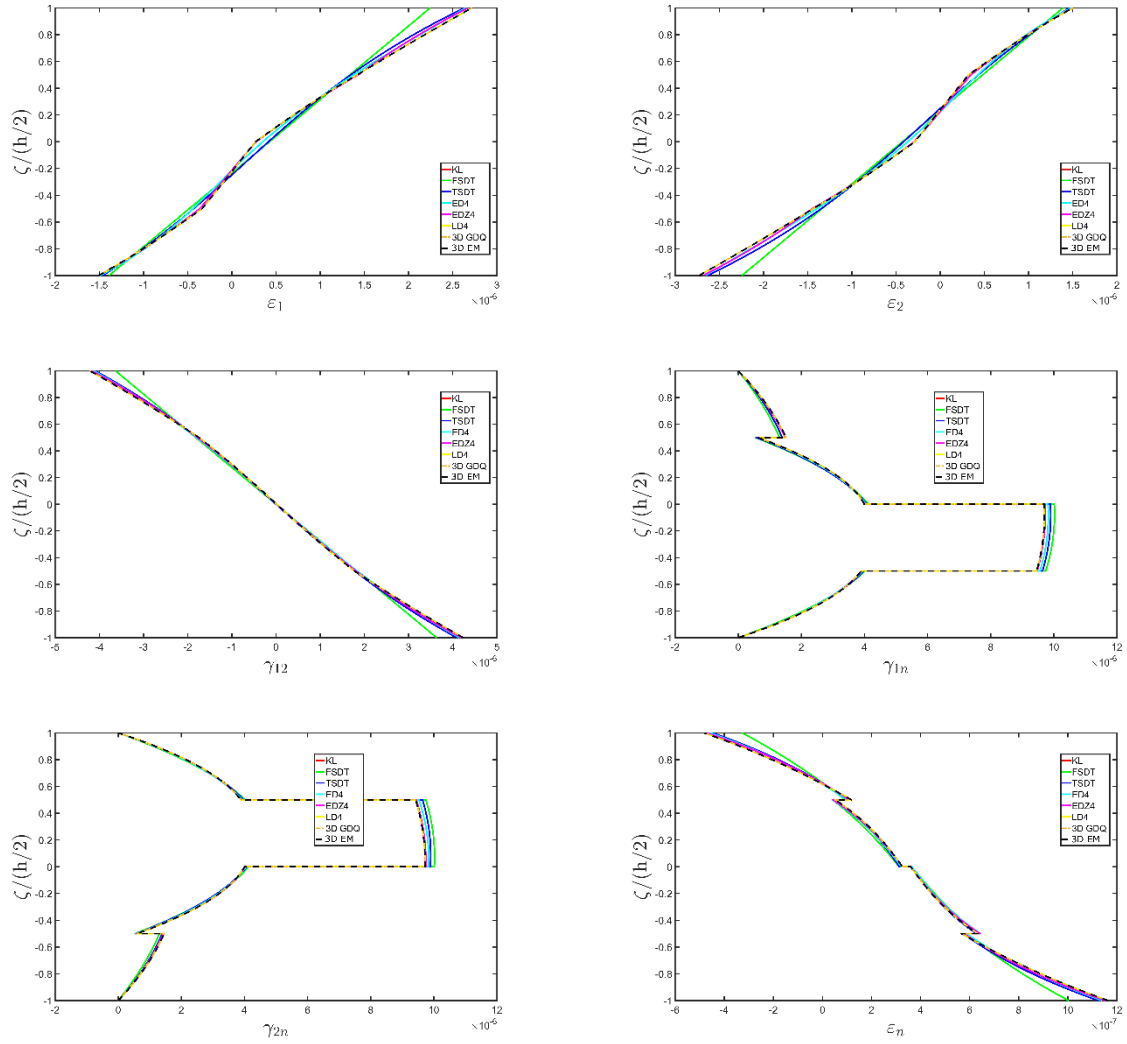
Figure 3. Through-the-thickness variation of strain components for a SSSS square plate $(a/h = 10)$ made of four layers $(0/90/0/90)$ with $h_1 = h_2 = h_3 = h_4 = h/4$ at the point $P = (0.25a, 0.25b)$ subjected to a normal sinusoidal pressure $q_3^{(+)} = 10000\,\text{Pa}$ with $n = 1, m = 1$ on the top surface. Comparison between different structural theories.
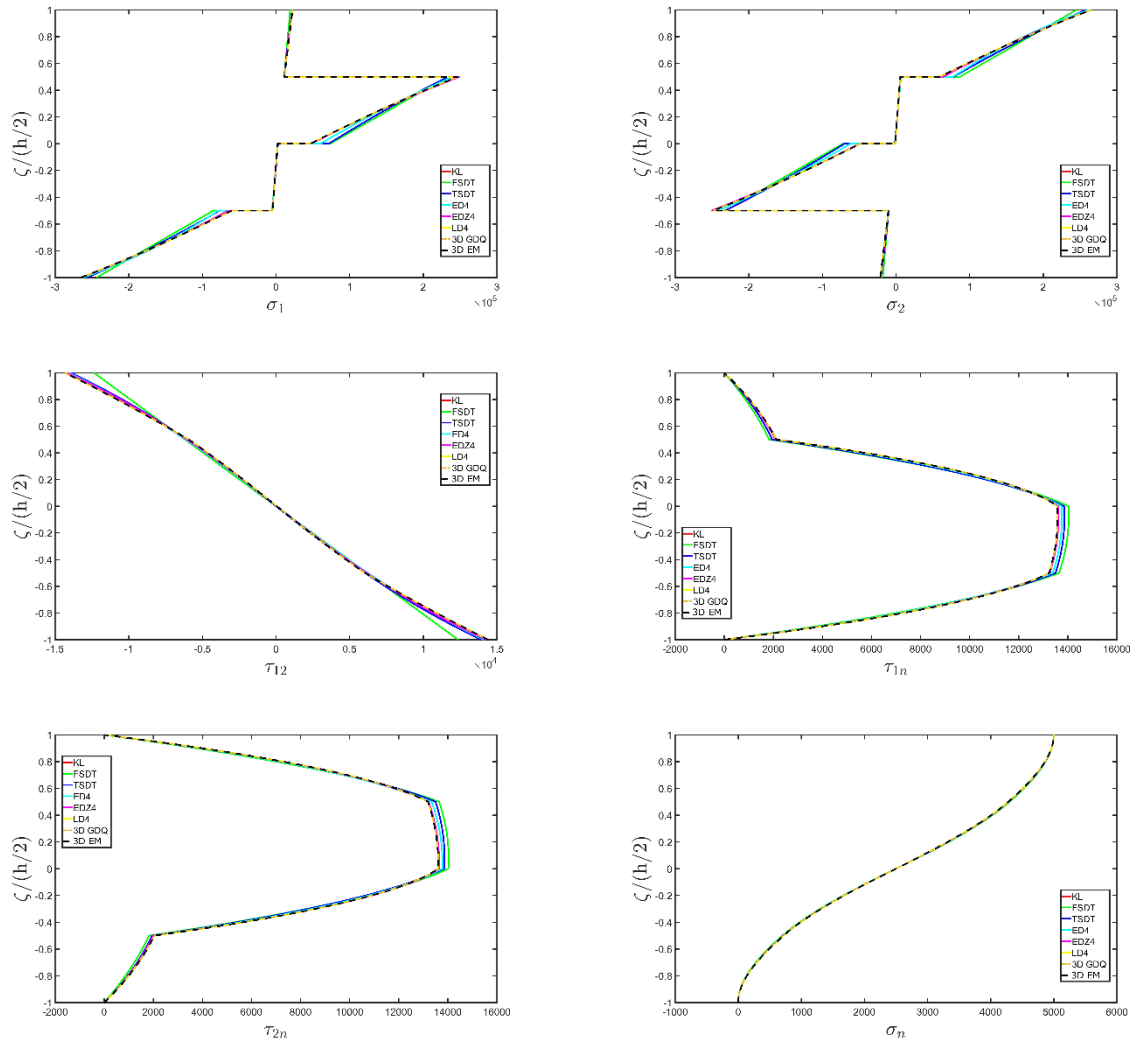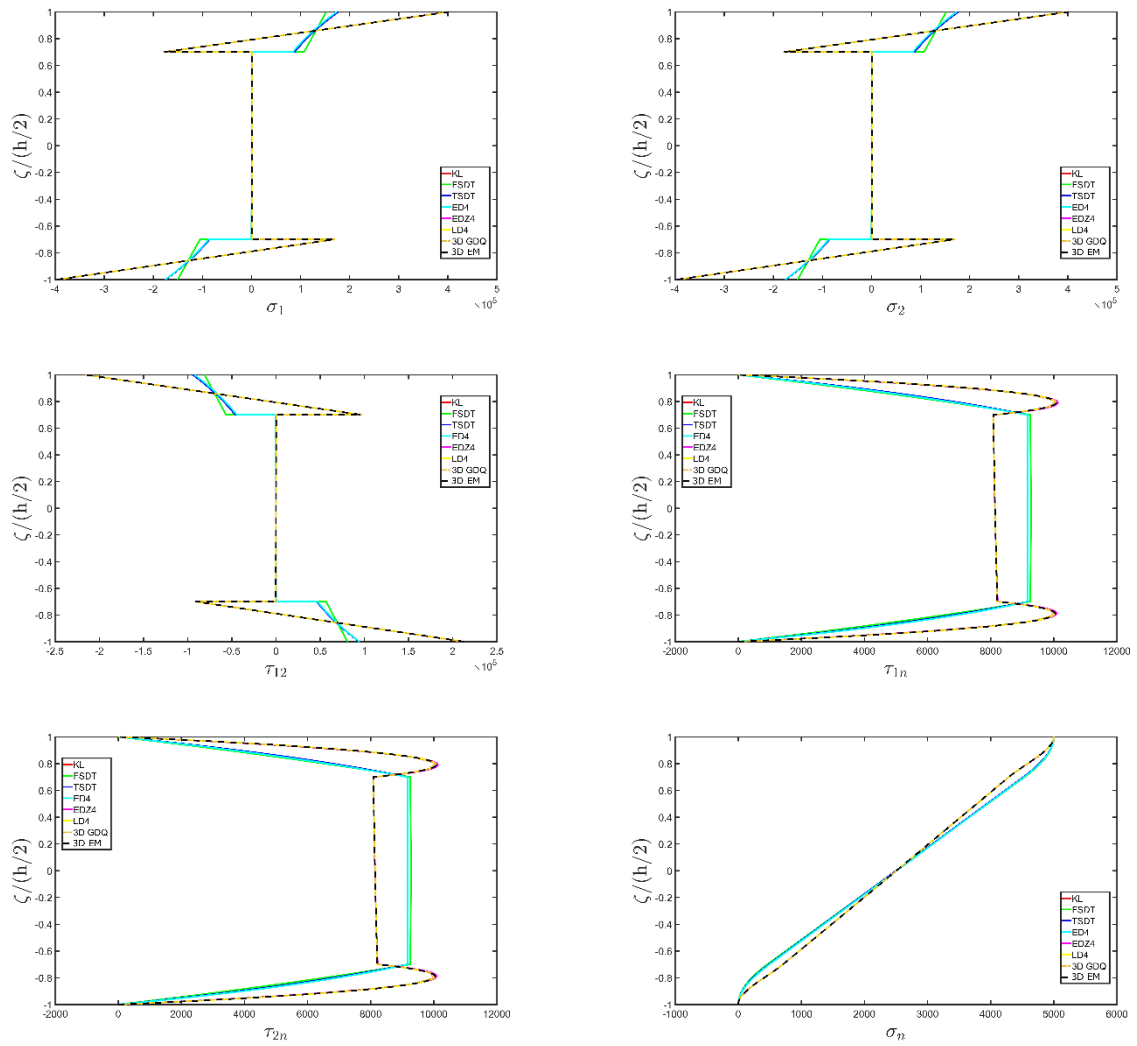
Figure 4. Through-the-thickness variation of stress components [Pa] for a SSSS square plate $\left(a/h=10\right)$ made of four layers $\left(0/90/0/90\right)$ with $h_1=h_2=h_3=h_4=h/4$ at the point $P=\left(0.25\,a,0.25\,b\right)$ subjected to a normal sinusoidal pressure $q_3^{(+)}=10000\,\mathrm{Pa}$ with $n=1,m=1$ on the top surface. Comparison between different structural theories.
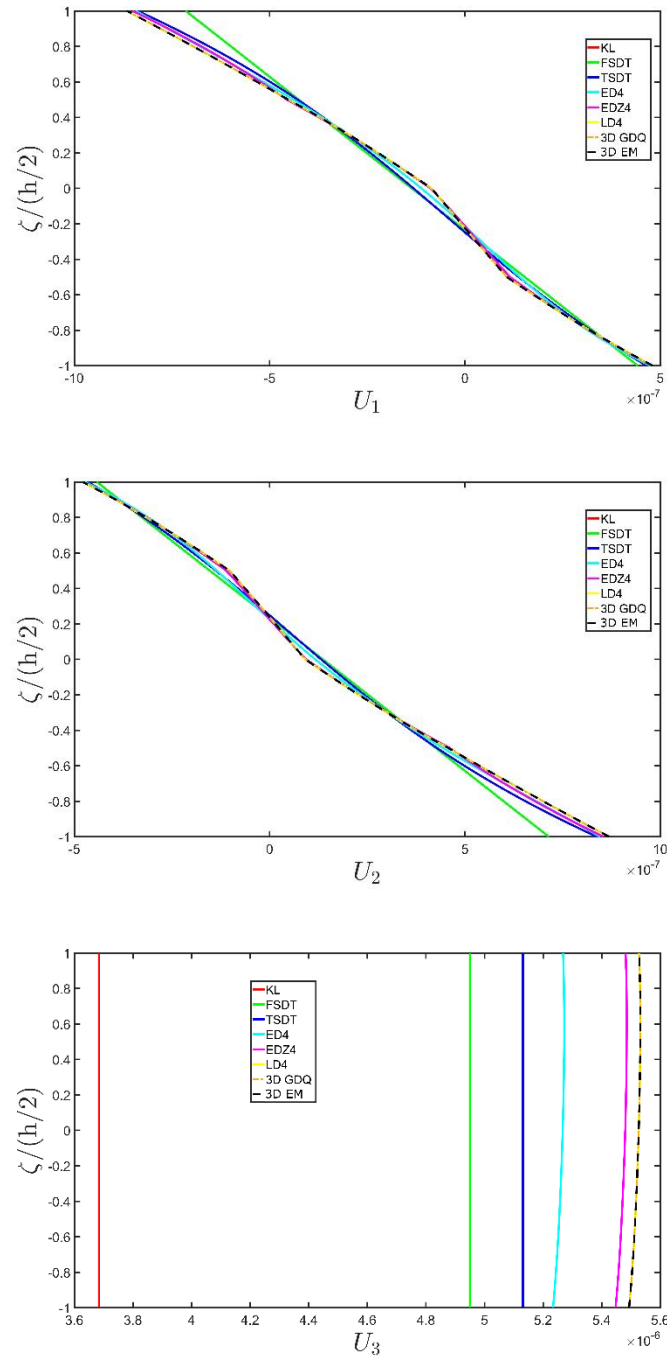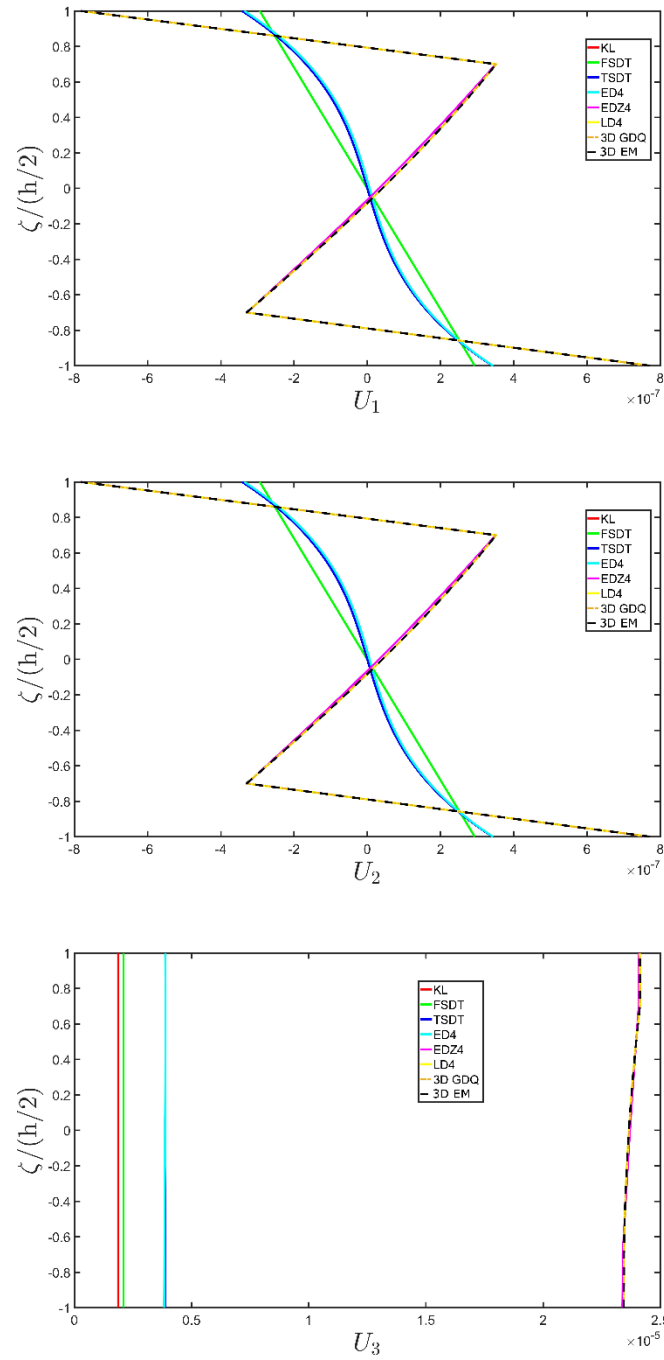
Figure 5. Through-the-thickness variation of displacement components [m] for a SSSS square plate $(a/h = 10)$ made of four layers $(0/90/0/90)$ with $h_1 = h_2 = h_3 = h_4 = h/4$ at the point $P = (0.25a, 0.25b)$ subjected to a normal sinusoidal pressure $q_3^{(+)} = 10000 \, \text{Pa}$ with $n = 1, m = 1$ on the top surface. Comparison between different structural theories.
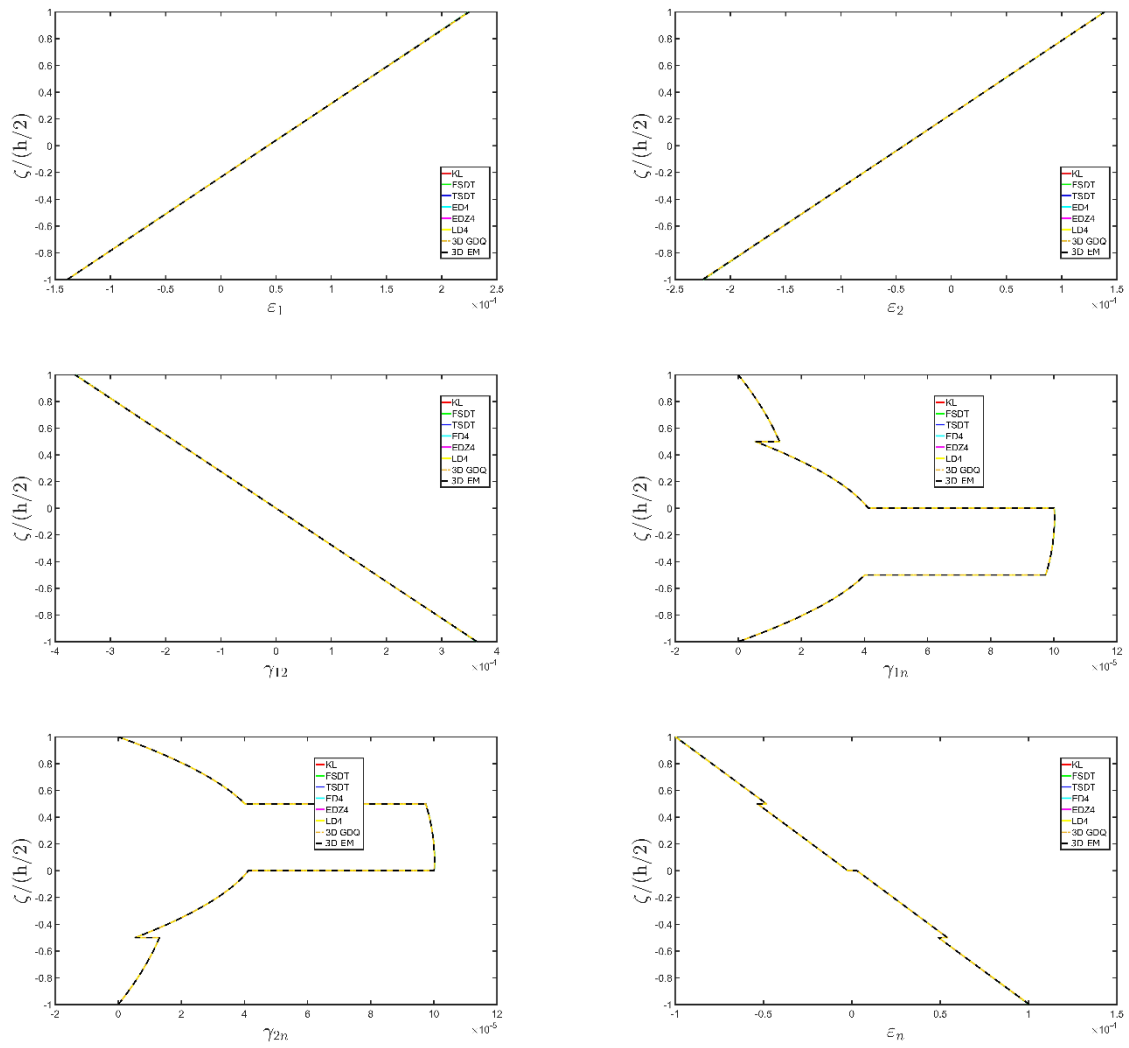
Figure 6. Through-the-thickness variation of strain components for a SSSS square plate $(a/h = 100)$ made of four layers $(0/90/0/90)$ with $h_1 = h_2 = h_3 = h_4 = h/4$ at the point $P = (0.25\,a, 0.25\,b)$ subjected to a normal sinusoidal pressure $q_3^{(+)} = 10000\,\text{Pa}$ with $n = 1, m = 1$ on the top surface. Comparison between different structural theories.
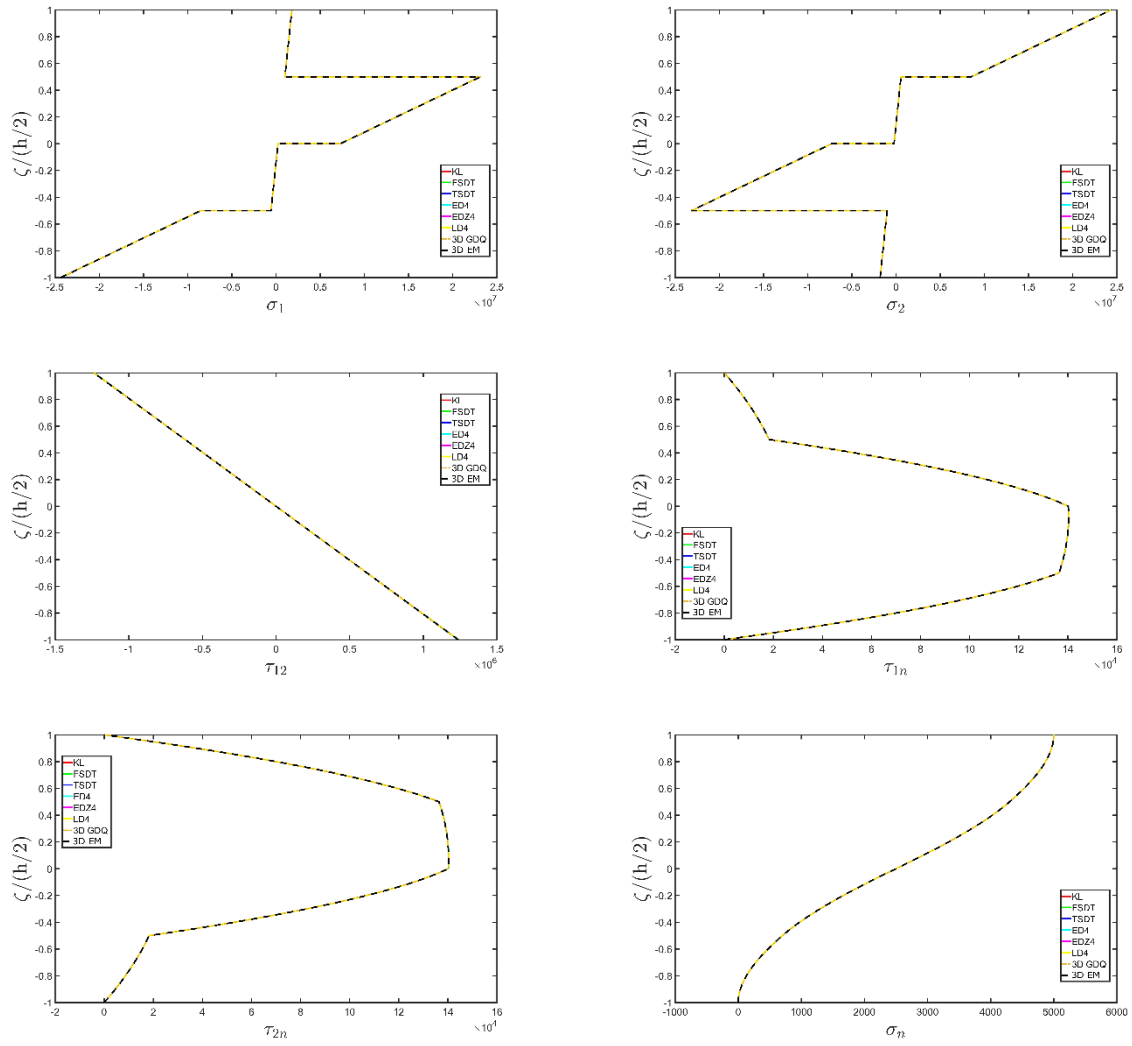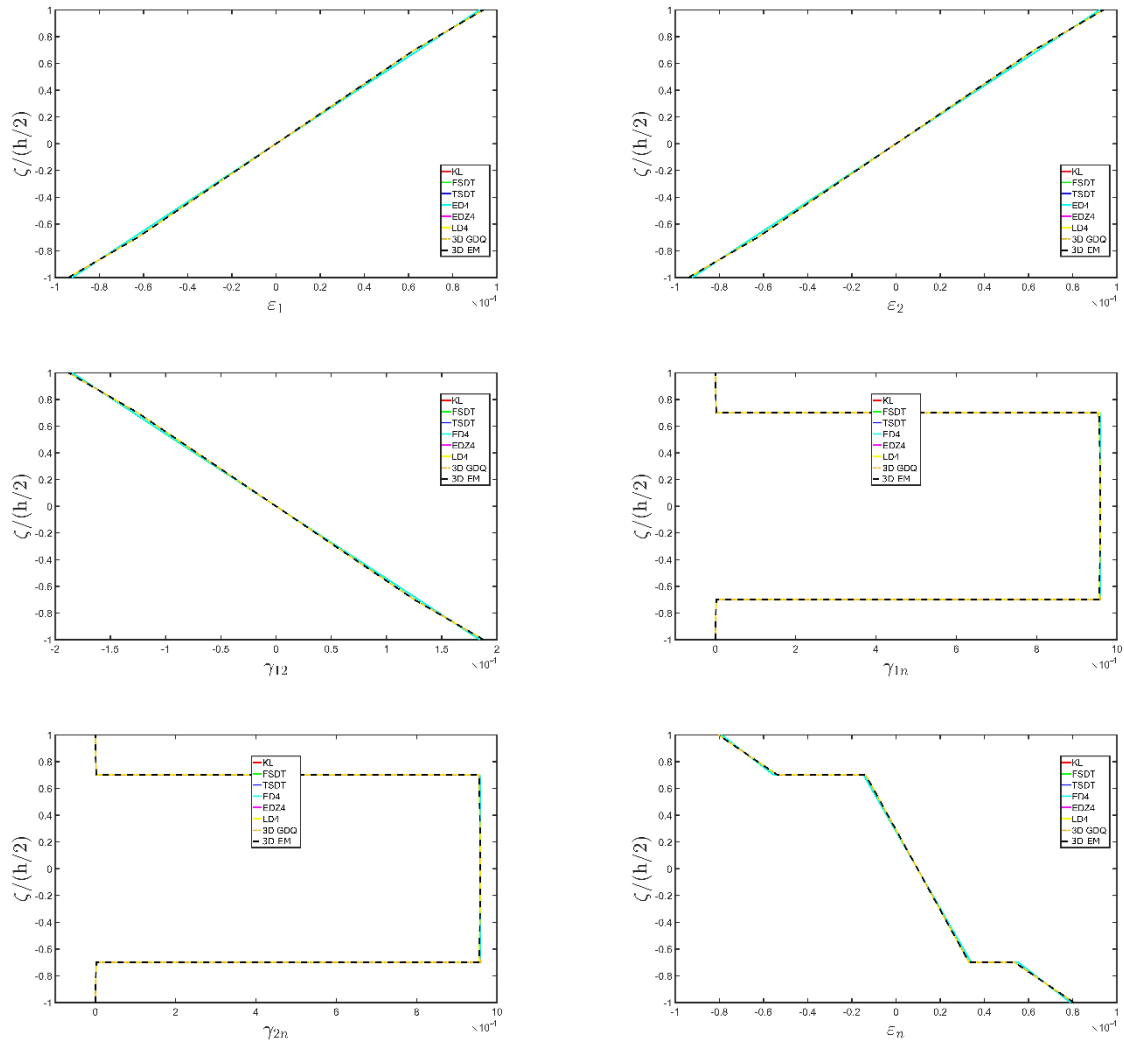
Figure 7. Through-the-thickness variation of stress components [Pa] for a SSSS square plate $(a/h = 100)$ made of four layers $(0/90/0/90)$ with $h_1 = h_2 = h_3 = h_4 = h/4$ at the point $P = (0.25\,a, 0.25\,b)$ subjected to a normal sinusoidal pressure $q_3^{(+)} = 10000\,\text{Pa}$ with $n = 1, m = 1$ on the top surface. Comparison between different structural theories.
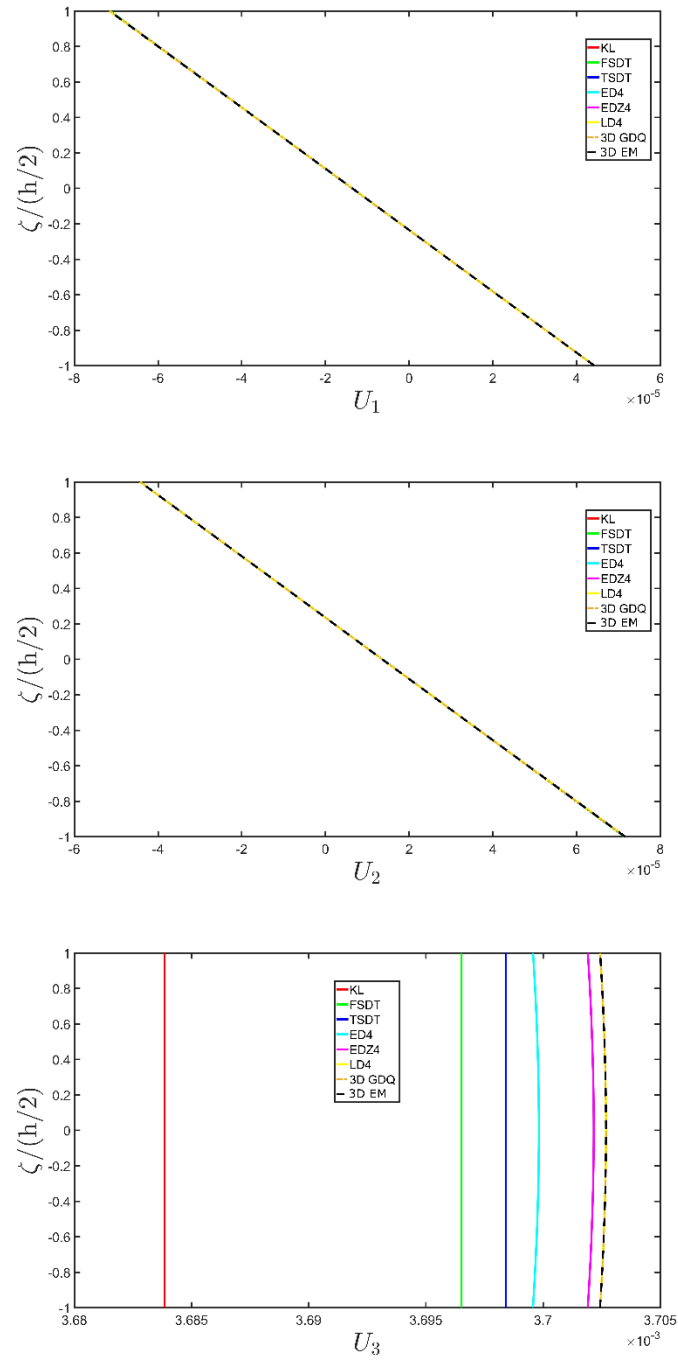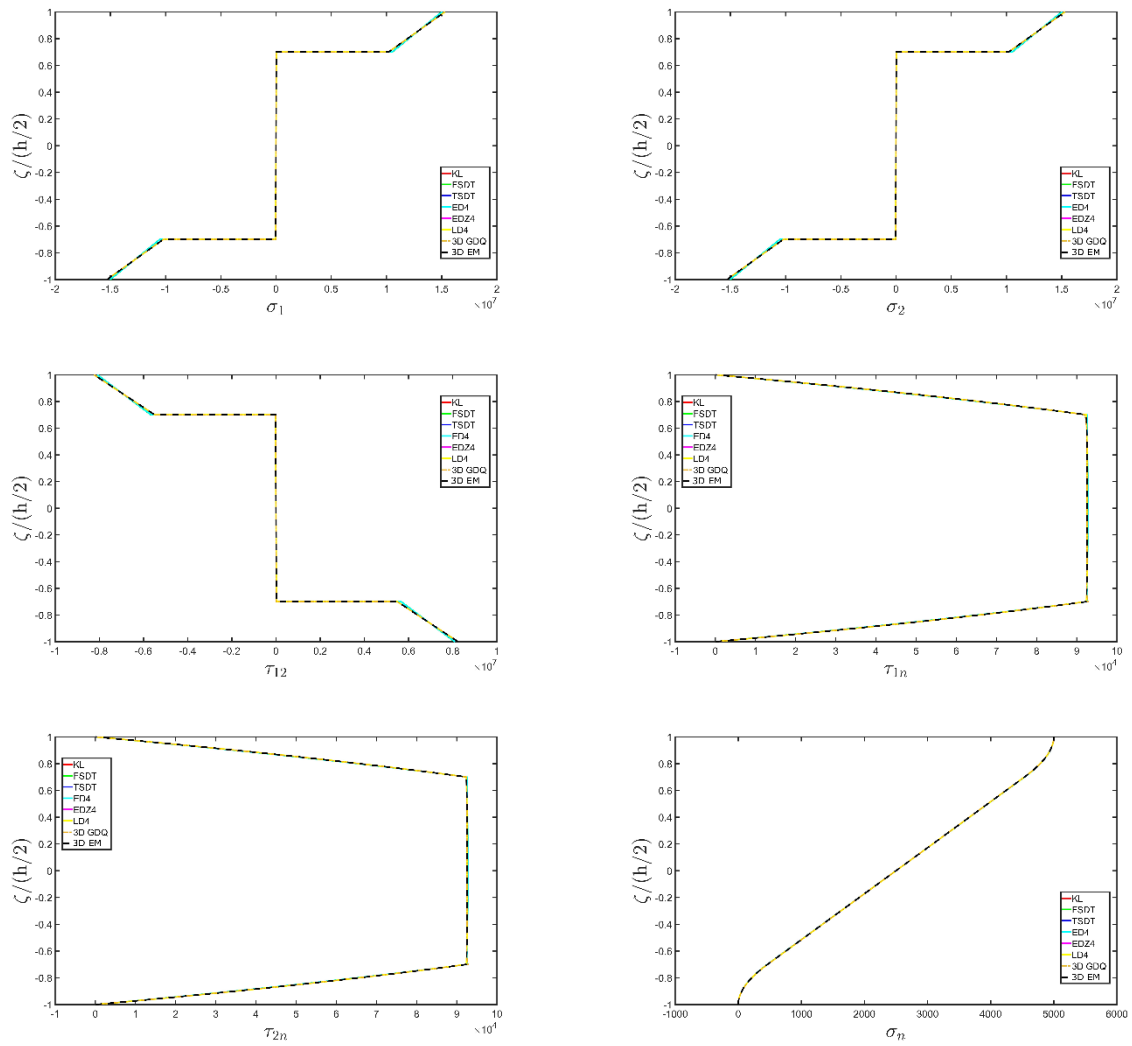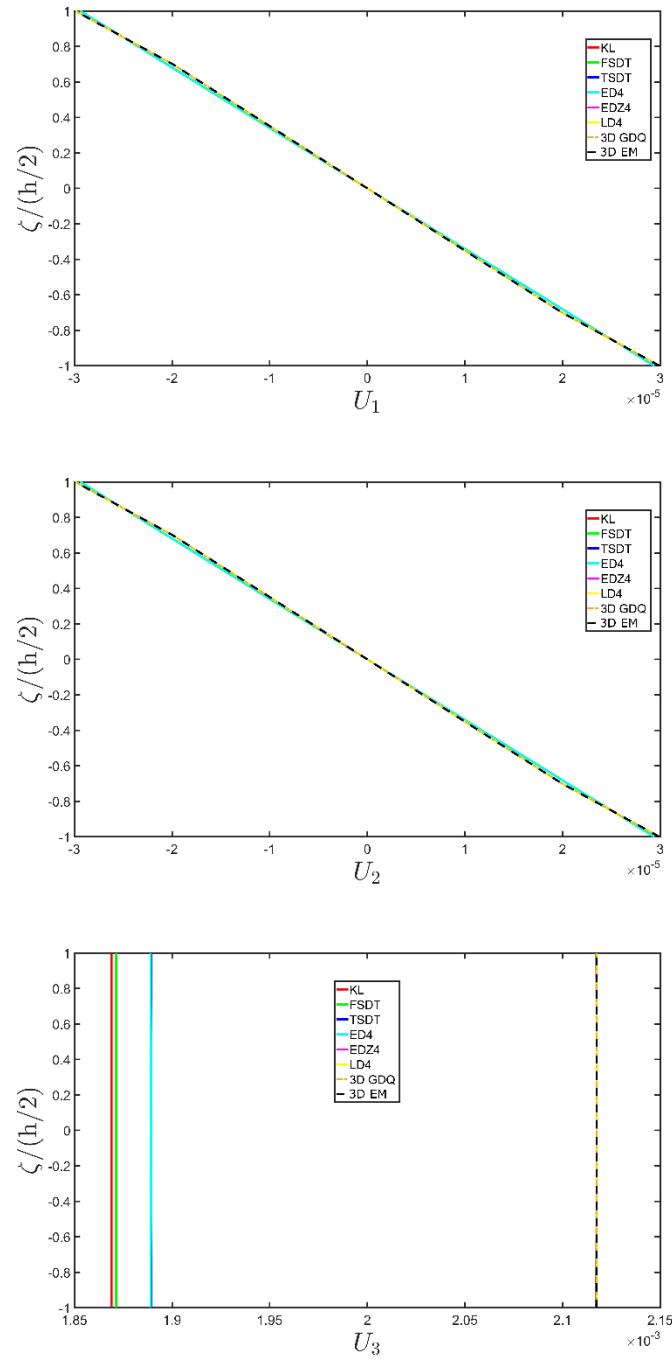
Figure 8. Through-the-thickness variation of displacement components [m] for a SSSS square plate $(a/h = 100)$ made of four layers $(0/90/0/90)$ with $h_1 = h_2 = h_3 = h_4 = h/4$ at the point $P = (0.25a, 0.25b)$ subjected to a normal sinusoidal pressure $q_3^{(+)} = 10000\,\text{Pa}$ with $n = 1, m = 1$ on the top surface. Comparison between different structural theories.

Figure 9. Through-the-thickness variation of strain components for a SSSS square plate $(a/h=10)$ made of three layers $(\text{Titanium}/\text{Foam}/\text{Titanium})$ with $h_1 = h_3 = 0.15\,h$, $h_2 = 0.7\,h$ at the point $P = (0.25\,a, 0.25\,b)$ subjected to a normal sinusoidal pressure $q_3^{(+)} = 10000\,\text{Pa}$ with $n=1, m=1$ on the top surface. Comparison between different structural theories.
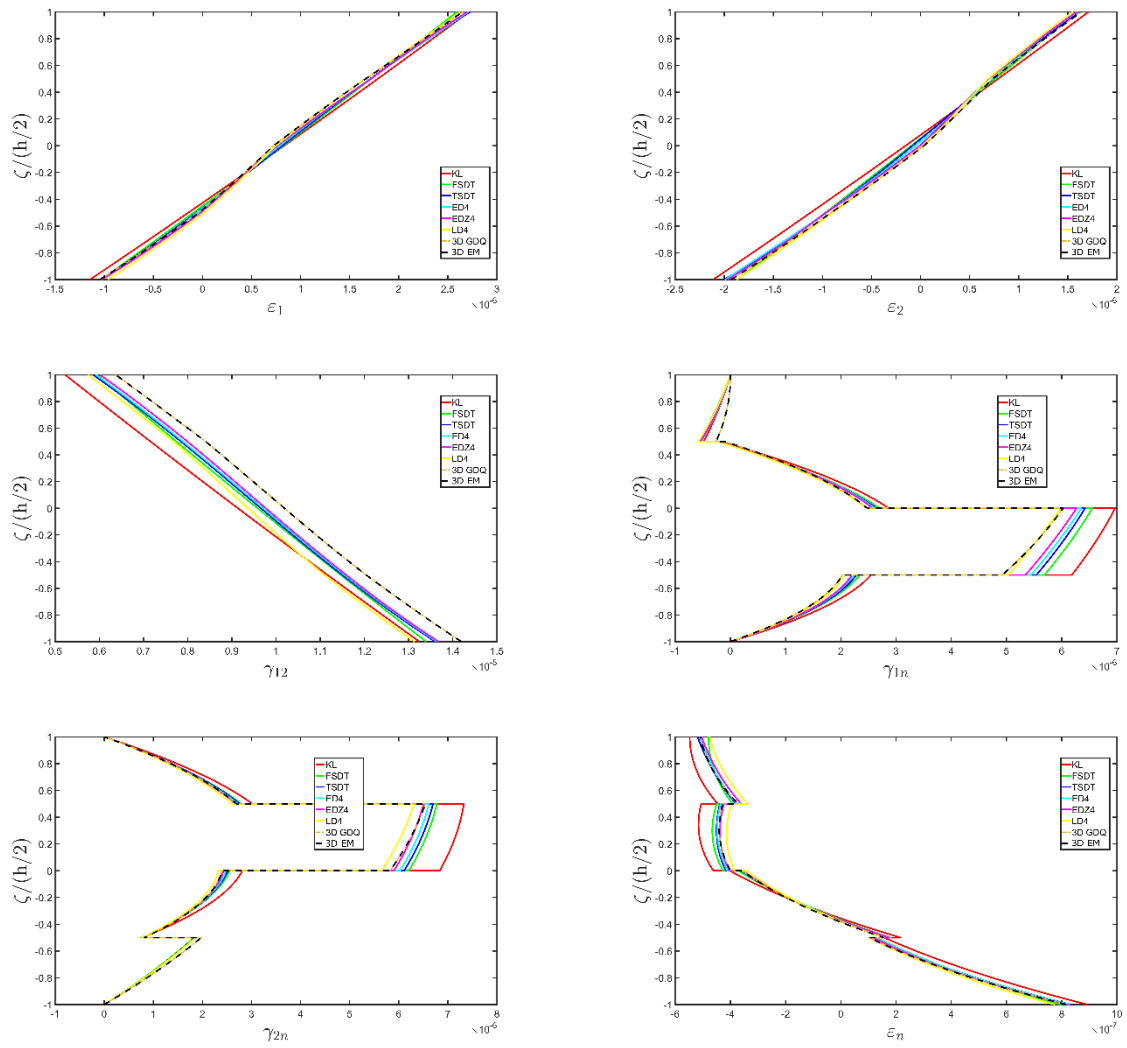
Figure 10. Through-the-thickness variation of stress components [Pa] for a SSSS square plate $\left(a/h=10\right)$ made of three layers $\left(\text{Titanium}\,/\,\text{Foam}\,/\,\text{Titanium}\right)$ with $h_1=h_3=0.15\,h,\,h_2=0.7\,h$ at the point $P=\left(0.25\,a,0.25\,b\right)$ subjected to a normal sinusoidal pressure $q_3^{(+)}=10000\,\text{Pa}$ with $n=1,m=1$ on the top surface. Comparison between different structural theories.
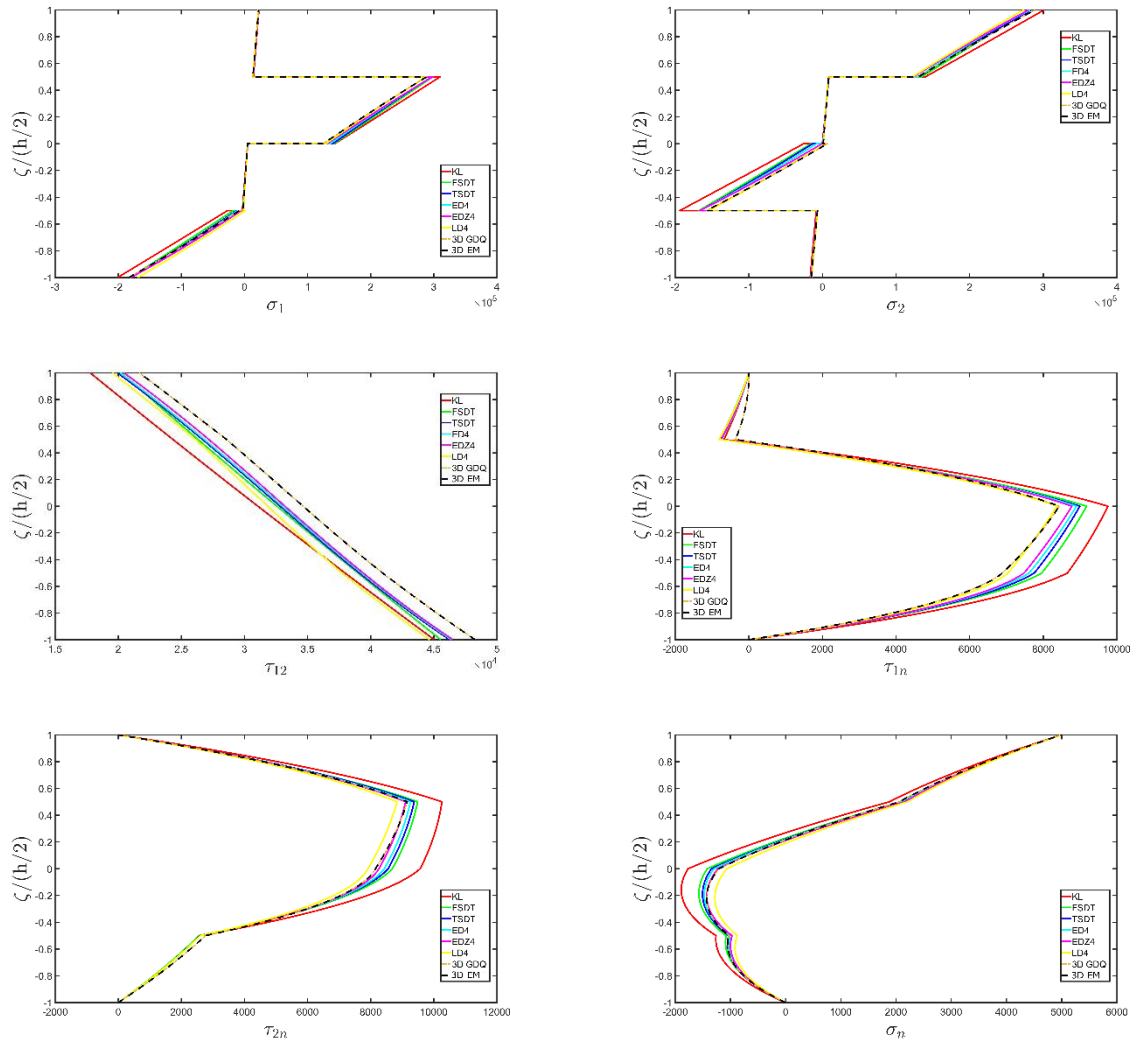
Figure 11. Through-the-thickness variation of displacement components [m] for a SSSS square plate $(a/h = 10)$ made of three layers $(\text{Titanium}/\text{Foam}/\text{Titanium})$ with $h_1 = h_3 = 0.15h,\ h_2 = 0.7h$ at the point $P = (0.25a, 0.25b)$ subjected to a normal sinusoidal pressure $q_3^{(+)} = 10000\,\text{Pa}$ with $n = 1, m = 1$ on the top surface. Comparison between different structural theories.
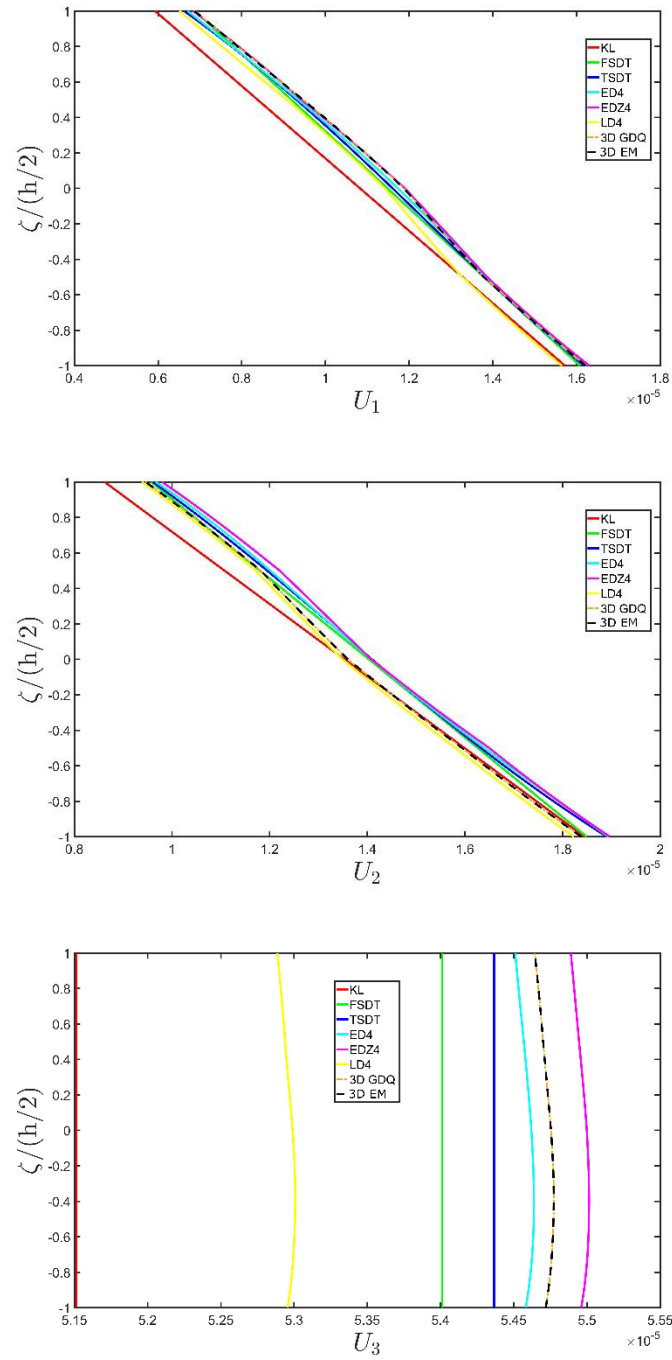
Figure 12. Through-the-thickness variation of strain components for a SSSS square plate $(a/h = 100)$ made of three layers $(\text{Titanium} / \text{Foam} / \text{Titanium})$ with $h_1 = h_3 = 0.15\,h$, $h_2 = 0.7\,h$ at the point $P = (0.25\,a, 0.25\,b)$ subjected to a normal sinusoidal pressure $q_3^{(+)} = 10000\,\text{Pa}$ with $n = 1, m = 1$ on the top surface. Comparison between different structural theories.

Figure 13. Through-the-thickness variation of stress components [Pa] for a SSSS square plate $\left(a/h=100\right)$ made of three layers $\left(\text{Titanium}/\text{Foam}/\text{Titanium}\right)$ with $h_1=h_3=0.15h$, $h_2=0.7h$ at the point $P=\left(0.25a,0.25b\right)$ subjected to a normal sinusoidal pressure $q_3^{(+)}=10000\,\text{Pa}$ with $n=1,m=1$ on the top surface. Comparison between different structural theories.
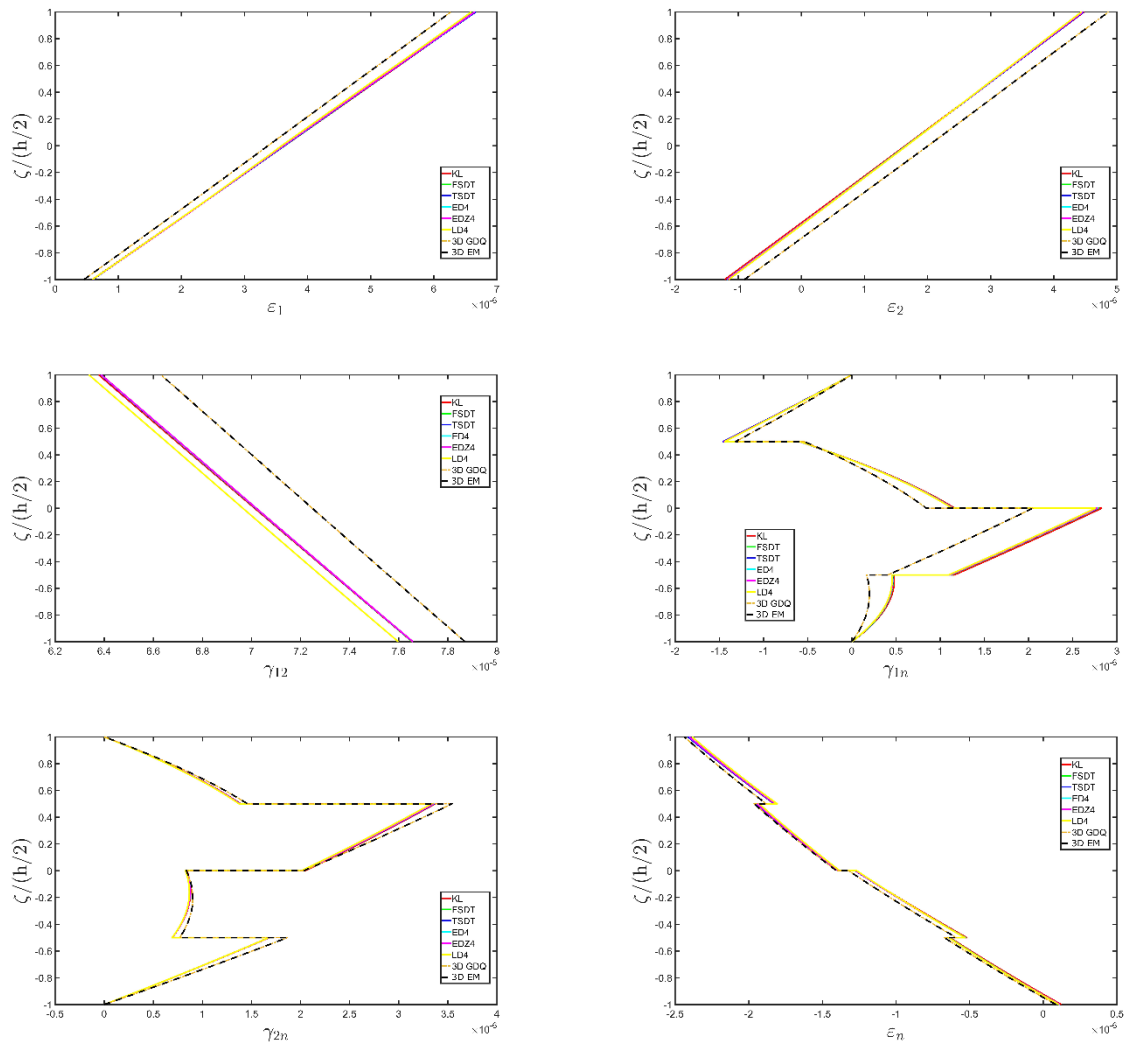
Figure 14. Through-the-thickness variation of displacement components [m] for a SSSS square plate $\left(a/h=100\right)$ made of three layers $\left(\text{Titanium}/\text{Foam}/\text{Titanium}\right)$ with $h_1=h_3=0.15h$, $h_2=0.7h$ at the point $P=\left(0.25a,0.25b\right)$ subjected to a normal sinusoidal pressure $q_3^{(+)}=10000\,\text{Pa}$ with $n=1,m=1$ on the top surface. Comparison between different structural theories.

Figure 15. Through-the-thickness variation of strain components for a SSSS spherical panel $\left(R/h=20\right)$ made of four layers $\left(0/90/0/90\right)$ with $h_1=h_2=h_3=h_4=h/4$ at the point $P=\left(0.25\left(\alpha_1^1-\alpha_1^0\right),0.25\left(\alpha_2^1-\alpha_2^0\right)\right)$ subjected to a normal sinusoidal load $q_3^{(+)}=10000\,\text{Pa}$ with $n=1, m=1$ on the top surface. Comparison between different structural theories.
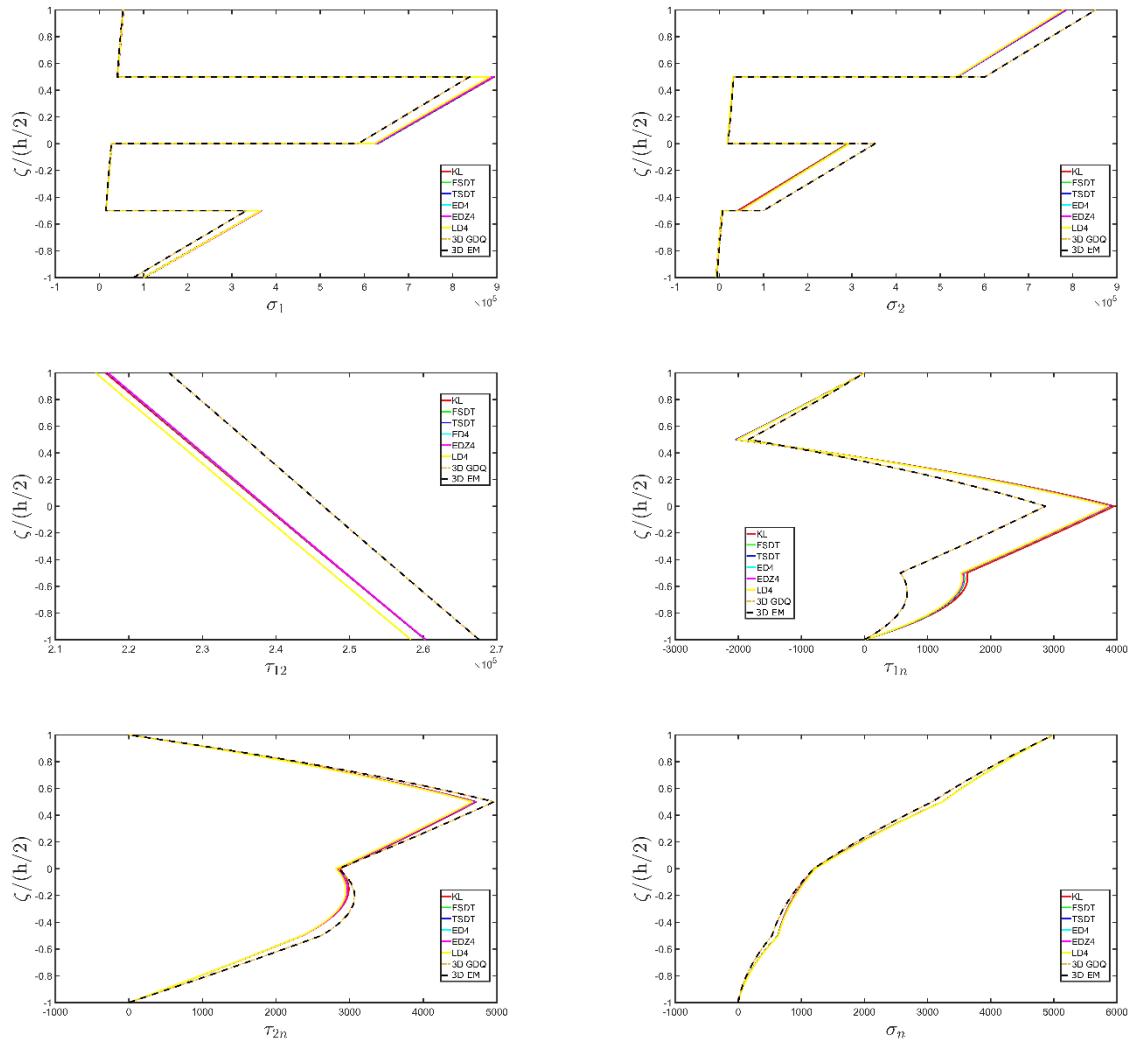
Figure 16. Through-the-thickness variation of stress components [Pa] for a SSSS spherical panel $\left(R/h=20\right)$ made of four layers $\left(0/90/0/90\right)$ with $h_1=h_2=h_3=h_4=h/4$ at the point $P=\left(0.25\left(\alpha_1^1-\alpha_1^0\right),0.25\left(\alpha_2^1-\alpha_2^0\right)\right)$ subjected to a normal sinusoidal load $q_3^{(+)}=10000\,\text{Pa}$ with $n=1,m=1$ on the top surface. Comparison between different structural theories.
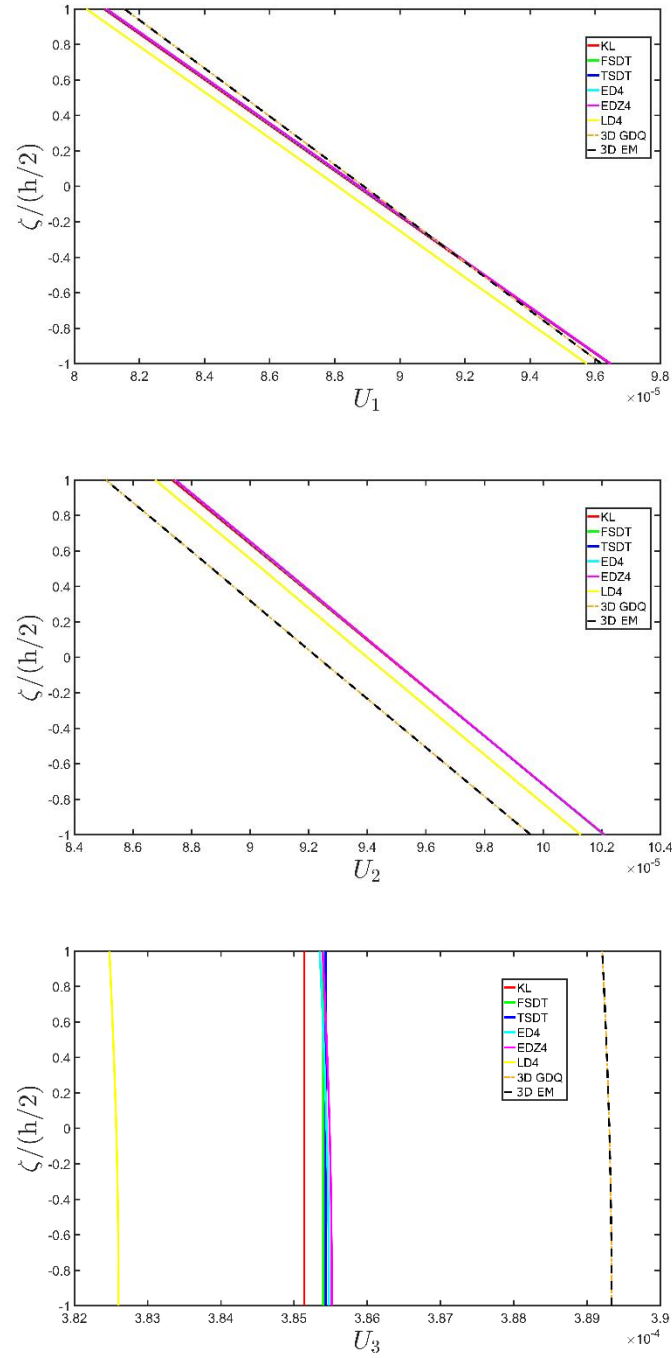
Figure 17. Through-the-thickness variation of displacement components [m] for a SSSS spherical panel $\left(R/h = 20 \right)$ made of four layers $\left(0/90/0/90 \right)$ with $h_1 = h_2 = h_3 = h_4 = h/4$ at the point $P = \left(0.25\left(\alpha_1^1 - \alpha_1^0 \right), 0.25\left(\alpha_2^1 - \alpha_2^0 \right) \right)$ subjected to a normal sinusoidal load $q_3^{(+)} = 10000 \, \text{Pa}$ with $n = 1, m = 1$ on the top surface. Comparison between different structural theories.

46

Figure 18. Through-the-thickness variation of strain components for a SSSS spherical panel $\left(R/h=100\right)$ made of four layers $\left(0/90/0/90\right)$ with $h_1=h_2=h_3=h_4=h/4$ at the point $P=\left(0.25\left(\alpha_1^1-\alpha_1^0\right),0.25\left(\alpha_2^1-\alpha_2^0\right)\right)$ subjected to a normal sinusoidal load $q_3^{(+)}=10000\,\mathrm{Pa}$ with $n=1,m=1$ on the top surface. Comparison between different structural theories.
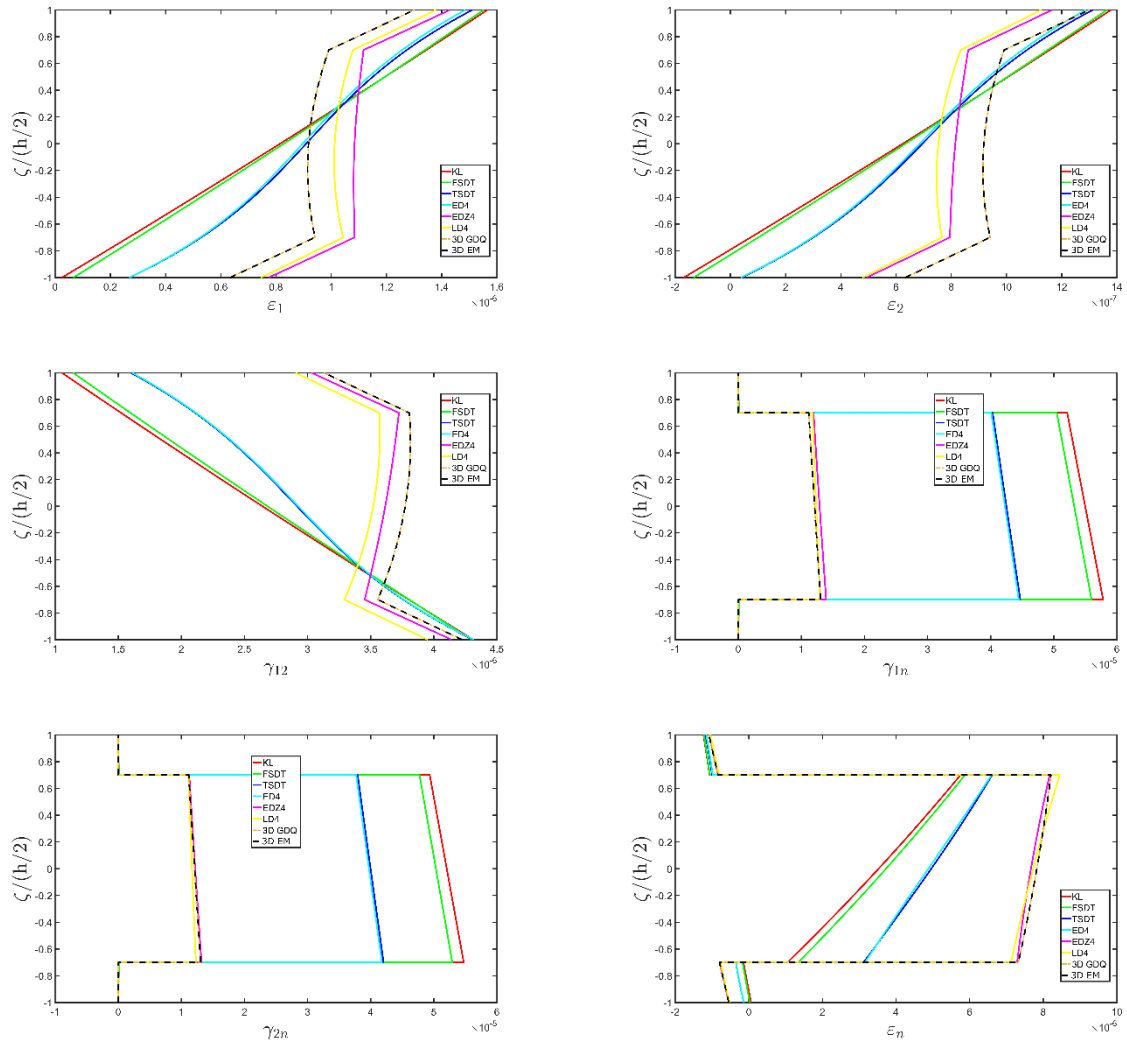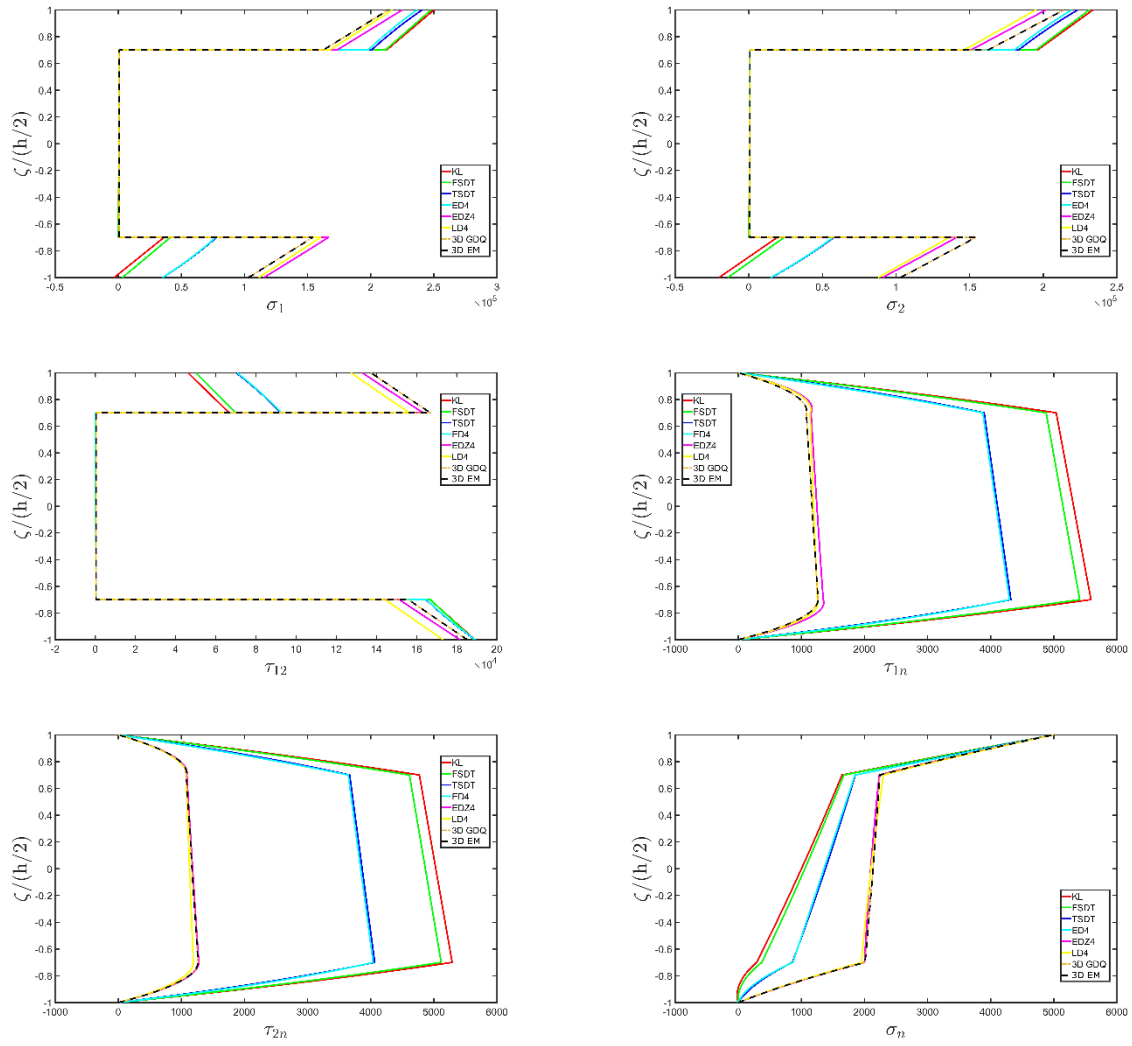
Figure 19. Through-the-thickness variation of stress components [Pa] for a SSSS spherical panel $\left(R/h=100\right)$ made of four layers $\left(0/90/0/90\right)$ with $h_1=h_2=h_3=h_4=h/4$ at the point $P=\left(0.25\left(\alpha_1^1-\alpha_1^0\right),0.25\left(\alpha_2^1-\alpha_2^0\right)\right)$ subjected to a normal sinusoidal load $q_3^{(+)}=10000\,\text{Pa}$ with $n=1,m=1$ on the top surface. Comparison between different structural theories.
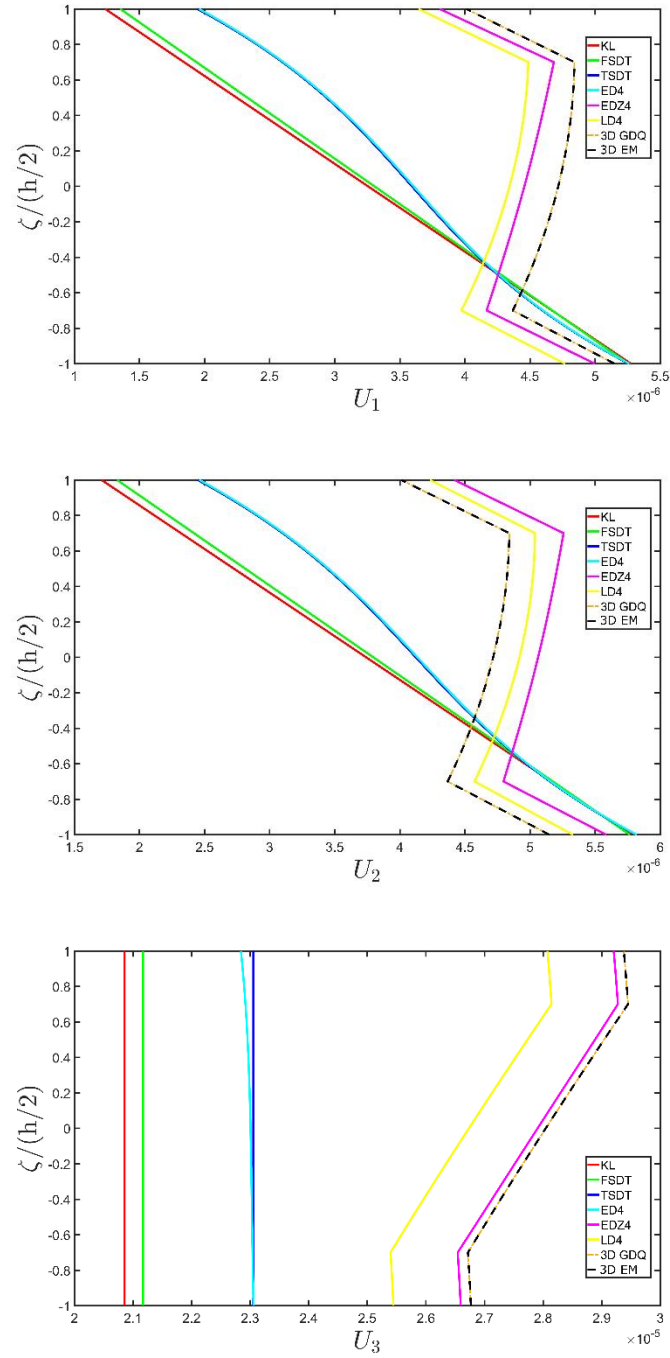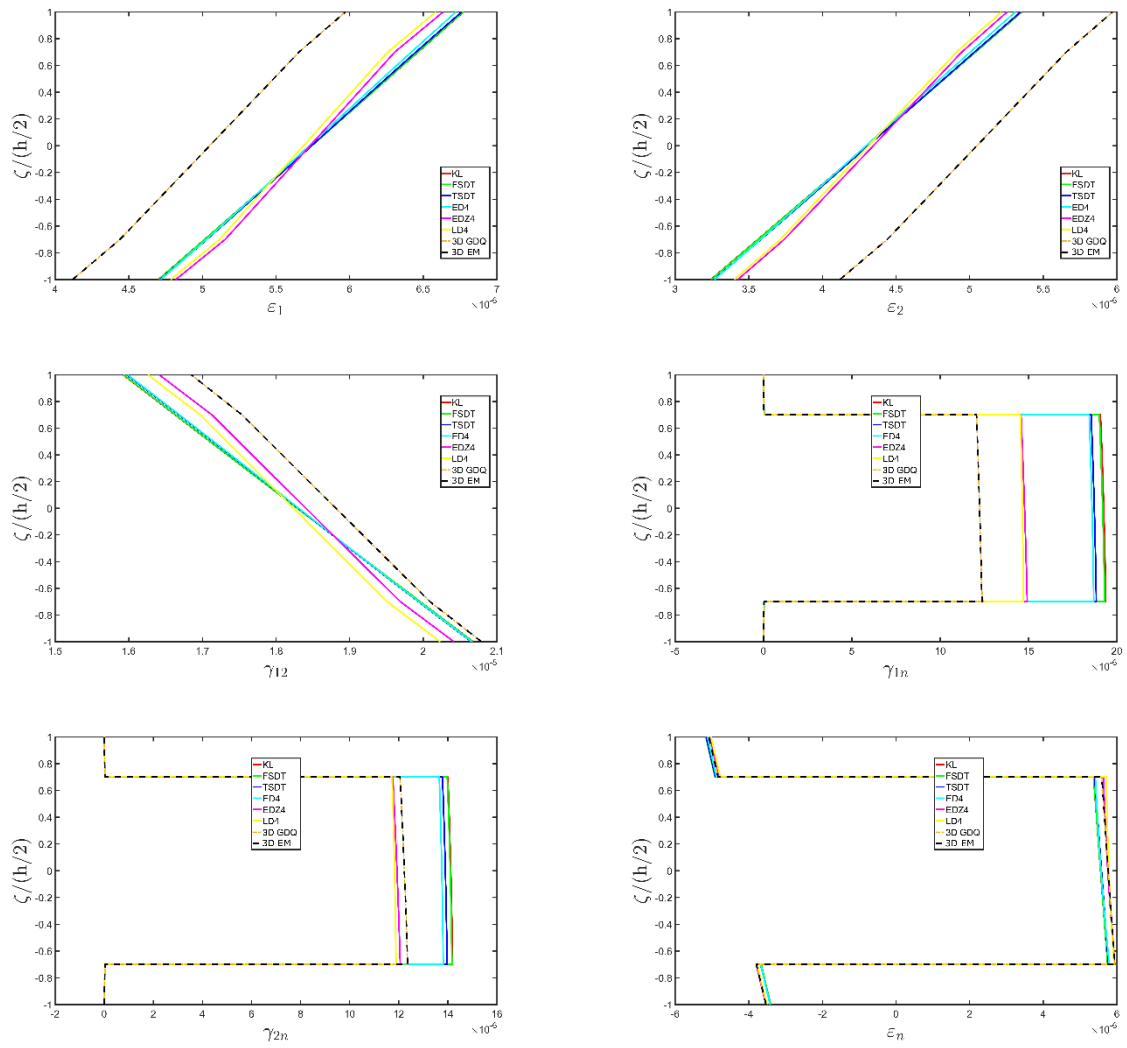
Figure 20. Through-the-thickness variation of displacement components [m] for a SSSS spherical panel $\left(R/h = 100 \right)$ made of four layers $\left(0/90/0/90 \right)$ with $h_1 = h_2 = h_3 = h_4 = h/4$ at the point $P = \left(0.25 \left(\alpha_1^1 - \alpha_1^0 \right), 0.25 \left(\alpha_2^1 - \alpha_2^0 \right) \right)$ subjected to a normal sinusoidal load $q_3^{(+)} = 10000 \, \text{Pa}$ with $n = 1, m = 1$ on the top surface. Comparison between different structural theories.

Figure 21. Through-the-thickness variation of strain components for a SSSS spherical panel $\left(R/h=20\right)$ made of three layers $\left(\text{Titanium}/\text{Foam}/\text{Titanium}\right)$ with $h_1=h_3=0.15\,h,\ h_2=0.7\,h$ at the point $P=\left(0.25\left(\alpha_1^1-\alpha_1^0\right),0.25\left(\alpha_2^1-\alpha_2^0\right)\right)$ subjected to a normal sinusoidal load $q_3^{(+)}=10000\,\text{Pa}$ with $n=1,m=1$ on the top surface. Comparison between different structural theories.
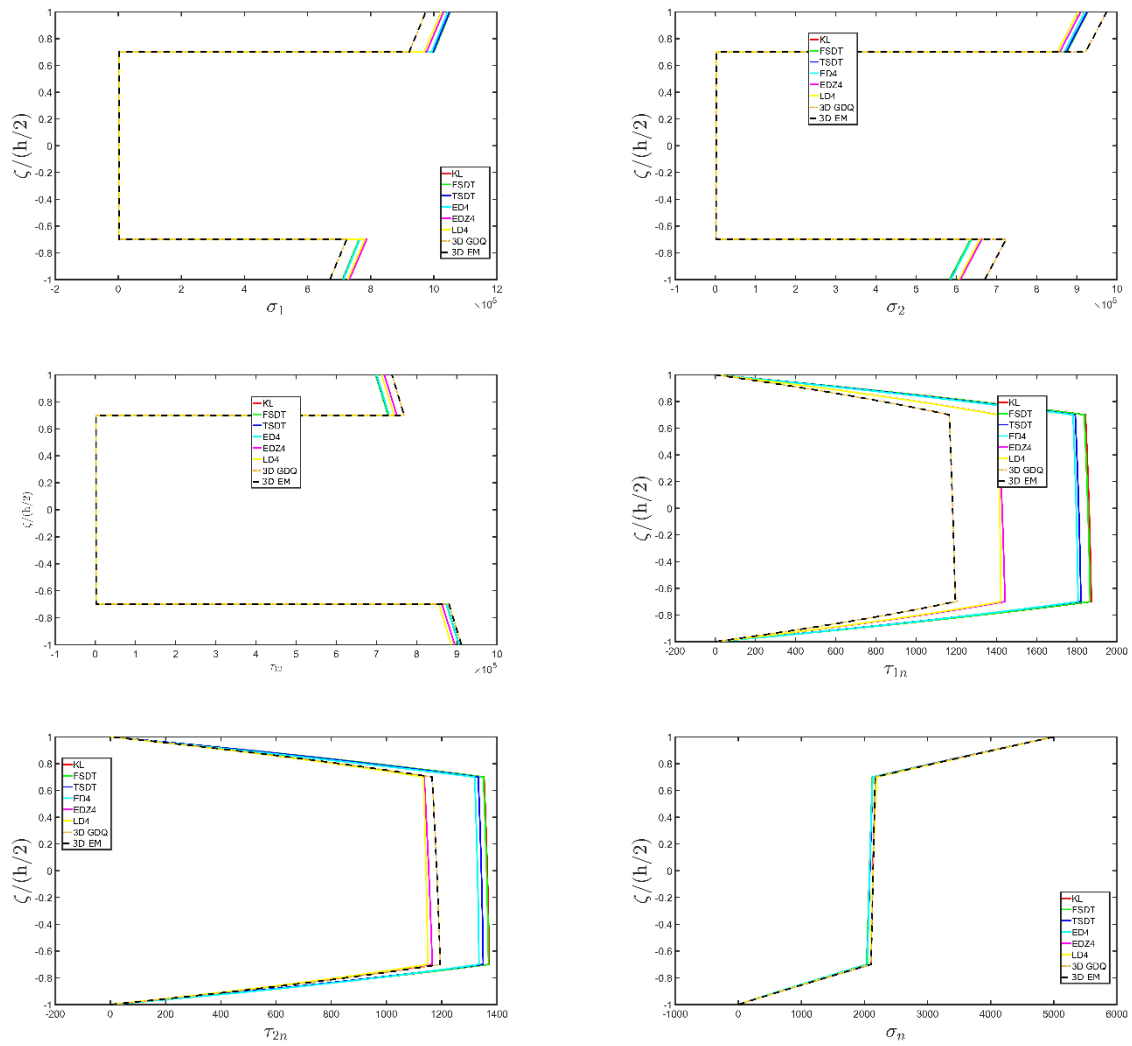
Figure 22. Through-the-thickness variation of stress components [Pa] for a SSSS spherical panel $\left(R/h = 20\right)$ made of three layers $\left(\text{Titanium / Foam / Titanium}\right)$ with $h_1 = h_3 = 0.15\,h$, $h_2 = 0.7\,h$ at the point $P = \left(0.25\left(\alpha_1^1 - \alpha_1^0\right), 0.25\left(\alpha_2^1 - \alpha_2^0\right)\right)$ subjected to a normal sinusoidal load $q_3^{(+)} = 10000\,\text{Pa}$ with $n = 1, m = 1$ on the top surface. Comparison between different structural theories.
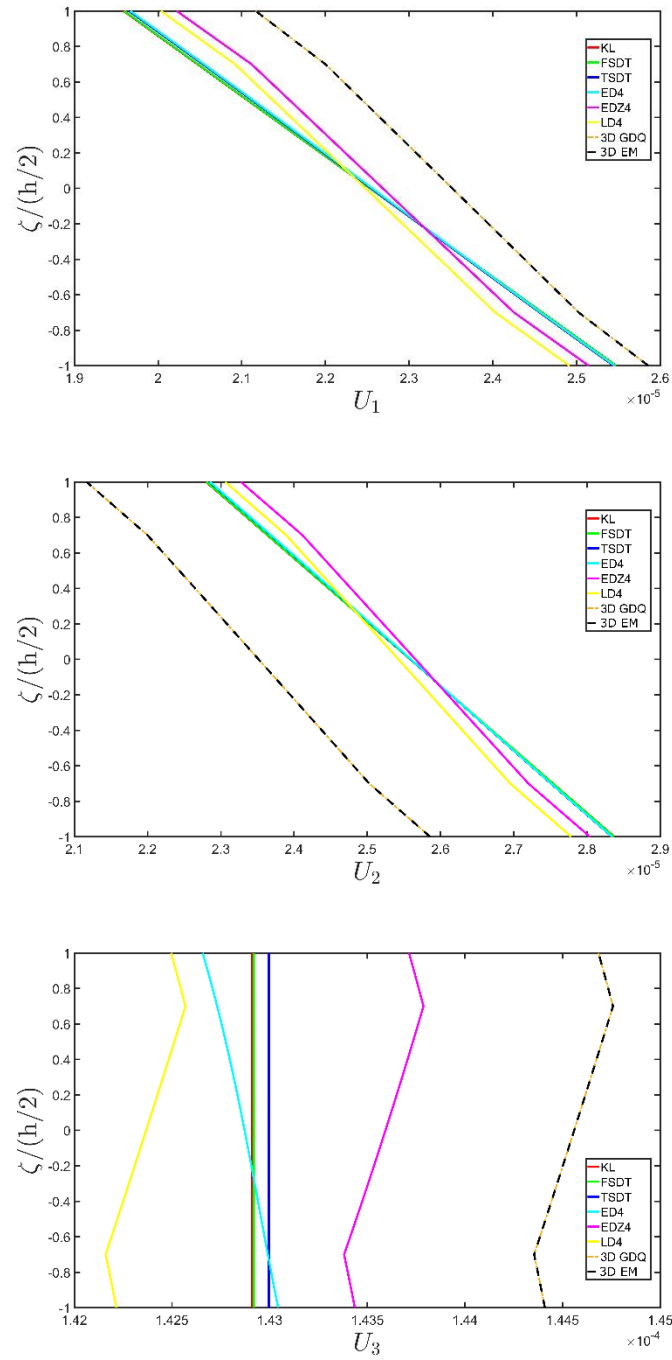
51

Figure 23. Through-the-thickness variation of displacement components [m] for a SSSS spherical panel $(R/h = 20)$ made of three layers $(\text{Titanium} / \text{Foam} / \text{Titanium})$ with $h_1 = h_3 = 0.15\,h$, $h_2 = 0.7\,h$ at the point $P = \left(0.25\left(\alpha_1^1 - \alpha_1^0\right), 0.25\left(\alpha_2^1 - \alpha_2^0\right)\right)$ subjected to a normal sinusoidal load $q_3^{(+)} = 10000\,\text{Pa}$ with $n = 1, m = 1$ on the top surface. Comparison between different structural theories.

Figure 24. Through-the-thickness variation of strain components for a SSSS spherical panel $(R/h = 100)$ made of three layers $(\text{Titanium}/\text{Foam}/\text{Titanium})$ with $h_1 = h_3 = 0.15\,h,\ h_2 = 0.7\,h$ at the point $P = \left(0.25\left(\alpha_1^1 - \alpha_1^0\right), 0.25\left(\alpha_2^1 - \alpha_2^0\right)\right)$ subjected to a normal sinusoidal load $q_3^{(+)} = 10000\,\text{Pa}$ with $n = 1, m = 1$ on the top surface. Comparison between different structural theories.

53

Figure 25. Through-the-thickness variation of stress components [Pa] for a SSSS spherical panel $\left(R/h = 100\right)$ made of three layers $\left(\text{Titanium} / \text{Foam} / \text{Titanium}\right)$ with $h_1 = h_3 = 0.15\,h$, $h_2 = 0.7\,h$ at the point $P = \left(0.25\left(\alpha_1^1 - \alpha_1^0\right), 0.25\left(\alpha_2^1 - \alpha_2^0\right)\right)$ subjected to a normal sinusoidal load $q_3^{(+)} = 10000\,\text{Pa}$ with $n = 1, m = 1$ on the top surface. Comparison between different structural theories.
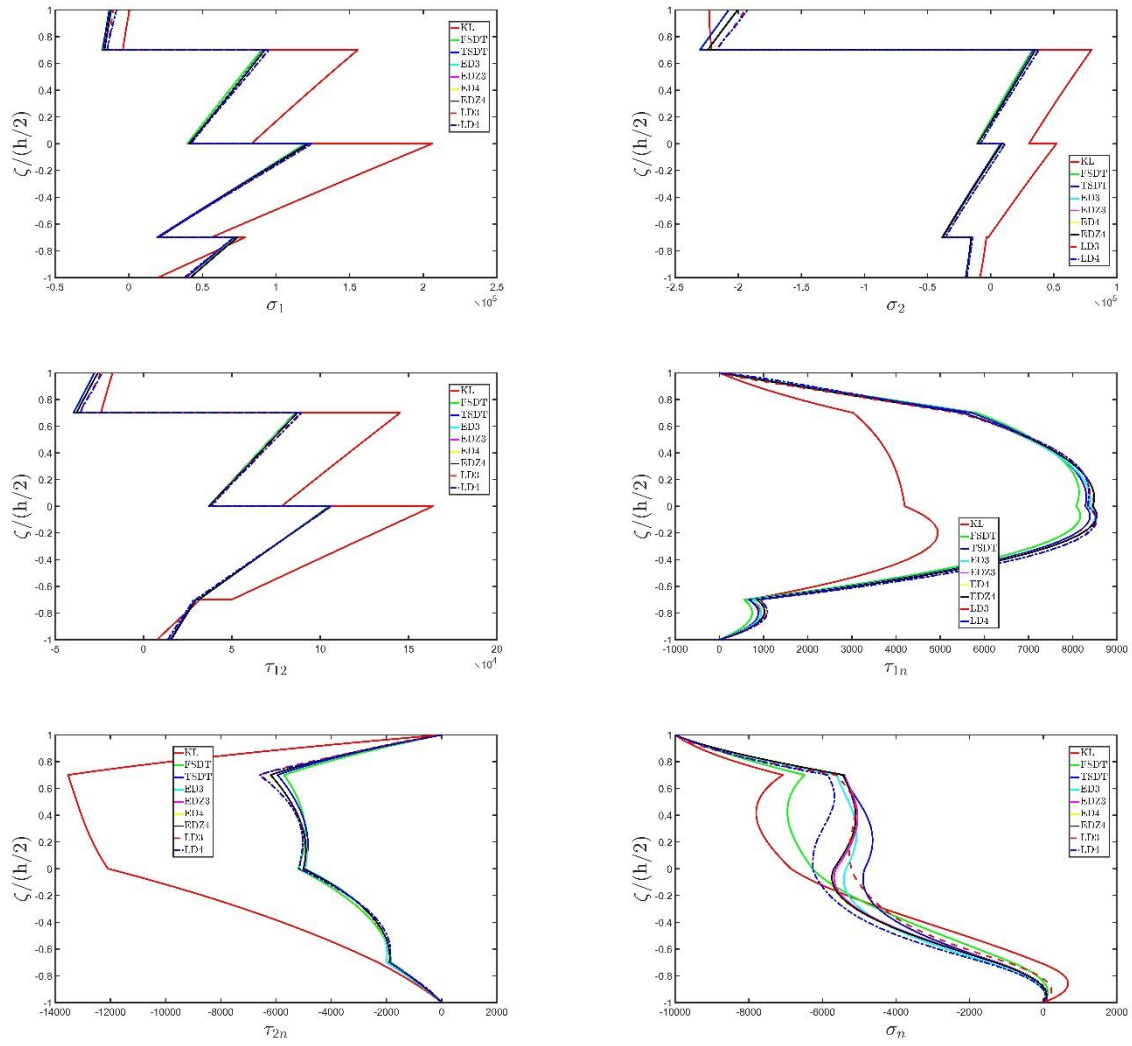
Figure 26. Through-the-thickness variation of displacement components [m] for a SSSS spherical panel $\left(R/h = 100 \right)$ made of three layers $\left(\text{Titanium} / \text{Foam} / \text{Titanium} \right)$ with $h_1 = h_3 = 0.15\,h$, $h_2 = 0.7\,h$ at the point $P = \left(0.25 \left(\alpha_1^1 - \alpha_1^0 \right), 0.25 \left(\alpha_2^1 - \alpha_2^0 \right) \right)$ subjected to a normal sinusoidal load $q_3^{(+)} = 10000\,\text{Pa}$ with $n = 1, m = 1$ on the top surface. Comparison between different structural theories.
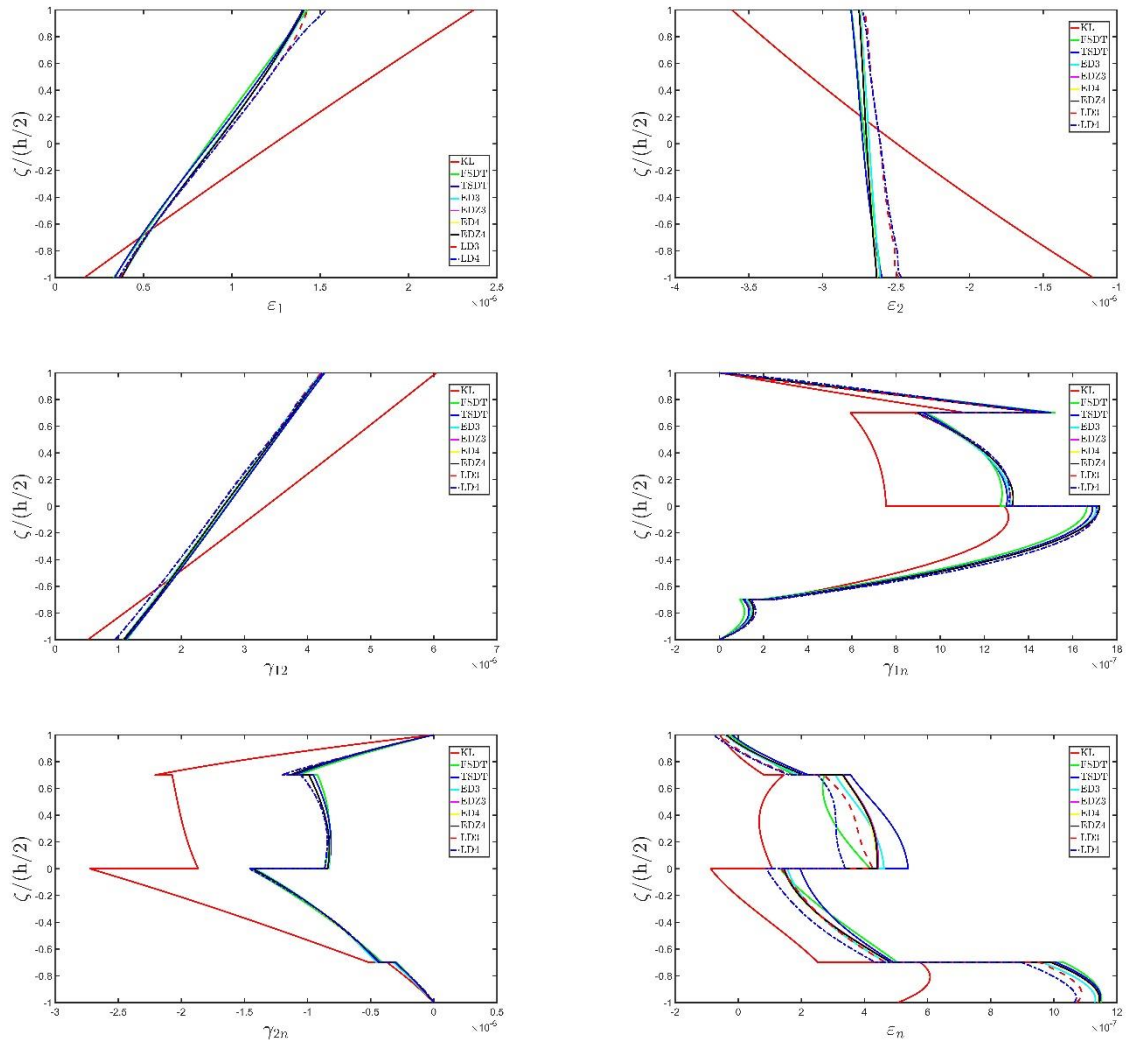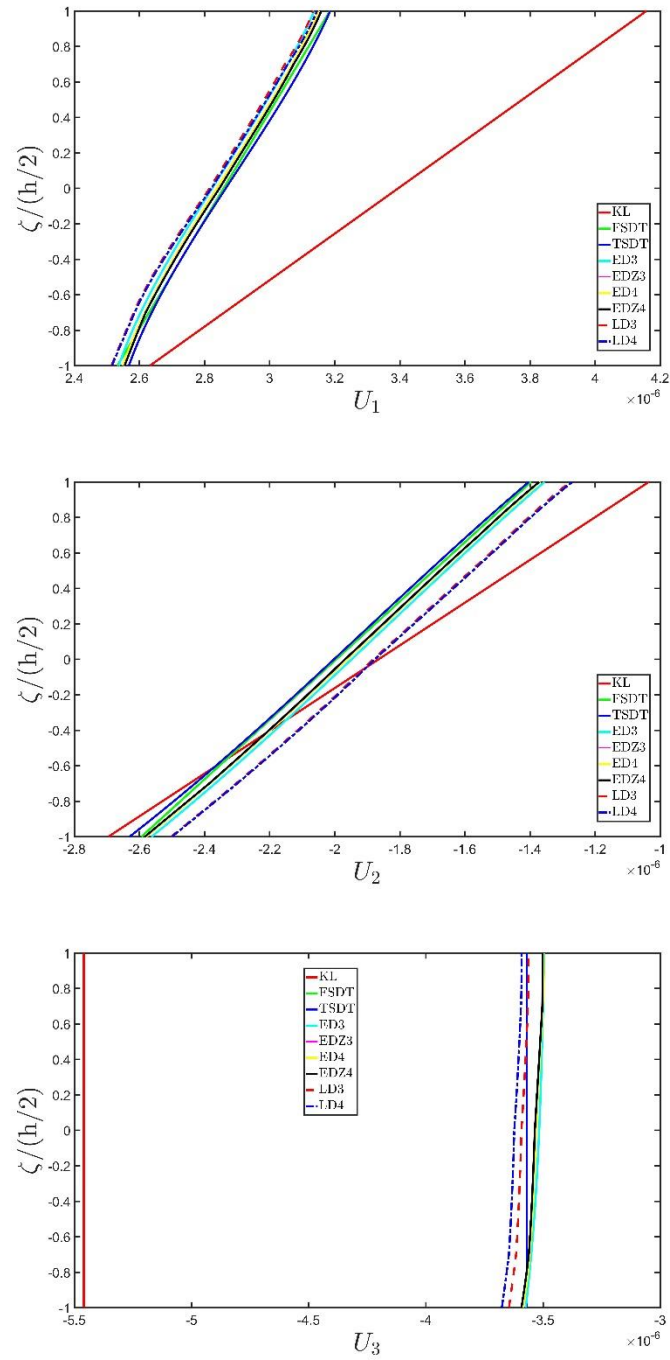
Figure 27. Through-the-thickness variation of strain components for a CFCF elliptic pseudosphere (Figure 2c) made of four layers $(20/35/45/70)$ with $h_1 = h_4 = 0.03\,\text{m}$, $h_2 = h_3 = 0.07\,\text{m}$ at the point $P = \left(0.25\left(\alpha_1^1 - \alpha_1^0\right), 0.25\left(\alpha_2^1 - \alpha_2^0\right)\right)$ subjected to a uniform load $q_3^{(+)} = -10000\,\text{Pa}$ on the top surface. Comparison between different structural theories.

Figure 28. Through-the-thickness variation of stress components [Pa] for a CFCF elliptic pseudosphere (Figure 2c) made of four layers $\left(20/35/45/70\right)$ with $h_1 = h_4 = 0.03\,\text{m},\ h_2 = h_3 = 0.07\,\text{m}$ at the point $P = \left(0.25\left(\alpha_1^1 - \alpha_1^0\right), 0.25\left(\alpha_2^1 - \alpha_2^0\right)\right)$ subjected to a uniform load $q_3^{(+)} = -10000\,\text{Pa}$ on the top surface. Comparison between different structural theories.

Figure 29. Through-the-thickness variation of displacement components [m] for a CFCF elliptic pseudosphere (Figure 2c) made of four layers $\left(20/35/45/70\right)$ with $h_1 = h_4 = 0.03\,\mathrm{m}$, $h_2 = h_3 = 0.07\,\mathrm{m}$ at the point $P = \left(0.25\left(\alpha_1^1 - \alpha_1^0\right), 0.25\left(\alpha_2^1 - \alpha_2^0\right)\right)$ subjected to a uniform load $\mathrm{q}_3^{(+)} = -10000\,\mathrm{Pa}$ on the top surface. Comparison between different structural theories.